Astronomy & Astrophysics manuscript no. hper
March 1, 2016
©ESO 2016

arXiv:1602.03696v2 [astro-ph.SR] 29 Feb 2016

Supersaturation and activity-rotation relation in PMS stars: the young cluster h Per⋆

C. Argiroffi[1,2], M. Caramazza[2], G. Micela[2], S. Sciortino[2], E. Moraux[3], J. Bouvier[3], and E. Flaccomio[2]

[1] Dip. di Fisica e Chimica, Università di Palermo, Piazza del Parlamento 1, 90134, Palermo, Italy, e-mail: argi@astropa.unipa.it
[2] INAF - Osservatorio Astronomico di Palermo, Piazza del Parlamento 1, 90134, Palermo, Italy,
[3] Univ. Grenoble Alpes, IPAG, F-38000 Grenoble, France
CNRS, IPAG, F-38000 Grenoble, France

Received May 18, 2015; accepted February 10, 2016

ABSTRACT

Context. Several studies showed that the magnetic activity of late-type main-sequence (MS) stars is characterized by different regimes and that their activity levels are well described by the Rossby number, *Ro*, defined as the ratio between the rotational period $P_{\rm rot}$ and the convective turnover time. Very young pre-main-sequence (PMS) stars show, similarly to MS stars, intense magnetic activity. However, they do not show clear activity-rotation trends, and it still debated which stellar parameters determine their magnetic activity levels.
Aims. To bridge the gap between MS and PMS stars, we studied the activity-rotation relation in the young cluster h Persei, a ~ 13 Myr old cluster, that contains both fast and slow rotators. The cluster members have ended their accretion phase and have developed a radiative core. It therefore offers us the opportunity of studying the activity level of intermediate-age PMS stars with different rotational velocities, excluding any interactions with the circumstellar environment.
Methods. We constrained the magnetic activity levels of h Per members by measuring their X-ray emission from a *Chandra* observation, while rotational periods were obtained previously in the framework of the MONITOR project. By cross-correlating these data, we collected a final catalog of 414 h Per members with known rotational period, effective temperature, and mass. In 169 of these, X-ray emission has also been detected.
Results. We found that h Per members with $1.0\,M_{\odot} < M_{\star} < 1.4\,M_{\odot}$ display different activity regimes: fast rotators clearly show supersaturation, while slower rotators have activity levels compatible to the non-saturated regime. At 13 Myr, h Per is therefore the youngest cluster showing activity-rotation regimes analogous to those of MS stars, indicating that at this age, magnetic field production is most likely regulated by the $\alpha\Omega$ type dynamo. Moreover, we observed that supersaturation is better described by $P_{\rm rot}$ than *Ro*, and that the observed patterns are compatible with the hypothesis of centrifugal stripping. In this scenario we inferred that coronae can produce structures as large as $\sim 2\,R_{\star}$ above the stellar surface.

Key words. Stars: activity – Stars: coronae – Stars: pre-main sequence – Stars: rotation – X-rays: stars

1. Introduction

Main-sequence (MS) late-type stars, including the Sun, produce intense magnetic fields, as evidenced by many observational features: photometric variability that is due to spots, enhanced chromospheric lines, frequent flaring activity, and intense X-ray emission (e.g., Berdyugina 2005; Kővári & Oláh 2014). In these stars X-rays are emitted by the stellar coronae, the outer stellar atmosphere where hot plasma is confined and heated by the stellar magnetic field (e.g., Favata & Micela 2003; Güdel 2004). This makes stellar X-ray emission one of the best probes of stellar magnetic activity.

Stellar magnetic fields are thought to be produced by dynamo processes that in turn are caused by plasma motions in the stellar interior. The role of stellar rotation and how stellar activity increases with stellar rotational velocity was initially described by Skumanich (1972) and Pallavicini et al. (1981). Then Noyes et al. (1984) also included the role of convective motions and proved that stellar activity levels do not depend on rotation alone, but are indeed better described by the Rossby number, *Ro*, defined as the ratio between the rotational period $P_{\rm rot}$ and the convective turnover time τ, which is the characteristic time taken by the plasma to cover a given distance in the convective envelope. Considering these results and what is known for the Sun, it is believed that all the stars with an inner radiative core and an outer convective envelope develop a $\alpha\Omega$ type dynamo, originating in a thin shell named tachocline at the interface between these two regions (Parker 1955; Spiegel & Weiss 1980).

Several studies based on large samples of late-type MS stars showed that stellar activity is characterized by different regimes (e.g., Dobson & Radick 1989; Pizzolato et al. 2003; Wright et al. 2011). In the non-saturated regime, that is, for $Ro > 0.13$, the stellar X-ray luminosity anticorrelates with *Ro*, with the fractional X-ray emission $L_{\rm X}/L_{\rm bol}$ scaling as $Ro^{-2.7}$ (Wright et al. 2011). This non-saturated regime, showing how activity levels and internal motions are linked, shows that stellar activity is indeed produced by a dynamo mechanism. For increasing rotational velocities, or more precisely, for $Ro < 0.13$, the $L_{\rm X}/L_{\rm bol}$ of MS stars saturates to its maximum level, which is $L_{\rm X}/L_{\rm bol} \approx 10^{-3}$, defining the so-called saturated regime. It is still debated whether this saturated level is due to an intrinsic saturation of the dynamo efficiency or to external constraints, like the full coverage of stellar surface with active regions. In ad-

⋆ Tables 1 and 2 Tables are available in electronic form at the CDS via anonymous ftp to cdsarc.u-strasbg.fr (130.79.128.5) or via http://cdsweb.u-strasbg.fr/cgi-bin/qcat?J/A+A/...

dition to non-saturation and saturation, a few studies suggested that in very rapidly rotating MS stars, a third regime probably occurs. These very rapid rotators show L_X/L_{bol} ratios lower than the saturated level (Randich et al. 1996; Prosser et al. 1996; James et al. 2000; Jeffries et al. 2011), which indicates the existence of a third regime, called supersaturation. This behavior was observed only for a very few stars belonging to young clusters ($\sim 30-50$ Myr), probably because of the decreasing stellar rotational velocities in older clusters.

Similarly to what occurs in MS stars, late-type pre-main-sequence (PMS) stars are also magnetically active, producing strong magnetic fields and manifesting intense coronal emission. Several studies investigated the properties of coronal activity of PMS stars, focusing almost entirely on very young ($\sim 1-3$ Myr) clusters. These studies found that in PMS stars, differently than in MS stars, L_X/L_{bol} and *Ro* are not correlated, with L_X/L_{bol} showing a very large scatter (e.g., Stassun et al. 2004; Preibisch et al. 2005; Briggs et al. 2007). The activity level of PMS stars, always showing a huge scatter, correlates with the accretion status, with accreting stars displaying on average lower L_X/L_{bol} than non-accreting stars (e.g., Flaccomio et al. 2003; Preibisch et al. 2005). It is still debated which mechanism causes this difference (e.g., Preibisch et al. 2005; Telleschi et al. 2007; Flaccomio et al. 2010, 2012). Some studies moreover also observed a positive correlation between L_X/L_{bol} and the stellar rotational period (Feigelson et al. 2003; Stassun et al. 2004; Preibisch et al. 2005; Henderson & Stassun 2012), a trend analogous the supersaturation phenomenon observed in young MS stars. However, this trend is not ubiquitous (Rebull et al. 2006; Alexander & Preibisch 2012). These results indicate that it is still unclear which stellar parameters determine the magnetic activity levels in PMS stars. Identifying this would help in constraining the physical mechanism causing or regulating their magnetic activity.

Diverse mechanisms could generate the different magnetic properties between MS and PMS stars. First, PMS and MS stars have different internal structures: PMS stars have deeper and more massive convective envelopes than MS stars, with very young stars (with mass of up to $\sim 1.0\,M_\odot$) being even fully convective. Moreover, considering that the different layers of internal stellar structure may have different rotational velocity, and that these velocities evolve on different timescales (Gallet & Bouvier 2013), then the different magnetic properties of PMS and MS stars could also be related to a different internal distribution of rotational velocities. Finally it is worth noting that PMS stars, especially at very young ages, still accrete material from their circumstellar disks, experiencing exchange of mass, energy, and angular momentum. The accretion process, braking or affecting stellar rotation or interacting with the stellar magnetosphere, might affect the magnetic activity of accreting stars.

To bridge the gap between the well-constrained case of MS stars and the puzzling case of very young PMS stars, we studied the activity-rotation relation in the young cluster h Per, which is a rich cluster, ~ 13 Myr old, located at 2290 pc, and characterized by a moderate interstellar absorption ($E(B-V) \sim 0.55$, which corresponds to $A_V = 1.7$). Because of its age, the h Per cluster offers several advantages: *a)* it contains both fast and slow rotators, allowing us therefore to test the different regimes of stellar dynamo, and in particular to search for and investigate the supersaturation phenomenon; *b)* accretion processes are completed, allowing us therefore to test the stellar magnetic activity excluding any interactions with the circumstellar environment; *c)* all the stars with $0.5\,M_\odot < M < 1.5\,M_\odot$ at the h Per age have already developed a radiative core and still preserve a convective envelope, which means that they have an internal structure similar to that of slightly older MS stars, where the $\alpha\Omega$ dynamo is already at work. Investigating the case of a young cluster also allows us to constrain whether stellar activity depends on Rossby number alone, as for MS stars, or whether it behaves differently, which would indicate that magnetic activity also depends on stellar evolutionary phase, hence on mass and age.

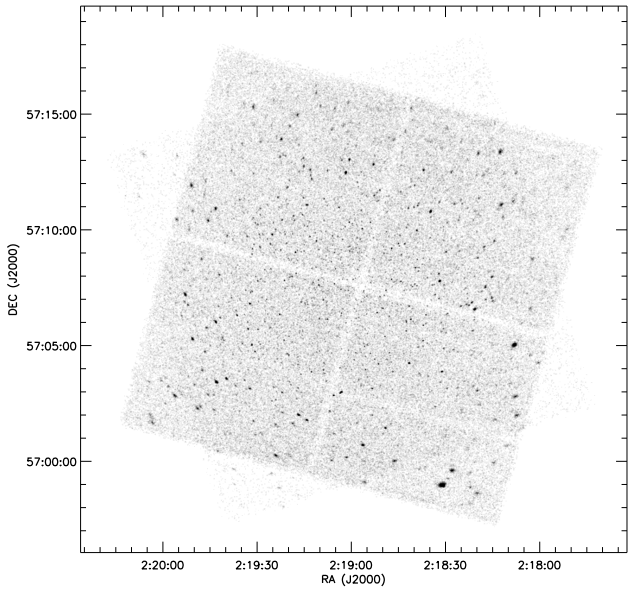

Fig. 1. $17' \times 17'$ field of view of the Chandra/ACIS-I observation of h Per. In this image we detected 1002 X-ray sources.

This paper is organized as follows: observation properties, data analysis, source identification, and parameter determination are reported in Sect. 2; properties of the selected sample of h Per members are presented in Sect. 3; Sect. 4 describes the search for activity-rotation relation, and the results are discussed in Sect. 5.

2. Data analysis

To investigate the activity-rotation relation in the h Per cluster, we constrained the magnetic activity levels of h Per members from a deep *Chandra* observation. Rotational periods were obtained by Moraux et al. (2013) in the framework of the MONITOR project.

2.1. X-ray source detection

We obtained a deep *Chandra*/ACIS-I observation of the h Per cluster in 2009. This observation has an exposure time of 189.8 ks, it is divided into three observing segments (Obs ID 09912, 09913, and 12021, PI G. Micela), and it is centered on $RA = 02^h\,19^m\,02\overset{s}{.}20$ and $DEC = +57^\circ07'12\overset{''}{.}00$. Data reduction was performed in a standard way, using the CIAO 4.1 package and following the threads provided by the *Chandra* X-ray Center. X-ray data were finally filtered considering only events with energy ranging between 0.5 and 8.0 keV.

We searched for X-ray sources using the `PWDetect` code (Damiani et al. 1997a,b), a wavelet-based detection algorithm. We set the significance threshold to 4.7σ, which, considering the background level of our observation, corresponds to an expected number of spurious detections of ten sources. For each detected

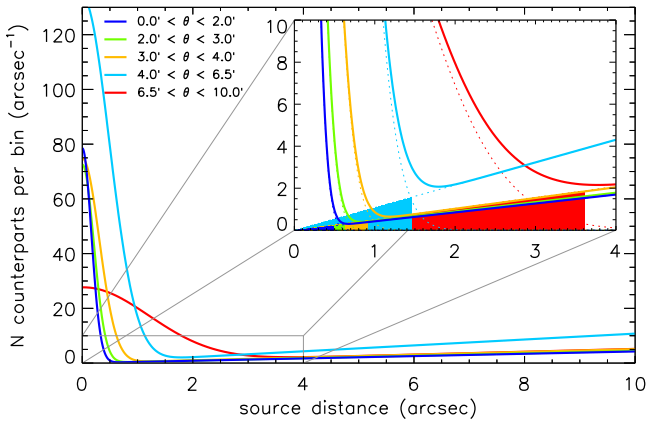

Fig. 2. Best-fit functions obtained from the distance distributions between X-ray sources and Moraux et al. catalog counterparts. We separately computed the distributions corresponding to X-ray sources located at different off-axis angle θ in the *Chandra* fov. The two components of each best-fit function, the Gaussian and the linear function, are indicated with dotted lines in the inset plot. The areas of the solid triangles indicate the expected number of spurious identification, assuming a matching radius of 3σ for each off-axis interval.

source this code provides in addition to the source position and detection significance the background-subtracted count rate in the 0.5 – 8 keV band. We applied the `PWDetect` code to the superposition of the three observing segments, shown in Fig. 1, collecting a list of 1010 X-ray sources. After a careful inspection, we rejected eight entries, corresponding to sources detected twice, obtaining therefore a final catalog of 1002 distinct X-ray sources, whose position and X-ray properties are reported in Table 1. The sensitivity of our X-ray survey is not uniform over the *Chandra* field of view (fov): it is higher near the telescope axis, where the weakest X-ray sources detected have fluxes of $\sim 10^{-7}$ ph s^{-1} cm^{-2}, while it diminishes in the outer regions (off axis $\sim 10'$), where the limiting flux is $\sim 5 \times 10^{-7}$ ph s^{-1} cm^{-2}.

2.2. X-ray source identification

To identify the detected X-ray sources, we first cross-correlated them with the catalog presented by Moraux et al. (2013) that contains 586 h Per members with a measured rotational period, 541 of which fall within the *Chandra* fov. For a correct comparison of the two catalogs we corrected the X-ray positions for a systematic offset, with respect to the Moraux et al. catalog, of $\Delta RA = -0.28''$ and $\Delta DEC = 0.28''$. To infer the best-matching radius for the source identification, we constructed and inspected the distribution of distances of Moraux et al. sources with respect to X-ray sources. This distribution is well described by a Gaussian, centered on a distance of $0''$, plus a linear function. These two components represent correlated and spurious identifications, respectively. This distribution is not the same over the *Chandra* fov, in particular, the Gaussian function becomes broader for increasing off-axis angle because of the decreasing accuracy of the X-ray position. We show in Fig. 2 the best-fit functions that describe these distributions, computed for different off-axis angle intervals. Considering these Gaussian functions, we adopted a matching radius of 3σ, which corresponds to $\sim 0.5''$ for sources near the telescope axis, and increases up to $\sim 3.6''$ for large off-axis angle. From this comparison with the Moraux et al. catalog, we found h Per member counterparts for 201 X-ray sources (with one X-ray source, X source ID = 187, being associated to two different counterparts). Considering the best-fit components describing the spurious associations (see Fig. 2), and integrating them up to the assumed matching radii, we expect five spurious identifications. 384 h Per members of the Moraux et al. catalog were left with no X-ray information. Since 339 of them are located within the *Chandra* fov, we estimated their upper limits in the X-ray band using the `PWDetect` code.

To search for other h Per members among the X-ray sources with no counterparts in the Moraux et al. catalog, we cross-correlated them with the h Per member list presented by Currie et al. (2010, Table 6). Again we corrected the X-ray source positions for a systematic offset ($\Delta RA = -0.43''$ and $\Delta DEC = 0.07''$) emerged from a first comparison with the source position of Currie et al. (2010). We computed and investigated the distribution of distances between X-ray and optical sources, applying the same procedure as was adopted for the counterparts search in the Moraux et al. catalog. In this case, the adopted matching radius ranges from $\sim 0.6''$ to $\sim 3.0''$ (corresponding to 3σ in this case as well) for increasing off-axis. Among the 801 X-ray sources not identified with the Moraux et al. catalog, we found h Per member counterparts for other 251 X-ray sources (with three sources, X source ID = 4, 273, and 858, having a double identification), of which nine are expected spurious identifications. The expected number of spurious identification is higher than for the identifications with the Moraux et al. sources because of the higher source density in the Currie et al. catalog.

Our final X-ray selected catalog of h Per members, listed in Table 2, is composed of 452 X-ray detected h Per members, 201 of which have a measured rotational period, and 420 have apparent magnitudes m_V and m_{I_C}. In the second part of Table 2 we also report the list of the 339 h Per members with measured rotational period that are not detected in X-rays.

2.3. Parameter determination

Our aim is to study the relationship between activity and rotation in h Per members. The stellar activity level is well probed by the X-ray luminosity L_X, and in particular by the ratio between L_X and the bolometric luminosities L_{bol}. The dynamo efficiency is expected to depend on the Rossby number *Ro*, that is, on the ratio between the stellar rotational period P_{rot} and the convective turnover time τ. The available measurements from which we started are the X-ray fluxes obtained from the *Chandra* data and the rotational period and mass are taken from the Moraux et al. catalog, and from the Currie et al. catalog we retrieved the m_V and m_{I_C} apparent magnitudes together with (whenever available) spectral type, individual $E(B-V)$, and luminosity class. Below we describe how, starting from these available measurements, we computed L_X, L_{bol}, and τ together with other parameters needed for their estimation.

2.3.1. Reddening and absolute magnitudes

To derive the interstellar absorption of each h Per member, we started from the $E(B-V)$ values published by Currie et al. (2010). Individual $E(B-V)$ values are only available for h Per members observed with optical spectroscopy and range from 0.188 to 1.137, with an uncertainty of 0.013. We adopted their average value, $E(B-V) = 0.55 \pm 0.1$, as reddening for the other h Per members. From the $E(B-V)$ we derived the A_V and A_I, (assuming $A_V = 3.12 \times E(B-V)$ and $A_I = 1.87 \times E(B-V)$, as re-

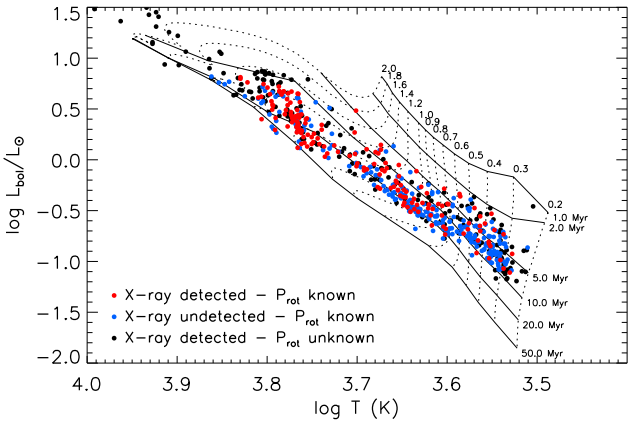

Fig. 3. HR diagram of h Per members. Evolutionary models, with labels indicating masses (in solar units) and ages, are taken from Siess et al. (2000).

ported in Currie et al. 2010), and then inferred the hydrogen column density $N_{\rm H}$, adopting an $N_{\rm H}$ to $A_{\rm V}$ ratio of 2.21×10^{21} cm^{-2} (Güver & Özel 2009). The $A_{\rm V}$ and $A_{\rm I}$ values associated with each source, together with the known cluster distance, allowed us to compute the absolute $M_{\rm V}$ and $M_{\rm I_C}$ magnitudes and dereddened $(V - I_{\rm C})$ color for those sources with known apparent $m_{\rm V}$ and $m_{\rm I_C}$ magnitude.

2.3.2. Effective temperature

For h Per members observed with optical spectroscopy by Currie et al. (2010) and classified as luminosity class V stars, we derived the effective temperatures $T_{\rm eff}$ by converting the reported spectral class following Kenyon & Hartmann (1995). For the other h Per members with no spectroscopic information, but with known absolute $M_{\rm V}$ and $M_{\rm I_C}$ magnitude, we derived the effective temperatures $T_{\rm eff}$ from their intrinsic $(V - I_{\rm C})$ color, according again to Kenyon & Hartmann (1995). The errors on $T_{\rm eff}$ were obtained by propagating the errors on spectral class or $(V - I_{\rm C})$; the obtained uncertainties are smaller than 10% for $T < 10^4$ K, and increase to 30-50% for hotter stars.

2.3.3. Bolometric luminosity

We derived the stellar bolometric luminosity $L_{\rm bol}$ starting from the absolute $M_{\rm V}$ magnitude and converting it into $L_{\rm bol}$ by adopting the Kenyon & Hartmann (1995) bolometric corrections corresponding to the evaluated $T_{\rm eff}$ of each source. We computed the uncertainties on $L_{\rm bol}$ taking into account both the uncertainty on $M_{\rm V}$ and bolometric corrections. From the inferred $L_{\rm bol}$ and $T_{\rm eff}$ values we constructed the HR diagram of the h Per members considered, as shown in Fig. 3.

2.3.4. X-ray luminosity

We derived the X-ray luminosity of h Per members by multiplying their observed X-ray photon flux by $k\,4\pi\,d^2$, with d being the cluster distance and k the average photon energy. The observed X-ray fluxes provided by the source detection algorithm correspond to the whole exposure time. Therefore the X-ray luminosities obtained correspond to values averaged over a time interval of 190 ks. This interval is long enough to ensure that individual strong flares do not affect the spread in the activity-rotation pattern (Preibisch et al. 2005). The parameter k depends on the adopted energy band, on the shape of the emitted spectrum, and on the interstellar absorption. We considered the 0.5 – 8.0 keV energy band[1] and assumed that the X-rays are emitted by an optically thin plasma, at a temperature of 10 MK, with heavy element abundances of 0.2 in solar units (this temperature and metallicity are typical values for low-mass PMS stars of a few Myr, Argiroffi et al. 2006). Taking into account the hydrogen column density of each source, we obtained k values ranging between 2.5×10^{-9} and 1.1×10^{-8} erg ph^{-1}. The derived X-ray luminosities of h Per members are reported in Table 2.

2.3.5. Convective turnover time

To compute the Rossby number $Ro = P_{\rm rot}/\tau$, it is necessary to estimate the convective turnover time τ for each star. While the rotational period is directly measured, τ is not directly observable. Two different convective turnover times are usually defined: the global convective turnover time, τ_g, defined as the time taken by the plasma to rise through the convective envelope, and the local convective turnover time, τ_l, defined considering not the whole convective envelope, but only a characteristic length at its base. Previous studies usually adopted the local convective turnover time τ_l to compute the Rossby number because the $\alpha\Omega$ type dynamo is expected to originate at the base of the convective envelope. For MS stars τ_l is commonly estimated empirically starting from the $(B - V)$ color (e.g., Noyes et al. 1984; Pizzolato et al. 2003), a proxy of stellar temperature. h Per is an intermediate-age PMS cluster, many of the h Per members lie well above the main sequence (see Fig. 3), indicating that they are still contracting, and that their internal structure is not settle to the MS status. The τ of PMS stars can only be estimated by referring to stellar evolutionary models that provide details on the stellar internal structure (e.g., Feigelson et al. 2003; Preibisch et al. 2005; Alexander & Preibisch 2012). As a consequence, results based on the inferred τ values might depend on the accuracy of stellar evolutionary models[2].

To derive the convective turnover time we followed the same procedure as was used by Flaccomio et al. (2004) for PMS stars in the Orion nebula cluster. This procedure is based on PMS evolutionary models of Ventura et al. (1998, and private communication) and allows estimating the global convective turnover time τ_g. These models provide τ_g values that depend almost only on the relative dimension of the convective envelope with respect to the stellar radius, $\Delta R_{\rm conv}/R_\star$. To show that we report in Fig. 4 the tracks followed by stars of different mass ($0.6\,{\rm M}_\odot \le M \le 1.6\,{\rm M}_\odot$) during their evolution toward the MS (1 Myr ≤ age ≤ 30 Myr) in the τ_g vs $\Delta R_{\rm conv}/R_\star$ space: these tracks perfectly overlap and allow identifying one well-defined relation between τ_g and $\Delta R_{\rm conv}/R_\star$, regardless of stellar mass and age. As a first step, we therefore derived the ratio $\Delta R_{\rm conv}/R_\star$

[1] Previous studies on activity-rotation relation where based on the *ROSAT* 0.1 – 2.4 keV band and not on the *Chandra* 0.5 – 8.0 keV band. This difference implies that a correction must be considered in the saturated $L_{\rm X}/L_{\rm bol}$ level observed for MS stars to compare it with our data. Wright et al. (2011) found a saturated level of $\log L_{\rm X}/L_{\rm bol} = -3.13$ and computed a factor of 0.676 to convert $L_{\rm X}$ from the 0.5 – 8.0 keV to 0.1 – 2.4 keV band. This means that the saturation level should be set to $\log L_{\rm X}/L_{\rm bol} = -2.96$. For simplicity we set it to $\log L_{\rm X}/L_{\rm bol} = -3$, since in the following analysis this value is used only as a reference.

[2] It is known that PMS evolutionary models show systematic mass-dependent discrepancies with observations (Hillenbrand et al. 2008). These discrepancies also emerge for h Per, where the comparison between empirical and theoretical cluster sequences suggests a younger age for low-mass members than for higher mass members (Fig. 3).

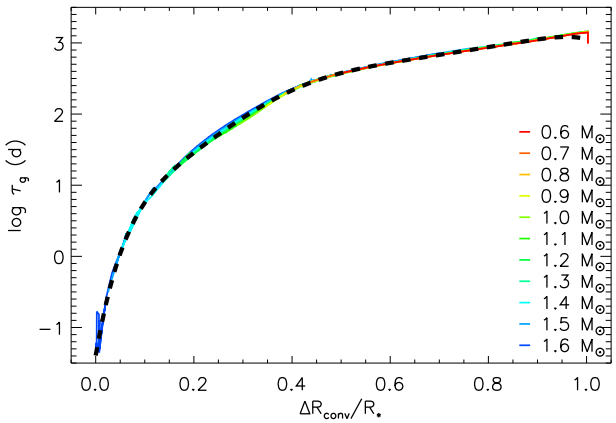

Fig. 4. Global convective turnover time, τ_g, vs relative convective envelope radius, $\Delta R_{conv}/R_\star$, derived from the PMS evolutionary models of Ventura et al. (1998), with ages ranging between 1 and 30 Myr. The black dashed line indicates the best-fit function adopted to convert the inferred convective radius of h Per members to derive their τ_g.

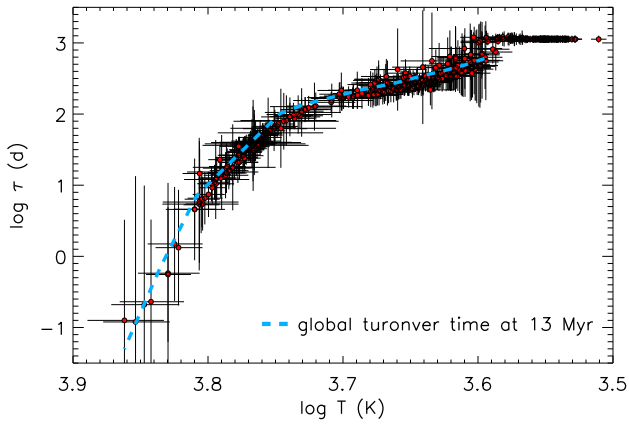

Fig. 5. Red circles indicate the global convective turnover time inferred for h Per members. The blue dashed line shows the global convective turnover time provided by Ventura et al. (1998) for 13 Myr old stars.

for each star by comparing its position on the HR diagram with the evolutionary tracks of Siess et al. (2000), that provide this information. We also computed the uncertainty on $\Delta R_{conv}/R_\star$ considering the uncertainties on T_{eff} and L_{bol}. Then, we inferred the τ_g corresponding to the estimated $\Delta R_{conv}/R_\star$ values, adopting the best-fit relation obtained from the Ventura et al. models[3] that are shown in Fig. 4. This method, being based on stellar position on the HR diagram, has the advantage of taking into account possible age spreads. The stellar formation process appears to be not instantaneous, but to last a few Myr (e.g., Burningham et al. 2005). This might produce significant differences in the internal structures of stars with similar mass at the age of h Per.

In Fig. 5 we show the τ_g values vs T_{eff} obtained for h Per members with known rotational period (either detected in X-rays or not), reporting also the resulting error bars on T_{eff} and τ_g. As shown in the plot, the estimated values scatter around the predicted value for 13 Myr old stars (blue dashed line), as expected. The coolest stars in our sample ($\log T_{eff} \lesssim 3.6$) have τ_g values that saturate at $\sim$ 1200 d. These stars appear slightly younger than the estimated h Per age because of their position in the HR diagram, and their inferred internal structure is that of fully convective stars (i.e., $\Delta R_{conv}/R_\star = 1$).

As specified above, with this procedure we inferred the global convective turnover time, τ_g. We decided to use the τ_g values in our analysis instead of τ_l because τ_g can also be defined for fully convective stars, other than for stars with outer convective envelope (τ_l can instead be defined only for the latter). This choice allows us to include both these stellar categories in our analysis, and investigate whether their activity behaves differently. However, we note that the τ_g and τ_l values provided by the Ventura et al. (1998) models differ by a factor $\sim$ 3 regardless of the stellar temperature. Hence the choice of using τ_g or τ_l in this work does not affect any possible activity-rotation observed trend, but can only change the absolute *Ro* values at which trends or regimes occur.

[3] We note that the use of two different evolutionary models, i.e. Ventura et al. (1998) and Siess et al. (2000), is required because the Ventura et al. models that provide τ_g consider only stars with masses ranging between 0.6 and 1.6 $M_\odot$, while the Siess et al. models also allow exploring stars down to 0.1 $M_\odot$. We therefore assume that the $\Delta R_{conv}/R_\star$ vs τ_g relation of Ventura et al. (1998) also holds for lower mass stars.

3. Properties of the X-ray selected catalog of h Per members

Our X-ray survey of h Per cluster and its comparison with the catalogs of Moraux et al. (2013) and Currie et al. (2010) provided a list of 452 X-ray sources identified as h Per members. Of these, 201 have a measured rotational period. We also computed upper limits in the X-ray band to other 339 h Per members with known rotational periods (see Table 2). The HR diagram of the h Per members considered is shown in Fig. 3.

We based our activity-rotation analysis on the subsample h Per members with known rotational period and effective temperature, both X-ray detected and undetected. This subsample is composed of 414 stars with masses ranging between 0.32 and 1.6 $M_\odot$, periods ranging between 0.15 and 16 d, and Rossby numbers ranging between 2.2×10^{-4} and 6.4. Of these 414 stars, 169 were detected in the X-ray *Chandra* observation, showing L_X ranging between $3.5{\times}10^{29}$ and $1.1{\times}10^{31}$ erg s^{-1}. In the whole subsample of 414 stars, 105 where flagged as candidate binaries by Moraux et al. (2013). However, in the analysis presented in this work, we do not distinguish between single or binary systems because the results obtained were the same for the two stellar subsets, which supports the finding of Wright et al. (2011), who did not find any significant difference in the activity-rotation behavior of single vs binary stars.

The contamination of field stars in the h Per period catalog from Moraux et al. (2013) is expected to be $\sim$ 2%. Because our catalog is X-ray selected, it is conceivable that the final contamination of field stars is even lower. In parallel we estimated the spurious identifications of X-ray sources to be $\sim$ 2%. Therefore the whole contamination of erroneous sources (because of incorrect identification or false membership) in our subsample is expected to be negligible.

The period catalog of Moraux et al. is characterized by a period detection rate that ranges between $\sim$ 80% for stars at $I_{CFHT} = 15.5$ (corresponding to $M \sim 1.5\,M_\odot$), and $\sim$ 5% at $I_{CFHT} = 19.5$ (corresponding to $M \sim 0.3 - 0.4\,M_\odot$). Our X-ray survey, being a flux-limited survey, is likewise characterized by a detection rate that decreases for lower mass stars. In the upper panel of Fig. 6 we show the mass vs X-ray luminosity scatter plot, including the upper limits of X-ray undetected h Per members as well, and distinguishing between single and binary stars. In the lower panel of Fig. 6 we report the detection rate in the X-ray band with respect to the Moraux et al. catalog: the fraction of

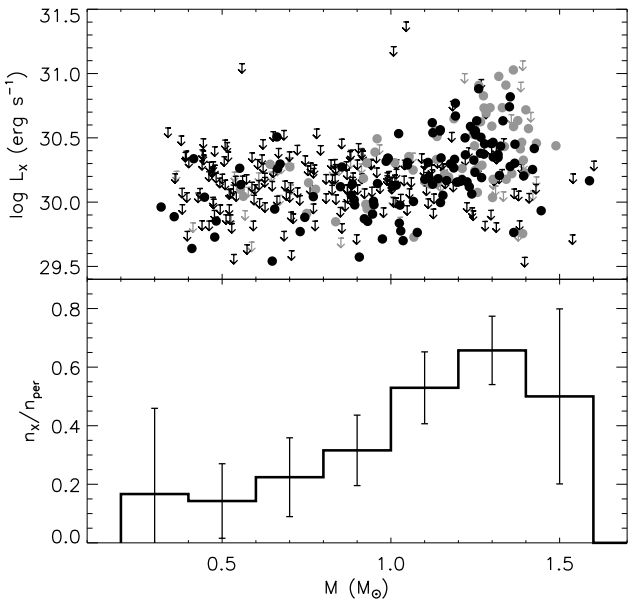

Fig. 6. *Upper panel*: L_X vs mass for h Per members, with black and gray symbols indicating single and binary stars, respectively. *Lower panel*: Fraction of sources of the Moraux et al. (2013) catalog detected in the X-ray band.

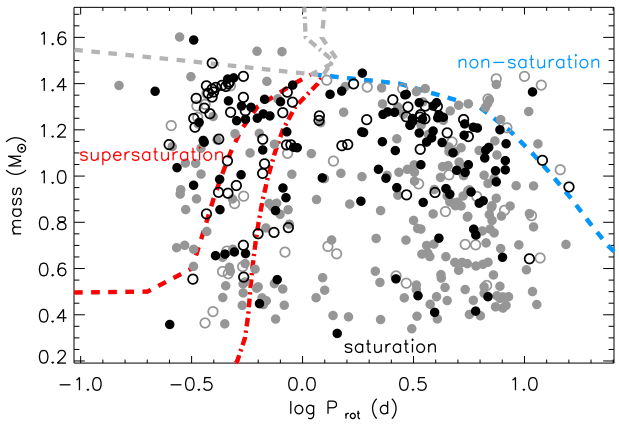

Fig. 7. Mass vs period of X-ray selected h Per members detected (black) and undetected (gray) in X-rays. Filled and open symbols indicate single and binary stars, respectively. Red lines separate the loci corresponding to supersaturation and saturation, assuming centrifugal stripping (dash-dotted line) or polar updraft (dashed line) theories. The blue dashed line marks the expected separation between non-saturation and saturation.

stars detected in the X-ray band is ∼ 15% for ∼ 0.5 $M_\odot$ stars and increases to ∼ 70% for ∼ 1.3 $M_\odot$. Therefore the completeness of X-ray detected h Per subsample, with respect to the total cluster population, is ∼ 40% – 50% for stars with $M \sim 1.3 - 1.5\,M_\odot$, and lower than 1% for stars with $M \sim 0.3 - 0.4\,M_\odot$. We note moreover that $P_{\rm rot}$ and $L_{\rm X}$ detections are highly correlated, since the most active stars on average display both higher X-ray emission and larger amplitude in their photometric variability, which increases the period detection rate. Therefore the X-ray detected h Per members our sample, for each mass bin, are preferentially the most active stars.

We first checked which activity regimes can be explored with the 13 Myr old stellar sample obtained. To this aim we show in Fig. 7 the scatter plot of mass vs period of h Per members, including detected and non-detected X-ray sources.

For MS stars the separation between saturated and non-saturated regimes occurs at fixed *Ro* values, regardless of stellar mass. When *Ro* is computed as $P_{\rm rot}/\tau_l$, this threshold occurs at $Ro \approx 0.13$ (Wright et al. 2011), which turns into $Ro \approx 0.04$ when it is taken into account that $\tau_g \approx 3\tau_l$. Therefore, assuming that the same applies to intermediate-age PMS stars and considering the internal structures of 13 Myr old stars of different masses, it is possible to compute rotational periods corresponding to this *Ro* value. We report in Fig. 7 this expected separation between non-saturated and saturated regimes (blue dashed line).

We also computed where the supersaturated regime is expected to occur. However, the paucity of observational constraints of supersaturation makes this prediction more uncertain. Hence we considered the two physical mechanisms suggested to explain the supersaturation: centrifugal stripping (Jardine & Unruh 1999) and polar updraft migration (Stępień et al. 2001). The centrifugal stripping mechanism predicts that coronal emission might be reduced when rotational velocity increases because the largest coronal structures might be disrupted by the centrifugal force. This mechanism takes place when the largest coronal structures extend beyond the co-rotation radius[4]. Assuming therefore that centrifugal stripping becomes effective when the co-rotation radius is smaller than $3\,R_\star$ (i.e., assuming that coronal structures extending up to $2\,R_\star$ above the photosphere), as suggested by Wright et al. (2011), we obtained the dash-dotted red line shown in Fig. 7. The polar updraft effect instead predicts that when the rotational velocity increases, then the magnetic flux emergence becomes more efficient near stellar poles, leaving the equatorial regions free of magnetic flux tubes and hence without coronal structures. Wright et al. (2011) quantified the efficiency of this mechanism by defining the parameter

$$G_X = \frac{\omega_{\rm core}^2 R_{\rm core}^3 \sin^2\theta}{G M_{\rm core}},$$

where $M_{\rm core}$ and $R_{\rm core}$ are the mass and radius of the radiative core, $\omega_{\rm core}$ is its rotational angular velocity, and θ is the colatitude on stellar surface. Considering MS stars, they suggested that supersaturation occurs where $G_X < 0.01$. Considering again the internal structures of 13 Myr old stars, assuming that the core rotates with the same period as the convective envelope and averaging $\sin^2\theta$ over the stellar surface, we computed the locus corresponding to $G_X = 0.01$ and report this threshold with a red dashed line in Fig. 7. A more detailed discussion on centrifugal stripping and poleward migration is reported in Sect. 5.

The two thresholds that identify the supersaturation regime differ among themselves and with respect to MS stars, where they almost overlap (Fig. 6 in Wright et al. 2011). In particular, the centrifugal stripping threshold for PMS stars is located at periods longer than those of MS stars (because of the larger stellar radii of PMS stars) and longer than those corresponding to the polar updraft threshold. Moreover, the two transitions show large differences for very low mass stars: the polar updraft can operate only in stars with a radiative inner core, and at an age of 13 Myr, stars with $M \sim 0.3 - 0.5\,M_\odot$ have not developed it as yet.

[4] The co-rotation radius is defined as the distance from the star at which the orbital period equals the stellar rotational period. Beyond this distance it is not possible to have gravitationally bound structures that rotate with the same angular velocity as the central star.

The thresholds shown in Fig. 7 indicate that our stellar sample provides a good coverage of supersaturation and saturation regimes. This should allow us to check whether or not at 13 Myr old these activity regimes are analogous to those of MS stars, or whether, even at this age, PMS stars still show activity levels scattered over several order of magnitudes. In particular, the large number of stars with short rotational periods provide the opportunity of deeply investigating the supersaturated regime, whose occurrence, parameter dependence, and physical origin are still elusive.

4. Activity vs rotation analysis

We based our activity-rotation analysis on the sample of h Per members with known rotational period and effective temperature, both X-ray detected and undetected. This sample is composed of 414 stars with masses ranging between 0.3 and 1.6 $M_\odot$. To check whether the mass is an important parameter in determining the stellar activity level, we divided our stellar sample into different mass bins. The adopted mass grid is $0.3 - 0.7$, $0.7 - 1.0$, $1.0 - 1.2$, $1.2 - 1.4$, and $1.4 - 1.6\,M_\odot$. The aim is to obtain a minimum number of stars in each mass bin to perform a statistically meaningful analysis. The last bin, $1.4 - 1.6\,M_\odot$, is poorly populated, but we decided to keep it separated because in this mass range the expected behavior is significantly different from that of lower mass stars (see Fig. 7). All but one of the stars populating the first bin, that is, $0.3\,M_\odot < M_\star < 0.7\,M_\odot$, are fully convective stars ($\Delta R_{\rm conv}/R_\star > 0.95$), but some fully convective stars also populate ($\sim 30\%$) the second mass bin. Each mass bin is also composed of a significant percentage (ranging between 20% and 50%) of candidate binary stars. In our analysis we investigated whether and how different parameters could be relevant for determining stellar activity in PMS stars, and to this aim we considered separately single vs binary stars, and fully convective from partially convective stars. The different subsamples obtained showed no significant differences, however. Therefore in the analysis presented here we did not consider these classes separately.

To search for intrinsic correlations among variables, we used the `ASURV` software package (Isobe & Feigelson 1990; Lavalley et al. 1992), which implements methods presented in Isobe et al. (1986) that provide correlation and regression techniques for samples containing both detections and upper limits. In particular, we searched for significant correlations by using Spearman's rho test and computed linear regression with the EM algorithm.

We searched for a significant correlation between $\log L_{\rm X}$ vs $\log P_{\rm rot}$ considering separately stars with different mass. We separated stars by mass because the completeness of our sample depends on stellar mass, and because we cannot exclude that stellar activity at this age are mass dependent. The resulting scatter plots are shown in the left panels of Fig. 8.

Inspecting these plots and considering that MS stars show different activity regimes, we guessed that different correlations corresponding to different regimes may exist also for intermediate-age PMS stars. We did not assume a priori at which $P_{\rm rot}$ value regime switches take place. We therefore investigated separately different $P_{\rm rot}$ subintervals. In particular, for each mass bin, we divided the entire $P_{\rm rot}$ range into two adjacent subintervals, searched for correlations separately in the two subintervals, and repeated this analysis considering different $P_{\rm rot}$ separating values.

We assumed 99% as confidence level. The best fits corresponding to all the significant correlations obtained are indicated in Fig. 8 with gray lines. Since in several cases significant correlations are present for a vast range of $P_{\rm rot}$ separating values, we identified the positive and negative correlations corresponding to the highest significance to synthesize these results in a more compact way. We highlight these correlations in Fig. 8 with red dashed lines. For some mass bins, none, or only one kind of correlation emerges. For the $1.0 - 1.2$ and $1.2 - 1.4\,M_\odot$ bins we instead found both positive and negative correlations. In these cases we note that positive and negative correlations are present also in non-overlapping and hence independent ranges. This renders the detection of different regimes statistically reliable. The fact that significant correlations are obtained for a vast range of $P_{\rm rot}$ separating values could pinpoint the uncertainty on the exact $P_{\rm rot}$ value at which these regimes switch, but it could also indicate that the regime switch is not as sharp.

To summarize, and taking into account the highest significance correlations, we found a clear evidence of correlations between $\log L_{\rm X}$ and $\log P_{\rm rot}$ for stars with masses in the ranges $0.7 - 1.0\,M_\odot$, $1.0 - 1.2\,M_\odot$, and $1.2 - 1.4\,M_\odot$. In particular, for stars with masses between 0.7 and $1.0\,M_\odot$, the data indicate a negative correlation over the whole $P_{\rm rot}$ range, with a slope of -0.20 ± 0.07. For the $1.0 - 1.2\,M_\odot$ and $1.2 - 1.4\,M_\odot$ mass bins we found that for periods shorter than $\sim$ 1 d there is a positive correlation corresponding to slopes of 0.60 ± 0.16 and 0.86 ± 0.22. We also observed a significant negative correlation for periods longer than $\sim$ 1 d, with slopes of -0.31 ± 0.09 -0.51 ± 0.09, respectively.

We also searched for significant correlations between the logarithmic fractional X-ray luminosity, $\log R_{\rm X} = \log L_{\rm X}/L_{\rm bol}$, and $\log Ro$. For MS stars the relation between $R_{\rm X}$ and Ro is the same for stars of different masses. However, we first also inspected the $\log R_{\rm X}$ and $\log Ro$ patterns separating stars of different mass (right panels of Fig. 8) because *a*) we wished to check whether in intermediate-age PMS stars activity depends on mass, *b*) the completness of our stellar sample depends on stellar mass, and *c*) we aim at minimizing the effect of possible mass-dependent systematic uncertainty present in the evolutionary models used to infer stellar τ. After dividing the stars into different mass bins, it might be expected that a significant correlation between $\log L_{\rm X}$ and $\log P_{\rm rot}$ would correspond to a significant correlation between $\log R_{\rm X}$ and $\log Ro$, but this is not the case: in all the inspected cases we did not find evidence of significant correlations, with the only exception of a negative correlation for stars with $1.2\,M_\odot < M < 1.4\,M_\odot$ and $\log Ro \gtrsim -2$, corresponding a slope of -0.54 ± 0.09.

Inspecting the $\log R_{\rm X}$ vs $\log Ro$ scatter plots of Fig. 8, we note that even if significant correlations in most cases do not emerge, the typical $\log R_{\rm X}$ level decreases for increasing stellar mass. We cannot distinguish whether this effect is due to an intrinsic difference in the typical $\log R_{\rm X}$ level of stars of different mass or simply a consequence of the different X-ray sensitivity in different mass bins. We selected our stellar sample from a flux-limited X-ray survey (see Sect. 3), hence the survey reaches the lowest $R_{\rm X}$ for the highest mass stars. If the latter is the case, then lower mass stars might have a larger scatter in their $\log R_{\rm X}$ distribution than higher mass stars.

To investigate the $R_{\rm X}$ vs Ro relation for intermediate-age PMS stars in more detail, we considered the whole stellar sample, regardless of the different stellar masses, in analogy to the $R_{\rm X}$ vs Ro trends observed for MS stars. We show the $\log R_{\rm X}$ vs $\log Ro$ scatter plot of h Per members of our sample in Fig. 9, where we report as a reference the best-fit relation describing saturated and non-saturated regimes that was obtained by Wright et al. (2011) for MS stars, which we adjusted for the dif-

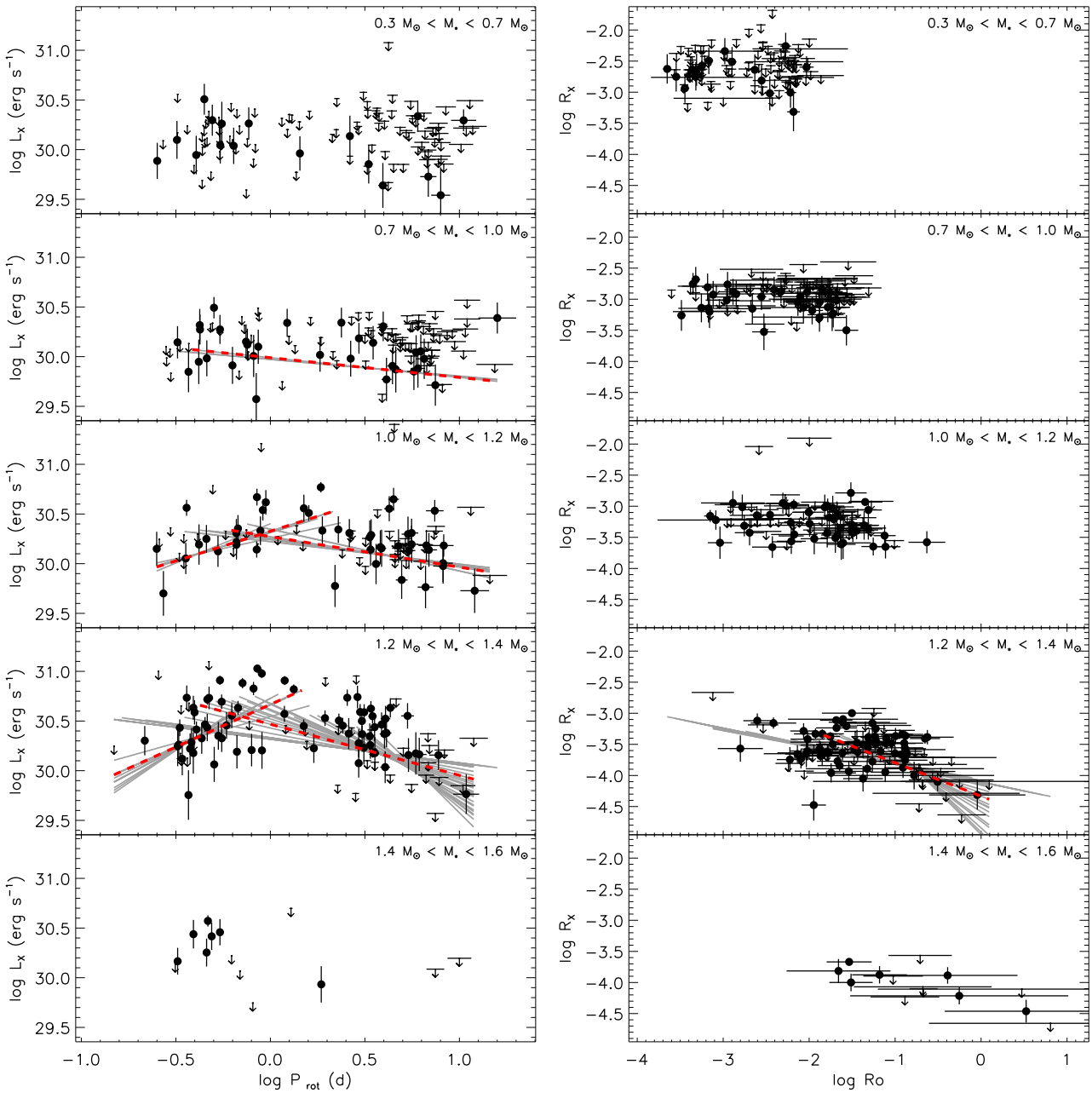

Fig. 8. *Left panel*: X-ray luminosity vs rotational period for h Per members of different mass. *Right panel*: Fractional X-ray luminosity vs Rossby number for h Per members of different mass. In both cases gray lines mark the best fit corresponding to intervals in which the two quantities have a significant correlation (confidence level higher than 99%), with red dot-dashed lines indicating the highest significant cases for both positive and negative correlation.

ferent τ used here. The whole stellar sample indicates a significant correlation over the whole *Ro* ranges with fractional X-ray luminosity increasing for decreasing Rossby number. As stressed above, this correlation might be due to the different X-ray sensitivity of our sample for different stellar masses: the lowest R_X values can be explored only for the highest mass stars, which on average have lower τ and hence higher *Ro*. This selection effect is evident from the left panel plots of Fig. 8. To avoid this mass selection effect, we searched for correlations considering only stars with $M_\star > 1.0\,M_\odot$, since our completeness is uniform over this mass range (see Fig. 6). In particular, examining only the *Ro* range corresponding to non-saturation (i.e., $Ro > 0.04$), we found a significant negative correlation, corresponding to a slope of -0.76 ± 0.10, which is shown by the red dashed line in Fig. 9.

From this analysis we found evidence that for long rotational periods (or large *Ro*) X-ray luminosity (or R_X) decreases for increasing P_{rot} (or *Ro*). We also found that for short rotational periods, stars with $1.0\,M_\odot < M < 1.4\,M_\odot$ show a positive correlation between L_X and P_{rot}. This trend is not observed in the R_X vs *Ro* space.

Before discussing these results, and in particular the positive correlation between L_X and P_{rot} that is not observed between R_X and *Ro*, we performed some additional checks. As a first step, to distinguish whether this positive correlation disappears in the R_X vs *Ro* space because of the L_X to R_X conversion or because of the change from P_{rot} to *Ro* , we inspected the R_X vs P_{rot} space. We

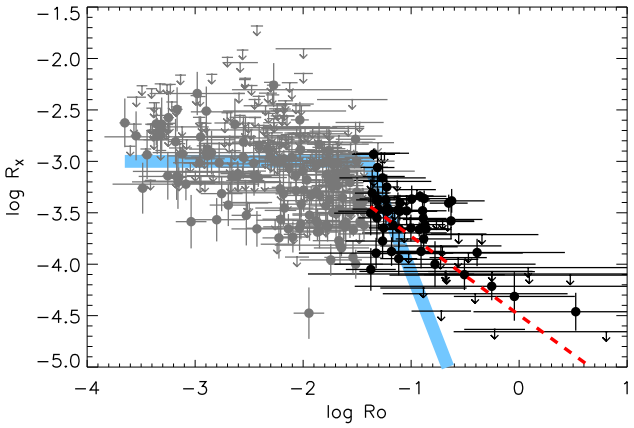

Fig. 9. Fractional X-ray luminosity vs Rossby number for h Per members. The light blue solid line indicates the saturated and non-saturated relation obtained for MS stars by Wright et al. (2011). Black symbols mark h Per members used to perform the best fit in the expected non-saturation regime (i.e., $Ro > 0.04$ and $M > 1.0\,M_{\odot}$), with the red dashed line being the best-fit relation. Gray symbols indicate the remaining h Per members.

found a significant positive correlation between R_X vs P_{rot} for the same mass bins and for short periods. This indicates that this positive correlation emerges only when L_X or R_X are considered with respect to P_{rot} and that it is not related to the known positive correlation between L_X and L_{bol} or L_X and stellar mass.

As already stressed in Sect. 2.3.5, the τ estimation is particularly critical for PMS stars because empirical relations calibrated on MS stars cannot be used. For PMS stars τ must be estimated considering stellar evolutionary models and inferring the internal structure of each star. Therefore we scrutinized the method adopted for estimating τ to try to evaluate whether and how our results depend on the peculiar evolutionary models considered, or on the method adopted.

We checked the theoretical τ values of Ventura et al., comparing them with the value provided by Landin et al.. The two models provide very similar values both for τ_l and τ_g. The Landin et al. models, however, range only from 0.6 to 1.2 $M_{\odot}$, which is at odds with the 0.6 to 1.6 $M_{\odot}$ range covered by Ventura et al. The τ vs M relation at 13 Myr changes significantly in slope in the $1.0\,M_{\odot} - 1.6\,M_{\odot}$ range (this slope change also emerges in the τ vs T_{eff} relation at $\log T_{eff} \approx 3.75$, see Fig. 5). This is because of the steep τ decrease during final PMS contraction stages, just before arriving at the zero-age main sequence. Consequently, considering the mass range of our stellar sample, we preferred to use the Ventura et al. models to derive τ , since they provide a better coverage of this mass range.

We examined whether and how the method employed to estimate τ , based on the position of each star in the HR diagram, affects the results. We performed different τ estimations, using a 13 Myr isochrone, and inferring τ from the T_{eff} or L_{bol} only. Both these estimates rely on assuming that all the stars are exactly coeval, and basing the τ estimation on only one stellar parameter. With these different τ derivation techniques the *Ro* vs R_X correlation search provides exactly the same results: a significant negative correlation for large *Ro* (the non-saturation regime), and no significant correlation for low *Ro*.

This comparison between models and methods demonstrates that they are all similar and that a specific choice of model and/or method does not significantly affect the inferred τ. Available evolutionary models are known to have mass-dependent systematic uncertainties (Hillenbrand et al. 2008), and hence possibly future model improvements might change our understanding of the R_X vs *Ro* correlation in PMS stars. We are confident that our analysis, performed on different mass bins, minimizes the effect of these possible systematic errors on the obtained results.

We also considered the random uncertainties on *Ro*, and in particular whether these errors, being larger than that on P_{rot}, could hide an underlying correlation. We evaluated that even if some stars have very large uncertainties, the average *Ro* error in the different mass bins is significantly smaller than the *Ro* range we explored. This suggests that random uncertainties are not large enough to completely bury a correlation, if present.

These checks and considerations indicate that the obtained results, and in particular the absence of any positive correlation between *Ro* and R_X in the low *Ro* range, which is at odds with that observed between P_{rot} and L_X, appears to be independent of systematic and/or random uncertainties in the inferred *Ro*. Therefore the positive correlation between activity and rotation occurring for fast rotators with $1.0\,M_{\odot} < M < 1.4\,M_{\odot}$, a pattern analogous to the supersaturation phenomenon, appears to be related to the stellar rotational period and not to the Rossby number.

5. Discussion

The stellar sample composed of 414 h Per members offered us the possibility of investigating correlations between activity and rotation in stars at 13 Myr. The first result we obtained is that h Per members, depending on mass, show relations between activity, probed by L_X, and rotation. In particular, inspecting the L_X vs P_{rot} space, we found a positive correlation for $P_{rot} \lesssim 1$ d for masses ranging between $1.0\,M_{\odot}$ and $1.4\,M_{\odot}$, while we found a negative correlation between L_X and P_{rot} for long P_{rot} for $0.7\,M_{\odot} < M < 1.4\,M_{\odot}$. Conversely, for lower mass stars ($M_{\star} < 0.7\,M_{\odot}$) we did not observe correlations between L_X and P_{rot}, with L_X displaying a significant scatter, and being compatible with a constant value, regardless of P_{rot}.

In the R_X and *Ro* space no clear relations were observed when we separately considered the different mass bins, with only one exception of a negative correlation in the $1.2 - 1.4\,M_{\odot}$ bin. This negative correlation also emerges significantly when all the $M_{\star} > 1.0\,M_{\odot}$ stars are considered, over the *Ro* range expected for non-saturated regime. No evidence of positive correlations is present in the R_X vs *Ro*, regardless of mass and *Ro* range. Here we discuss whether and how these observed trends are reconcilable to the supersaturated, saturated, and non-saturated regimes that are observed for MS stars, and what can be inferred, from this comparison, about the coronal properties of intermediate-age PMS stars.

5.1. Saturation and non-saturation

h Per stars show clear evidence of a negative correlation between $\log L_X$ and $\log P_{rot}$ for stars with $0.7\,M_{\odot} < M_{\star} < 1.4\,M_{\odot}$ and for long rotational periods. This negative correlation is contiguous (for $1.0\,M_{\odot} < M_{\star} < 1.4\,M_{\odot}$) to the positive correlation observed instead for $P_{rot} \lesssim 1$ d. The fact that these correlations are adjacent indicates that there is no clear evidence of an intermediate behavior between them. We interpret this observed negative correlation as the average effect due to the fact that stars with $1\,\mathrm{d} \lesssim P_{rot} \lesssim 10\,\mathrm{d}$ are mainly in the saturated regime, with only some of the slowest rotators being located in the non-saturated regime, and hence having a slightly lower L_X that provides the global negative correlation. This interpretation is also

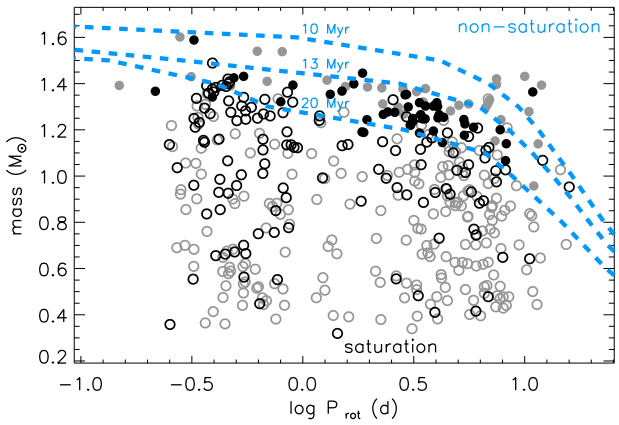

Fig. 10. Mass vs period of X-ray selected h Per members detected (black) and non-detected (gray) in X-rays. Filled and open symbols indicate non-saturated and saturated or supersaturated stars. The blue dashed line marks the expected separation between non-saturation and saturation ($Ro = 0.04$) at different ages, as labeled in the plot.

supported by the inspection of the R_X vs Ro space, where we found that stars with $M_\star > 1.0\,M_\odot$ whose Ro correspond to the non-saturated regime indeed display a significant negative correlation.

The fact that we found h Per members in the non-saturated regime apparently contradicts what was inferred from the mass vs P_{rot} scatter plot and the predicted thresholds between the different regimes (Fig. 7). The predicted edge between saturated and non-saturated regimes (the blue dashed line in Fig. 7) places almost all the h Per members in the saturated regime. However, the position of this threshold is uncertain. This threshold is highly sensitive to stellar age: a slightly older age would bring a significant fraction of stars into the non-saturated regime, as shown in Fig. 10. The Rossby number estimate for each h Per member, obtained taking into account possible age spread, provided several stars with $\log Ro$ larger than the limiting value for saturation ($Ro = 0.04$, these stars are indicated with filled circles in Fig. 10). Moreover, it may be inappropriate to assume that the threshold for intermediate-age PMS stars is the same as that for MS stars.

We finally note that all the negative correlations obtained show slopes significantly shallower than that observed for the non-saturated pattern in MS stars (i.e., ~ -2 or ~ -2.7, Pizzolato et al. 2003; Wright et al. 2011). However, no separation between saturation and non-saturation in our sample is evident, and hence the slope determination is likely affected by partial inclusion of a few saturated stars. Moreover, our survey, being an X-ray limited survey, only allowed us to detect the most active stars in the non-saturated regime. This means that we probe only the upper envelope of the R_X vs Ro parameter space, which in turn implies a highly uncertain estimate of the slope.

5.2. Supersaturation

h Per, thanks to its age, is well populated by very fast rotating stars. This makes it a unique benchmark to probe the supersaturated regime. Considering separately stars with different mass, we found clear evidence of a positive correlation between $\log L_X$ and $\log P_{rot}$ for stars with $1.0\,M_\odot < M_\star < 1.2\,M_\odot$ and $1.2\,M_\odot < M_\star < 1.4\,M_\odot$, and for periods shorter than ~ 1 d. The slopes in the two cases are 0.60 ± 0.16 and 0.86 ± 0.22, respectively. This pattern is compatible with the supersaturation behavior. Moreover, we observed that the activity level in this regime is better described by the rotational period than by the Rossby number: we did not observe any significant correlation, analogous to the supersaturation, between R_X and Ro, either by separating stars according to mass or considering the whole sample. As already discussed in Sect. 2.3.5 and 4, we note that this finding is model dependent, but this result strongly suggests that supersaturation is unrelated to the dynamo efficiency, in contrast to the non-saturated and saturated regimes. Therefore the dynamo-related mechanisms, which consider dynamo feedback effects and suggest that induced magnetic fields could reduce differential rotation and hence the efficiency of the dynamo itself (e.g., Kichatinov & Rudiger 1993; Rempel 2006), are very likely not responsible for supersaturation. The mechanism causing supersaturation has to be searched for among those related to other mechanisms, such as centrifugal stripping or polar updraft migration. Here we discuss our results by comparing them with predictions and indicators that can be deduced from these two mechanisms.

5.2.1. Centrifugal stripping

The centrifugal stripping mechanism predicts that in rapidly rotating stars the coronal emission is reduced because the co-rotation radius R_{cor}, and hence the volume within the co-rotation radius that is the one available for stable coronal structures, decreases (Jardine & Unruh 1999; Jardine 2004). To try to quantify how, in the centrifugal stripping scenario, L_X decreases for increasing rotational velocity, we assumed that L_X scales as the available volume and computed the available coronal volume for increasing rotational velocity (i.e., decreasing rotational period). Therefore we set

$$L_X = L_{X0}\frac{V_{red}}{V_0}$$

where V_0 is the coronal volume of a slowly rotating star that is not affected by centrifugal stripping, V_{red} indicates the reduced coronal volume, and L_{X0} is the X-ray luminosity corresponding to the saturated level. We assumed that the coronal volume of a slowly rotating star is a sphere shell extending from the stellar surface up to λ stellar radii above it. Jardine & Unruh (1999) computed the volume available for the corona, when both magnetic fields and centrifugal forces are taken into account. For an aligned quadrupolar magnetic field[5] they found that undisturbed corona extends up to the surface defined by

$$r = R_{co-rot}\left(\frac{3\cos^2\theta - 1}{\sin^2\theta\,(5\cos^2\theta - 1)}\right)^{1/3}$$

where θ is the stellar colatitude, and R_{co-rot} is the co-rotation radius,

$$R_{co-rot} = \left(\frac{GM_\star P_{rot}^2}{(2\pi)^2}\right)^{1/3}$$

[5] We considered a quadrupolar magnetic field since young stars usually have complex multipolar fields (Hussain et al. 2007; Gregory et al. 2008; Donati & Landstreet 2009, e.g.), however, even considering the dipole case provided by Jardine & Unruh (1999), the results are very similar.

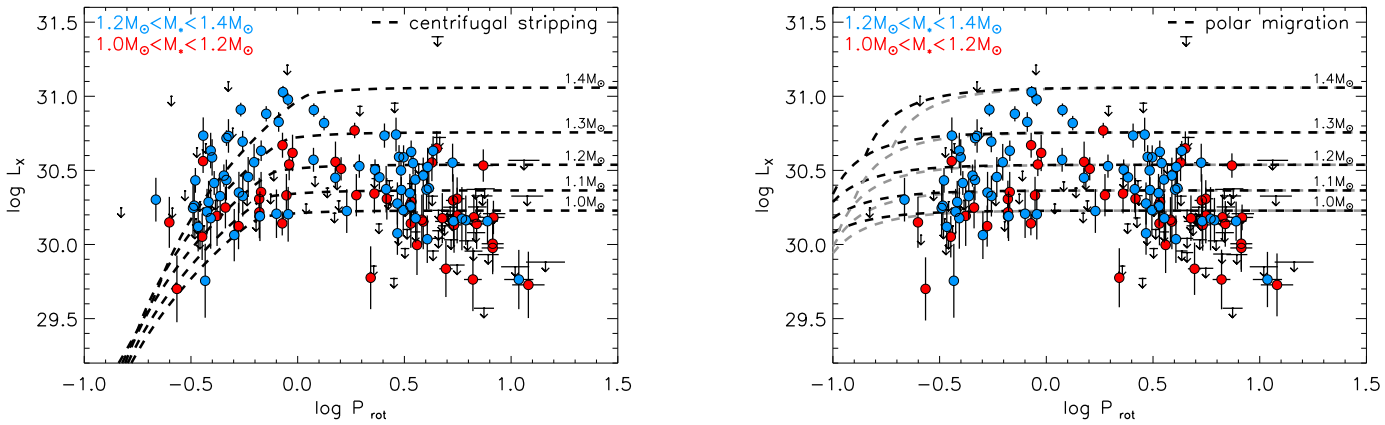

Fig. 11. X-ray luminosity vs rotational period for h Per members, with masses ranging between 1.2 and 1.4 $M_\odot$ (blue), and 1.0 and 1.2 $M_\odot$ (red), compared with supersaturation behavior predicted from centrifugal stripping models (*left panel*) or polar updraft migration models (*right panel*), obtained considering different stellar masses (dashed gray lines in the *right panel* are computed assuming that the radiative core has a 30% higher rotation than the convective envelope).

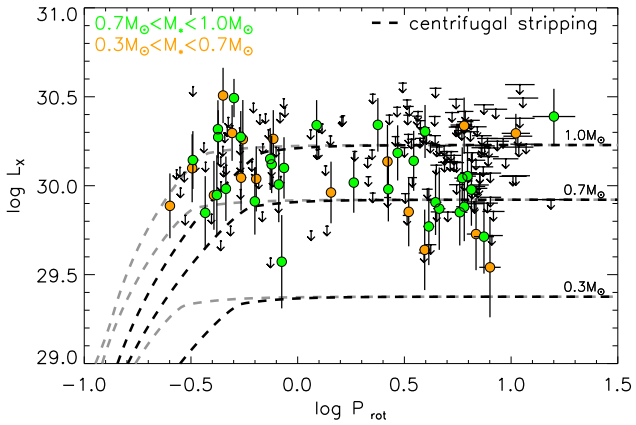

Fig. 12. X-ray luminosity vs rotational period for h Per members, with masses ranging between 0.7 and 1.0 $M_\odot$ (green), and 0.3 and 0.7 $M_\odot$ (orange), compared with supersaturation behavior predicted by centrifugal stripping models (dashed gray and black lines are computed assuming that the coronal extends up to 1 $R_\star$ and 2 $R_\star$ over the stellar surface).

We computed the available volume, $V_{\rm red}$, at each rotational period, as the intersection of the volume delimited by this surface with the sphere shell describing the coronal volume of a slowly rotating star.

The predicted curves obtained are shown in the left panel of Fig. 11, where we set $L_{\rm X0}$ as 10^{-3} with respect to the stellar bolometric luminosity, and V_0 as the volume corresponding to a sphere shell extending from the stellar surface up to two stellar radii above it (i.e., $\lambda = 2$). For each stellar mass we assumed for the stellar radius the value predicted by Siess et al. (2000) at an age of 13 Myr. We note that the value assumed for $L_{\rm X0}$ determines the vertical position of the predicted curves, while the value of V_0 determines at which rotational period the coronal stripping starts to occur (i.e., the lower V_0 the shorter the $P_{\rm rot}$ needed to have centrifugal stripping). Finally, we note that we focused here on saturation and supersaturation patterns, hence any prediction will include only these behaviors, and therefore we compare models and data in the short period range, that is, $P_{\rm rot} \lesssim 1$ d.

These predicted curves agree quite well with observed data. In particular, the predicted slopes between $\log L_{\rm X}$ and $\log P_{\rm rot}$, which vary between 1.7 and 1.0 for $-0.5 < \log P_{\rm rot} < 0$, are similar to the observed curves. This comparison indicates that despite the simplified assumptions made to compute the predicted $L_{\rm X}$, centrifugal stripping could be the mechanism responsible for the supersaturation. In this scenario the observed threshold of $P_{\rm rot} \sim 1$ d at which the supersaturation occurs, suggests that in 1.0 – 1.4 $M_\odot$ stars at 13 Myr age, coronal structures extend up to $\sim 2\,R_\star$ above the stellar surface. This value for coronal dimensions agrees with the value inferred by Wright et al. (2011), which was obtained by studying supersaturation in G-type and K-type MS stars. Moreover, both the analysis of flaring structures (Getman et al. 2008; Argiroffi et al. 2011) and the extrapolation coronal structures from magnetic maps (Johnstone et al. 2014) in PMS stars indicated that coronae can also have structures extending up to several stellar radii, which means that they are susceptible to coronal stripping.

We did not detect any supersaturation in the low-mass stars included in our sample, whose X-ray luminosities remained constant down to $P_{\rm rot} \sim 0.3$ d. We show in Fig. 12 the observed $L_{\rm X}$ vs $P_{\rm rot}$ scatter plot for stars with $M < 1.0\,M_\odot$, compared to predictions based on centrifugal stripping. This comparison indicates that centrifugal stripping was expected to occur for the most rapid rotators of our sample. We stress that in this mass range the completeness of our survey is too low (a few percent) and that we detected only the most active fraction of stars, therefore we cannot state that predictions and observation disagree. However, we could speculate that the dimensions of coronal structures in these stars might be smaller than that of solar-like mass stars. In this case, the $P_{\rm rot}$ threshold for centrifugal stripping should decrease (as shown by the gray dashed lines in Fig. 12, obtained by assuming coronal dimension of 1 $R_\star$).

With this further assumption all of our data become consistent with predictions based on centrifugal stripping. The hypothesis that centrifugal stripping is the mechanism responsible for supersaturation is also supported by the fact that supersaturation does not seem to be related to a reduced coverage of stellar surface by magnetically active regions, in fact, no evidence of supersaturation has been observed in chromospheric emission (Marsden et al. 2009; Christian et al. 2011). We finally note that depending on stellar mass and age, the hypothesis that supersaturation is caused by coronal stripping implies that fast rotators of different masses in the $R_{\rm X}$ vs *Ro* space settle on different tracks, and this can contribute to the observed spread.

5.2.2. Polar updraft migration

The alternative mechanism proposed to explain supersaturation, independent of the dynamo efficiency, is the polar updraft migration proposed by Stępień et al. (2001). This theory predicts that at high rotational velocity active regions preferentially concentrate near stellar poles, leaving the equatorial region free from magnetic structures and coronal plasma, reducing the filling factor, and hence decreasing the X-ray emission. This polar updraft migration is assumed to be caused by the non-uniform heating that at high rotational velocity characterizes the base of the convective envelope. The emerging energy flux F in the radiative core is proportional to the local effective gravitational acceleration $g_{\rm eff}$ (the von Zeipel theorem). In rapidly rotating stars, $g_{\rm eff}$ changes significantly with stellar latitude, it is lowest at the equator and highest at the poles. Hence the subsequent non-uniform heating at the base of the convective envelope might favor a magnetic field emergence higher near the stellar poles than in equatorial regions. This polar concentration might also be amplified by the Coriolis force, which tends to deflect the plasma rising across the stellar convective envelope and the frozen magnetic flux tubes toward the stellar poles (Solanki et al. 1997), even if the effect due to the Coriolis force has been predicted to be negligible with respect to the non-uniform heating at the base of the convective envelope (Stępień et al. 2001).

Starting from this supersaturation mechanism proposed by Stępień et al. (2001), we computed the expected variation in X-ray coronal emission with stellar rotation. Indicating with θ the stellar colatitude, then the local effective gravitational acceleration $g_{\rm eff}$ at the base of the convective envelope is

$$g_{\rm eff}(\theta) = g\left(1 - \frac{\omega^2 R_{\rm core}\sin^2\theta}{g}\right)$$

where $g = GM_{\rm core}/R^2_{\rm core}$ is the gravitational acceleration at the base of the convective envelope and $M_{\rm core}$ and $R_{\rm core}$ are the mass and radius of the inner radiative core. Considering that the energy flux at the base of the convective envelope $F(\theta)$ is proportional to $g_{\rm eff}(\theta)$, then the energy flux emerging through the convective envelope is expected to scale as $g^{\alpha}_{\rm eff}(\theta)$, with α being related to the dimension of the convective envelope (with $\alpha \sim 0.3$ for deep envelopes and $\alpha \sim 1$ for shallow envelopes, Stępień et al. 2001). We assumed that the magnetic field emergence, and hence the local X-ray luminosity of coronal plasma, has the same dependence on stellar colatitude θ as $g^{\alpha}_{\rm eff}$. Therefore, from integrating over the whole stellar surface, the $L_{\rm X}$ should follow the relation

$$L_{\rm X} = L_{\rm X0}\frac{1}{4\pi}\int_0^{\pi}\left(1 - \frac{\omega^2 R_{\rm core}\sin^2\theta}{g}\right)^{\alpha} 2\pi\sin\theta\,{\rm d}\theta$$

where $L_{\rm X0}$ is again the saturated X-ray luminosity, which we assumed to be 10^{-3} with respect to $L_{\rm bol}$. We assumed for $M_{\rm core}$ and $R_{\rm core}$ the values predicted by Siess et al. (2000) at an age of 13 Myr. In the right panel of Fig. 11 we show the comparison between this predicted relations and the observed values, with $\alpha = 1$ (a lower value for α would provide a shallower decrease of L_X for increasing rotational velocity). From this plot we observe that in the predicted patterns $L_{\rm X}$ starts to reduce for $P_{\rm rot} \lesssim 0.2$ d, while the data clearly suggest that supersaturation starts to become effective for significantly higher $P_{\rm rot}$ (i.e. $P_{\rm rot} \sim 1$ d).

Evolution of stellar rotation predicts that the radiative core and the convective envelopes should have different rotation, with the inner radiative core rotating faster (e.g., MacGregor & Brenner 1991; Gallet & Bouvier 2013). We considered the hypothesis that the radiative core rotates faster by 30% than the convective envelope, as suggested by rotational evolutionary models of Gallet & Bouvier (2013). The predicted patterns obtained (gray dashed lines in the right panel of Fig. 11) indicate again that supersaturation caused by poleward migration occurs at $P_{\rm rot}$ shorter than that observed. To reconcile this discrepancy, a core rotational velocity higher by a factor $\sim 2-3$ than that of the convective envelope has to be assumed. The other possibility is that the polar updraft migration of active regions should act in a more efficient way at $P_{\rm rot} \sim 0.5 - 1$ d to be able to explain the observed supersaturation of the X-ray luminosity. There is another quite strong evidence against polar updraft migration as the mechanism responsible for supersaturation. The poleward shift of magnetic flux tubes, and hence of active regions, would reduce the surface filling factor of magnetically active regions, but chromospheric activity indicators do not show any evidence of supersaturation (Marsden et al. 2009; Christian et al. 2011), indicating that the surface of supersaturated stars, in comparison to that of saturated stars, is probably not depleted of active regions.

5.3. Comparison with results obtained for younger or older stars

With its evidence of non-saturation, saturation, and supersaturation, h Per is the youngest cluster for which all the activity-rotation patterns have been observed. At an age of 13 Myr, the stellar activity therefore starts to resemble that observed for MS stars and is usually interpreted as the manifestation of the $\alpha\Omega$ type dynamo. There are two main differences between h Per members and younger stars: the internal structures, and the accretion status.

For the stellar internal structures, at an age of 13 Myr all stars with $M_\star > 0.5\,M_\odot$ have already developed an inner radiative core, and the core contains more than half of the stellar mass for stars with $M_\star > 1.0\,M_\odot$. At this age the internal structures are therefore analogous to those of MS stars, and in particular the $\alpha\Omega$ dynamo, which originates in the shell at the base of the convective envelope, can commence. Conversely, at an age of $1-3$ Myr (the typical ages of very young PMS stars previously inspected), stars with $1.0\,M_\odot < M_\star < 1.4\,M_\odot$ are fully convective, or (depending on mass and age) have the convective envelope overwhelm the stellar structure in terms of mass and volume, which means that the internal structure is different from that of MS stars. It is conceivable that in these very young stars the $\alpha\Omega$ dynamo efficiency is low because the base of the convective envelope is buried very deeply in the stellar interior. Hence other dynamo mechanisms, like the turbulent dynamo (e.g., Durney et al. 1993; Chabrier & Küker 2006) likely dominate. The coronal activity of very young stars is therefore very likely regulated by a different dynamo mechanism.

Compared with very young stars, h Per members also differ significantly because, at 13 Myr, they have already finished their accretion phase. Stars at a few Myr instead continue to accrete mass from their circumstellar disk. There are several pieces of evidence that the X-ray emission of accreting stars is significantly different from that of non-accreting stars: accreting stars on average show hotter coronal plasma, lower X-ray luminosity, and a higher variability (e.g., Tsujimoto et al. 2002; Stassun et al. 2004; Telleschi et al. 2007; Flaccomio et al. 2012). Several mechanisms have been proposed to explain the effect of accretion on coronal activity (e.g., Kastner et al. 2002; Telleschi et al. 2007; Brickhouse et al. 2010). However,

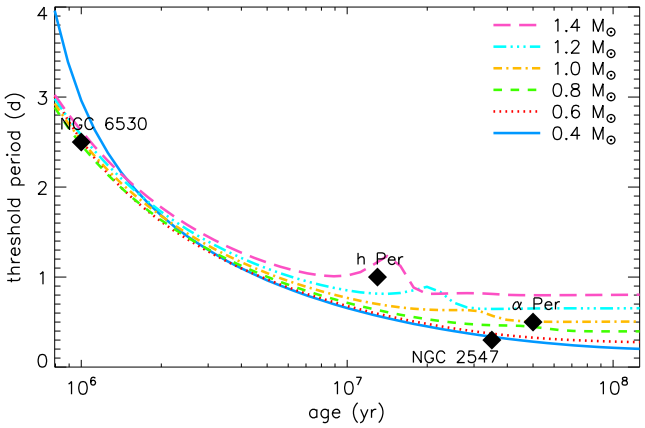

Fig. 13. Threshold value of $P_{\rm rot}$ for centrifugal stripping vs stellar age. These threshold values are computed assuming the Siess et al. (2000) evolutionary models and that coronal structures extend up to 2 stellar radii above the stellar photosphere.

this question is highly debated because the observed differences in the coronal emission of accreting and non-accreting stars could be explained in terms of different absorption suffered by the coronal emission (Flaccomio et al. 2010, 2012). It is worth noting that even considering only very young stars with no accretion, the activity-rotation pattern in very young stars is unclear (e.g., Preibisch et al. 2005). Therefore, even if accretion could affect magnetic activity of very young stars, it is probably not the cause of the observed difference of activity behavior between very young PMS and MS stars.

Assuming that centrifugal stripping is the mechanism causing supersaturation has important consequences when the results obtained from h Per are extrapolated to younger or older stars. We expect that the $P_{\rm rot}$ for which centrifugal stripping occurs has to change with stellar age. PMS stars, evolving toward the MS phase, reduce their radii significantly. This does not change the co-rotation radius, that depends only on stellar mass and rotational period. However, radius contraction changes the location of the stellar surface, and hence of the corona, which on average approaches the stellar rotational axis. Assuming that coronal dimensions scale as the stellar radius and indicating with λ the length of the largest coronal structures in units of stellar radii, centrifugal stripping becomes increasingly stronger for periods below the critical threshold of

$$P_{\rm rot} = 2\pi \sqrt{\frac{[(\lambda+1)R_\star]^3}{GM_\star}}$$

with $M_\star$ and $R_\star$ being stellar mass and radius. Therefore, since $R_\star$ decreases during PMS evolution, shorter $P_{\rm rot}$ are needed for centrifugal stripping and hence supersaturation when stars contract. We show in Fig. 13 the variation of this threshold period with stellar age for stars of different mass, assuming in all cases $\lambda = 2$ during the entire PMS evolution. In addition to h Per, hints of supersaturation were observed in a few clusters, and threshold periods were reported. In particular, Henderson & Stassun (2012), investigating a sample of $0.3 - 1.5\,M_\odot$ stars belonging to the NGC 6530 cluster (~ 1 Myr), found evidence of supersaturation for $P_{\rm rot} < 2.5$ d; Jeffries et al. (2011) concluded that supersaturation occurs only for $P_{\rm rot} < 0.3$ d, considering a sample of $0.55 - 0.95\,M_\odot$ stars of NGC 2547 (~ 35 Myr); the oldest cluster (α Per, age ~ 50 Myr) was reported by Randich et al. (1996), who observed supersaturation only for G and K-type stars with $P_{\rm rot} < 0.5$ d. We report these observed thresholds in Fig. 13, concluding that they perfectly fit predictions based on centrifugal stripping. This agreement might also suggest that young stars are able to produce significant amounts of coronal structures with lengths of up to $\sim 2\,R_\star$ during their entire PMS evolution, that is, from 1 to 50 Myr.

6. Conclusions

We studied the activity-rotation relation in the young cluster h Per, a ~ 13 Myr old cluster. This allowed us to investigate the processes in intermediate-age PMS stars, which, thanks to their age, show both fast and slow rotators, have completed the accretion process, and have developed an internal structure composed of an inner radiative core and an outer convective envelope.

We found that solar-like ($1.0\,M_\odot < M_\star < 1.4\,M_\odot$) h Per members show different activity regimes, analogous to that observed in MS stars. This result makes h Per the youngest cluster showing activity-rotation regimes. In particular, we clearly detected the supersaturation phenomenon for fast rotators, while slower rotators appear to be in the saturated or non-saturated regimes. Therefore when PMS stars develop a significant radiative core, their magnetic field production is most likely regulated by the $\alpha\Omega$ type dynamo, as occurs for MS stars.

The large numbers of fast rotating h Per members allowed us to investigate the supersaturation phenomenon. We observed that supersaturation is better described by $P_{\rm rot}$ than Ro. Therefore the supersaturation phenomenon, at odds with other activity regimes that depend on the Rossby number, is not due to feedback effects that might inhibit the dynamo efficiency. Specifically, the observed patterns in the supersaturation regime strongly suggest that in fast rotators coronal emission is reduced because of centrifugal stripping, and that coronal structures have dimensions as large as $\sim 2\,R_\star$ above the stellar surface. Moreover, the centrifugal stripping mechanism perfectly reproduces the observed evolution of the $P_{\rm rot}$ threshold for supersaturation with stellar age.

Acknowledgements. The scientific results reported in this paper are based on observations made by the *Chandra X-ray Observatory*.

References

Alexander, F. & Preibisch, T. 2012, A&A, 539, A64
Argiroffi, C., Favata, F., Flaccomio, E., et al. 2006, A&A, 459, 199
Argiroffi, C., Flaccomio, E., Bouvier, J., et al. 2011, A&A, 530, A1
Berdyugina, S. V. 2005, Living Reviews in Solar Physics, 2, 8
Brickhouse, N. S., Cranmer, S. R., Dupree, A. K., Luna, G. J. M., & Wolk, S. 2010, ApJ, 710, 1835
Briggs, K. R., Güdel, M., Telleschi, A., et al. 2007, A&A, 468, 413
Burningham, B., Naylor, T., Littlefair, S. P., & Jeffries, R. D. 2005, MNRAS, 363, 1389
Chabrier, G. & Küker, M. 2006, A&A, 446, 1027
Christian, D. J., Mathioudakis, M., Arias, T., Jardine, M., & Jess, D. B. 2011, ApJ, 738, 164
Currie, T., Hernandez, J., Irwin, J., et al. 2010, ApJS, 186, 191
Damiani, F., Maggio, A., Micela, G., & Sciortino, S. 1997a, ApJ, 483, 350
Damiani, F., Maggio, A., Micela, G., & Sciortino, S. 1997b, ApJ, 483, 370
Dobson, A. K. & Radick, R. R. 1989, ApJ, 344, 907
Donati, J.-F. & Landstreet, J. D. 2009, ARA&A, 47, 333
Durney, B. R., De Young, D. S., & Roxburgh, I. W. 1993, Sol. Phys., 145, 207
Favata, F. & Micela, G. 2003, Space Sci. Rev., 108, 577
Feigelson, E. D., Gaffney, III, J. A., Garmire, G., Hillenbrand, L. A., & Townsley, L. 2003, ApJ, 584, 911
Flaccomio, E., Micela, G., Favata, F., & Alencar, S. P. H. 2010, A&A, 516, L8
Flaccomio, E., Micela, G., Pizzolato, N., Sciortino, S., & Ventura, P. 2004, in IAU Symposium, Vol. 215, Stellar Rotation, ed. A. Maeder & P. Eenens, 429

Flaccomio, E., Micela, G., & Sciortino, S. 2003, A&A, 397, 611
Flaccomio, E., Micela, G., & Sciortino, S. 2012, A&A, 548, A85
Gallet, F. & Bouvier, J. 2013, A&A, 556, A36
Getman, K. V., Feigelson, E. D., Micela, G., et al. 2008, ApJ, 688, 437
Gregory, S. G., Matt, S. P., Donati, J.-F., & Jardine, M. 2008, MNRAS, 389, 1839
Güdel, M. 2004, A&A Rev., 12, 71
Güver, T. & Özel, F. 2009, MNRAS, 400, 2050
Henderson, C. B. & Stassun, K. G. 2012, ApJ, 747, 51
Hillenbrand, L. A., Bauermeister, A., & White, R. J. 2008, in Astronomical Society of the Pacific Conference Series, Vol. 384, 14th Cambridge Workshop on Cool Stars, Stellar Systems, and the Sun, ed. G. van Belle, 200
Hussain, G. A. J., Jardine, M., Donati, J.-F., et al. 2007, MNRAS, 377, 1488
Isobe, T. & Feigelson, E. D. 1990, in Bulletin of the American Astronomical Society, Vol. 22, Bulletin of the American Astronomical Society, 917–918
Isobe, T., Feigelson, E. D., & Nelson, P. I. 1986, ApJ, 306, 490
James, D. J., Jardine, M. M., Jeffries, R. D., et al. 2000, MNRAS, 318, 1217
Jardine, M. 2004, A&A, 414, L5
Jardine, M. & Unruh, Y. C. 1999, A&A, 346, 883
Jeffries, R. D., Jackson, R. J., Briggs, K. R., Evans, P. A., & Pye, J. P. 2011, MNRAS, 411, 2099
Johnstone, C. P., Jardine, M., Gregory, S. G., Donati, J.-F., & Hussain, G. 2014, MNRAS, 437, 3202
Kastner, J. H., Huenemoerder, D. P., Schulz, N. S., Canizares, C. R., & Weintraub, D. A. 2002, ApJ, 567, 434
Kenyon, S. J. & Hartmann, L. 1995, ApJS, 101, 117
Kővári, Z. & Oláh, K. 2014, Space Sci. Rev., 186, 457
Kichatinov, L. L. & Rudiger, G. 1993, A&A, 276, 96
Landin, N. R., Mendes, L. T. S., & Vaz, L. P. R. 2010, A&A, 510, A46
Lavalley, M. P., Isobe, T., & Feigelson, E. D. 1992, in Bulletin of the American Astronomical Society, Vol. 24, Bulletin of the American Astronomical Society, 839–840
MacGregor, K. B. & Brenner, M. 1991, ApJ, 376, 204
Marsden, S. C., Carter, B. D., & Donati, J.-F. 2009, MNRAS, 399, 888
Moraux, E., Artemenko, S., Bouvier, J., et al. 2013, A&A, 560, A13
Noyes, R. W., Hartmann, L. W., Baliunas, S. L., Duncan, D. K., & Vaughan, A. H. 1984, ApJ, 279, 763
Pallavicini, R., Golub, L., Rosner, R., et al. 1981, ApJ, 248, 279
Parker, E. N. 1955, ApJ, 122, 293
Pizzolato, N., Maggio, A., Micela, G., Sciortino, S., & Ventura, P. 2003, A&A, 397, 147
Preibisch, T., Kim, Y.-C., Favata, F., et al. 2005, ApJS, 160, 401
Prosser, C. F., Randich, S., Stauffer, J. R., Schmitt, J. H. M. M., & Simon, T. 1996, AJ, 112, 1570
Randich, S., Schmitt, J. H. M. M., Prosser, C. F., & Stauffer, J. R. 1996, A&A, 305, 785
Rebull, L. M., Stauffer, J. R., Ramirez, S. V., et al. 2006, AJ, 131, 2934
Rempel, M. 2006, ApJ, 647, 662
Siess, L., Dufour, E., & Forestini, M. 2000, A&A, 358, 593
Skumanich, A. 1972, ApJ, 171, 565
Solanki, S. K., Motamen, S., & Keppens, R. 1997, A&A, 324, 943
Spiegel, E. A. & Weiss, N. O. 1980, Nature, 287, 616
Stassun, K. G., Ardila, D. R., Barsony, M., Basri, G., & Mathieu, R. D. 2004, AJ, 127, 3537
Stępień, K., Schmitt, J. H. M. M., & Voges, W. 2001, A&A, 370, 157
Telleschi, A., Güdel, M., Briggs, K. R., Audard, M., & Palla, F. 2007, A&A, 468, 425
Tsujimoto, M., Koyama, K., Tsuboi, Y., Goto, M., & Kobayashi, N. 2002, ApJ, 566, 974
Ventura, P., Zeppieri, A., Mazzitelli, I., & D'Antona, F. 1998, A&A, 334, 953
Wright, N. J., Drake, J. J., Mamajek, E. E., & Henry, G. W. 2011, ApJ, 743, 48

Table 1. X-ray source detected in the CHANDRA/ACIS-I observations of h Per.

X source ID	RA (J2000)	DEC (J2000)	Pos. err. (″)	Count rate (10^{-5} cts s^{-1})	Flux (10^{-8} ph s^{-1} cm^{-2})
1	2:17:51.46	57:10:01.9	2.9	35.6 ± 11	107.0 ± 33
2	2:17:51.48	57:11:50.2	5.1	76.5 ± 20	229.6 ± 60
3	2:17:52.84	57:09:40.5	3.9	50.4 ± 14	151.3 ± 42
4	2:17:55.81	57:13:07.0	4.5	34.9 ± 12	104.8 ± 37
5	2:17:59.17	57:04:42.3	3.1	24.9 ± 8	74.8 ± 24
6	2:18:0 0.52	57:04:16.1	1.8	49.4 ± 8	148.3 ± 25
7	2:18:0 1.97	57:11:42.7	6.0	46.0 ± 15	138.1 ± 44
8	2:18:0 2.42	57:08:45.3	2.3	52.0 ± 9	156.3 ± 26
9	2:18:0 3.12	57:04:35.5	2.6	36.9 ± 10	111.0 ± 30
10	2:18:0 3.09	57:06:36.4	2.4	48.1 ± 9	144.6 ± 27
11	2:18:0 4.11	57:07:15.3	1.7	13.7 ± 5	41.0 ± 15
12	2:18:0 5.23	57:11:16.5	4.1	29.9 ± 9	89.9 ± 27
13	2:18:0 5.80	57:05:58.6	1.7	17.0 ± 7	50.9 ± 21
14	2:18:0 7.17	57:06:40.4	1.3	9.8 ± 4	29.4 ± 13
15	2:18:0 7.40	57:01:59.7	1.9	112.1 ± 12	336.8 ± 35
16	2:18:0 7.78	57:02:48.7	1.9	87.3 ± 10	262.1 ± 31
17	2:18:0 7.62	57:12:27.2	2.4	42.2 ± 8	126.7 ± 24
18	2:18:0 8.16	57:05:02.4	1.2	481.0 ± 21	1444.5 ± 62
19	2:18:0 8.60	57:11:14.1	1.3	29.3 ± 6	88.1 ± 17
20	2:18:0 9.08	57:01:21.0	2.4	17.4 ± 7	52.3 ± 20
21	2:18:0 9.02	57:04:50.8	1.4	8.6 ± 4	25.7 ± 13
22	2:18:0 9.15	57:02:26.5	1.8	12.4 ± 6	37.3 ± 19
23	2:18:0 9.05	57:07:01.3	3.1	18.9 ± 6	56.7 ± 19
24	2:18:0 9.36	57:03:22.8	3.0	25.9 ± 8	77.8 ± 25
25	2:18:10.22	57:07:53.6	3.2	18.8 ± 6	56.4 ± 19
26	2:18:10.63	57:00:40.5	2.8	34.4 ± 10	103.4 ± 31
27	2:18:11.37	57:12:26.3	3.0	25.2 ± 8	75.8 ± 24
28	2:18:11.78	57:10:33.2	2.4	37.8 ± 7	113.6 ± 21
29	2:18:12.37	57:03:56.1	1.3	10.1 ± 4	30.3 ± 13
30	2:18:12.27	57:11:05.6	1.8	105.4 ± 10	316.4 ± 30
31	2:18:12.65	57:13:22.0	1.7	145.3 ± 13	436.4 ± 38
32	2:18:13.44	57:00:26.9	2.6	18.8 ± 9	56.4 ± 27
33	2:18:13.88	57:03:17.8	1.3	10.8 ± 4	32.6 ± 13
34	2:18:14.30	57:01:48.7	2.7	35.9 ± 10	107.8 ± 30
35	2:18:14.38	57:14:36.4	2.3	22.2 ± 8	66.6 ± 25
36	2:18:14.54	57:09:31.5	1.2	40.8 ± 6	122.5 ± 19
37	2:18:14.78	56:59:56.9	2.4	53.4 ± 10	160.4 ± 29
38	2:18:14.71	57:08:13.1	1.3	10.0 ± 4	30.1 ± 12
39	2:18:14.80	57:03:60.0	1.8	11.4 ± 4	34.3 ± 13
40	2:18:15.29	57:07:58.5	1.4	55.7 ± 7	167.2 ± 21
41	2:18:15.33	57:07:04.5	1.6	43.3 ± 11	130.1 ± 32
42	2:18:15.48	57:10:00.0	1.7	11.3 ± 4	33.9 ± 13
43	2:18:16.24	57:08:12.7	3.1	20.8 ± 7	62.3 ± 20
44	2:18:16.50	57:04:29.6	1.4	8.0 ± 5	24.2 ± 14
45	2:18:16.61	57:12:01.2	2.4	13.7 ± 5	41.2 ± 15
46	2:18:17.27	57:06:59.8	1.3	30.8 ± 5	92.4 ± 16
47	2:18:17.37	57:07:32.6	1.9	77.7 ± 8	233.2 ± 23
48	2:18:17.75	57:09:16.3	1.6	34.7 ± 6	104.2 ± 18
49	2:18:17.76	57:09:08.2	1.3	8.0 ± 3	24.0 ± 10
50	2:18:18.11	57:02:55.3	1.3	9.7 ± 5	29.2 ± 16
51	2:18:18.03	57:12:21.5	2.6	36.5 ± 10	109.7 ± 30
52	2:18:18.48	57:07:21.0	2.1	17.0 ± 5	50.9 ± 16
53	2:18:18.95	57:04:40.7	1.0	7.6 ± 4	23.0 ± 12
54	2:18:19.19	57:02:27.7	2.7	33.8 ± 10	101.5 ± 29
55	2:18:19.36	57:03:42.3	1.3	10.5 ± 5	31.4 ± 14
56	2:18:19.43	57:11:22.4	1.4	21.9 ± 7	65.6 ± 20
57	2:18:19.52	57:07:19.7	1.0	7.7 ± 4	23.0 ± 12
58	2:18:19.59	57:13:18.8	2.0	63.3 ± 8	190.1 ± 24
59	2:18:19.79	57:08:47.8	1.6	32.3 ± 5	97.1 ± 15
60	2:18:20.00	56:58:38.2	2.2	79.3 ± 12	238.0 ± 36
61	2:18:19.94	57:03:03.9	1.2	39.0 ± 6	117.1 ± 18
62	2:18:19.94	57:10:44.2	5.3	50.6 ± 14	151.9 ± 42
63	2:18:20.10	57:09:55.4	1.6	18.6 ± 6	55.8 ± 19
64	2:18:20.14	57:12:21.7	1.7	14.5 ± 6	43.4 ± 17
65	2:18:20.59	57:07:19.0	1.0	6.8 ± 4	20.6 ± 11
66	2:18:20.71	57:06:34.8	1.1	158.2 ± 11	475.2 ± 34
67	2:18:20.64	57:10:49.2	2.9	28.5 ± 9	85.6 ± 26
68	2:18:20.79	57:07:59.4	1.6	13.5 ± 5	40.6 ± 14
69	2:18:20.87	57:06:14.1	1.7	19.5 ± 8	58.5 ± 23
70	2:18:20.92	57:06:07.2	1.1	24.9 ± 8	74.7 ± 24
71	2:18:21.21	57:03:15.2	1.2	11.7 ± 5	35.0 ± 14
72	2:18:21.21	57:10:25.5	1.2	14.3 ± 6	43.1 ± 17
73	2:18:21.36	57:05:04.0	1.0	7.3 ± 4	22.0 ± 11
74	2:18:21.42	57:05:38.9	1.3	26.3 ± 5	79.0 ± 14
75	2:18:21.73	57:06:51.9	0.8	41.3 ± 7	123.9 ± 20
76	2:18:21.82	57:04:36.1	2.2	19.3 ± 6	58.1 ± 19
77	2:18:22.15	56:58:53.3	1.8	43.0 ± 8	129.2 ± 25
78	2:18:22.15	56:59:31.6	2.8	41.0 ± 12	123.2 ± 36
79	2:18:22.20	56:58:11.2	4.0	52.3 ± 15	157.1 ± 46
80	2:18:22.33	57:08:09.0	1.2	10.0 ± 4	30.2 ± 12
81	2:18:22.56	57:06:45.1	1.0	25.1 ± 7	75.2 ± 21
82	2:18:23.06	57:00:33.5	4.0	40.2 ± 12	120.8 ± 36
83	2:18:22.96	57:13:01.9	3.2	21.4 ± 7	64.2 ± 22

Table 1. continued.

X source ID	RA (J2000)	DEC (J2000)	Pos. err. (″)	Count rate (10^{-5} cts s^{-1})	Flux (10^{-8} ph s^{-1} cm^{-2})
84	2:18:23.03	57:10:57.1	1.7	13.0 ± 5	38.9 ± 14
85	2:18:23.09	57:07:15.3	0.8	15.9 ± 6	47.8 ± 17
86	2:18:23.10	57:07:02.9	1.2	14.1 ± 5	42.2 ± 15
87	2:18:23.31	57:06:47.1	0.9	30.8 ± 9	92.6 ± 27
88	2:18:23.59	57:07:29.6	1.3	10.2 ± 4	30.7 ± 12
89	2:18:23.95	57:03:27.9	0.9	9.9 ± 4	29.7 ± 11
90	2:18:24.02	57:07:55.2	2.2	15.8 ± 5	47.6 ± 16
91	2:18:24.18	57:06:06.1	1.7	11.2 ± 4	33.8 ± 13
92	2:18:24.20	57:07:25.6	0.7	5.6 ± 3	16.8 ± 9
93	2:18:24.53	57:09:28.6	1.3	9.1 ± 4	27.3 ± 11
94	2:18:24.80	56:58:08.0	2.2	26.9 ± 10	80.7 ± 31
95	2:18:24.73	57:11:08.0	1.5	18.1 ± 6	54.4 ± 17
96	2:18:24.90	57:02:11.2	5.6	45.3 ± 13	136.1 ± 40
97	2:18:25.17	57:06:42.8	1.2	43.7 ± 7	131.2 ± 20
98	2:18:25.17	57:07:42.6	0.7	6.2 ± 3	18.7 ± 10
99	2:18:25.15	57:11:18.4	2.2	16.7 ± 6	50.1 ± 17
100	2:18:25.18	57:13:48.0	2.1	21.8 ± 7	65.5 ± 21
101	2:18:25.65	57:09:05.1	2.0	23.4 ± 7	70.1 ± 21
102	2:18:25.86	57:05:28.1	0.7	7.0 ± 4	21.1 ± 11
103	2:18:25.91	57:10:24.7	1.2	11.9 ± 4	35.8 ± 13
104	2:18:26.09	57:08:17.4	0.9	8.0 ± 3	24.0 ± 10
105	2:18:26.19	57:03:11.4	2.1	22.6 ± 7	68.0 ± 21
106	2:18:26.19	57:04:44.3	1.2	13.7 ± 5	41.1 ± 14
107	2:18:26.13	57:09:18.5	3.1	23.4 ± 8	70.2 ± 23
108	2:18:26.33	57:02:51.2	2.4	14.1 ± 5	42.4 ± 16
109	2:18:26.45	57:10:05.8	0.9	12.3 ± 6	37.1 ± 17
110	2:18:26.58	57:05:11.1	1.0	7.5 ± 3	22.5 ± 10
111	2:18:26.65	57:08:23.4	0.9	7.4 ± 3	22.3 ± 9
112	2:18:26.73	57:07:28.0	0.7	6.0 ± 3	18.0 ± 9
113	2:18:27.21	57:11:07.2	1.4	28.2 ± 8	84.8 ± 24
114	2:18:27.35	57:09:31.8	1.0	6.8 ± 5	20.3 ± 14
115	2:18:27.56	57:04:50.1	1.5	20.6 ± 6	61.9 ± 19
116	2:18:27.97	56:59:36.9	1.6	217.1 ± 17	651.9 ± 51
117	2:18:28.04	57:07:43.4	0.8	8.9 ± 3	26.6 ± 10
118	2:18:28.17	57:09:38.7	1.3	7.4 ± 3	22.4 ± 10
119	2:18:28.17	57:12:30.3	1.7	44.6 ± 7	133.8 ± 21
120	2:18:28.78	57:04:43.4	1.3	9.6 ± 4	28.9 ± 11
121	2:18:29.22	56:59:16.1	2.0	33.0 ± 10	99.0 ± 31
122	2:18:29.33	57:06:23.5	0.7	31.9 ± 9	95.7 ± 28
123	2:18:29.54	57:06:52.6	1.3	9.4 ± 4	28.1 ± 12
124	2:18:29.60	57:03:09.8	1.0	22.1 ± 6	66.4 ± 19
125	2:18:29.51	57:10:18.7	1.1	18.5 ± 6	55.6 ± 18
126	2:18:29.55	57:11:42.0	1.4	8.3 ± 4	24.8 ± 13
127	2:18:29.64	57:14:23.8	2.8	30.1 ± 9	90.5 ± 26
128	2:18:29.88	57:05:33.3	1.6	13.6 ± 5	40.8 ± 14
129	2:18:29.89	57:09:02.9	0.6	34.2 ± 5	102.8 ± 15
130	2:18:29.97	57:05:01.1	1.0	6.2 ± 3	18.5 ± 8
131	2:18:30.33	57:08:32.8	0.8	5.2 ± 4	15.6 ± 11
132	2:18:30.51	57:07:37.6	0.7	18.1 ± 6	54.2 ± 17
133	2:18:30.62	57:04:53.7	0.9	23.5 ± 7	70.6 ± 20
134	2:18:30.72	57:05:44.0	0.7	15.9 ± 5	47.6 ± 15
135	2:18:30.67	57:09:33.1	0.9	8.6 ± 3	25.7 ± 10
136	2:18:30.70	57:10:08.4	0.9	10.4 ± 4	31.3 ± 13
137	2:18:31.13	56:58:59.1	1.1	1026.0 ± 36	3081.1 ± 107
138	2:18:31.21	57:03:53.1	0.7	64.8 ± 7	194.7 ± 20
139	2:18:31.35	57:05:60.0	1.2	10.9 ± 4	32.8 ± 12
140	2:18:31.30	57:13:32.3	2.9	24.7 ± 8	74.2 ± 23
141	2:18:31.42	57:05:35.9	1.1	13.5 ± 5	40.6 ± 14
142	2:18:31.78	57:03:24.9	0.8	11.2 ± 4	33.8 ± 13
143	2:18:31.91	57:07:47.7	0.4	405.4 ± 16	1217.4 ± 49
144	2:18:31.97	57:11:12.1	1.8	33.6 ± 6	101.0 ± 19
145	2:18:32.10	57:02:26.5	1.3	8.0 ± 3	24.1 ± 10
146	2:18:32.13	57:07:01.9	0.7	22.6 ± 4	68.0 ± 12
147	2:18:32.18	57:08:06.7	0.8	32.4 ± 5	97.2 ± 15
148	2:18:32.42	57:04:16.6	0.7	7.9 ± 4	23.8 ± 11
149	2:18:32.48	57:09:47.6	0.9	7.7 ± 3	23.0 ± 9
150	2:18:33.11	57:03:46.0	0.7	5.8 ± 3	17.3 ± 10
151	2:18:33.33	57:02:22.7	1.4	24.7 ± 7	74.2 ± 22
152	2:18:33.33	57:07:12.3	0.5	19.4 ± 6	58.1 ± 17
153	2:18:33.60	57:07:38.6	0.7	18.6 ± 4	55.9 ± 11
154	2:18:33.93	57:11:47.6	2.3	13.9 ± 5	41.8 ± 15
155	2:18:34.23	57:07:37.7	0.4	6.0 ± 3	17.9 ± 9
156	2:18:34.33	57:05:09.5	1.3	8.2 ± 3	24.8 ± 10
157	2:18:34.39	57:06:41.5	0.4	6.4 ± 4	19.2 ± 13
158	2:18:34.53	57:06:58.4	0.7	6.9 ± 3	20.8 ± 9
159	2:18:34.63	57:08:06.3	1.3	7.5 ± 3	22.7 ± 9
160	2:18:34.74	57:10:33.1	1.5	19.3 ± 6	58.0 ± 18
161	2:18:34.78	57:10:47.5	0.5	242.2 ± 13	727.4 ± 39
162	2:18:34.92	57:09:39.7	0.8	16.0 ± 5	47.9 ± 15
163	2:18:35.07	57:13:50.4	5.4	47.7 ± 13	143.2 ± 40
164	2:18:35.18	57:08:44.0	0.5	5.9 ± 3	17.7 ± 8
165	2:18:35.48	57:04:16.6	0.8	5.8 ± 4	17.4 ± 12
166	2:18:35.50	57:03:41.1	1.2	11.4 ± 4	34.1 ± 12
167	2:18:35.64	57:02:23.0	1.0	7.3 ± 4	21.8 ± 13

Table 1. continued.

X source ID	RA (J2000)	DEC (J2000)	Pos. err. (″)	Count rate (10^{-5} cts s^{-1})	Flux (10^{-8} ph s^{-1} cm^{-2})
168	2:18:35.78	57:06:43.1	0.8	17.2 ± 6	51.6 ± 19
169	2:18:35.82	57:05:06.2	1.1	13.3 ± 4	40.0 ± 13
170	2:18:35.85	57:07:56.1	0.7	17.2 ± 5	51.8 ± 15
171	2:18:35.90	57:05:44.4	0.9	7.1 ± 3	21.2 ± 8
172	2:18:36.28	57:06:20.0	0.4	28.8 ± 5	86.4 ± 14
173	2:18:36.30	57:05:57.4	0.6	9.1 ± 3	27.4 ± 10
174	2:18:36.41	56:59:45.5	4.1	42.9 ± 13	128.9 ± 39
175	2:18:36.55	57:01:15.1	1.9	12.0 ± 6	36.2 ± 17
176	2:18:36.49	57:11:37.5	1.0	7.3 ± 3	22.0 ± 11
177	2:18:36.68	57:08:29.8	0.6	10.6 ± 4	31.8 ± 11
178	2:18:36.81	57:06:27.8	0.9	6.8 ± 3	20.5 ± 8
179	2:18:37.09	57:05:53.2	0.4	27.2 ± 4	81.7 ± 13
180	2:18:37.03	57:12:35.2	1.1	57.7 ± 7	173.4 ± 21
181	2:18:37.07	57:08:46.5	0.6	11.1 ± 4	33.4 ± 12
182	2:18:37.21	56:58:19.7	3.3	25.7 ± 9	77.3 ± 27
183	2:18:37.15	57:05:12.9	0.8	33.3 ± 5	99.9 ± 14
184	2:18:37.18	57:04:58.7	1.0	23.7 ± 7	71.2 ± 20
185	2:18:37.14	57:09:05.5	0.8	12.2 ± 4	36.6 ± 12
186	2:18:37.52	57:08:31.0	0.5	7.6 ± 3	22.9 ± 9
187	2:18:38.38	56:59:41.1	2.9	33.5 ± 10	100.7 ± 31
188	2:18:38.35	57:03:48.4	0.8	15.0 ± 5	45.1 ± 15
189	2:18:38.38	57:08:21.6	0.6	9.2 ± 3	27.7 ± 10
190	2:18:38.50	57:10:45.5	1.2	10.6 ± 4	31.9 ± 12
191	2:18:38.59	57:11:09.0	0.8	14.2 ± 5	42.8 ± 15
192	2:18:38.70	57:08:13.2	0.7	15.7 ± 5	47.0 ± 14
193	2:18:38.76	57:04:56.7	0.6	10.8 ± 4	32.5 ± 11
194	2:18:38.79	57:05:59.0	0.4	3.9 ± 2	11.8 ± 7
195	2:18:38.80	57:08:22.5	0.8	9.5 ± 3	28.5 ± 10
196	2:18:38.84	57:05:14.3	0.7	5.1 ± 3	15.3 ± 8
197	2:18:38.84	57:09:26.3	0.4	3.8 ± 2	11.4 ± 7
198	2:18:38.89	57:11:03.2	0.9	27.1 ± 5	81.4 ± 14
199	2:18:39.03	57:08:43.8	0.5	18.0 ± 5	54.1 ± 16
200	2:18:39.15	57:07:35.2	0.9	19.1 ± 4	57.5 ± 11
201	2:18:39.12	57:13:13.3	3.1	22.2 ± 7	66.7 ± 22
202	2:18:39.18	57:09:58.8	0.5	48.8 ± 6	146.5 ± 17
203	2:18:39.56	57:08:22.3	0.4	29.9 ± 8	89.8 ± 23
204	2:18:39.80	57:07:39.7	0.4	32.9 ± 8	98.9 ± 25
205	2:18:39.86	57:11:55.8	1.3	23.2 ± 4	69.8 ± 13
206	2:18:40.00	57:08:22.7	0.7	6.0 ± 3	18.0 ± 8
207	2:18:40.00	57:09:35.0	0.4	4.4 ± 2	13.3 ± 7
208	2:18:40.06	57:10:58.8	0.9	22.1 ± 4	66.2 ± 12
209	2:18:40.27	57:08:56.8	0.6	8.5 ± 3	25.5 ± 9
210	2:18:40.35	57:06:03.1	0.4	9.6 ± 3	28.8 ± 11
211	2:18:40.57	57:07:33.2	0.6	23.6 ± 4	70.8 ± 12
212	2:18:40.62	57:06:36.6	0.6	4.2 ± 2	12.7 ± 7
213	2:18:40.58	57:14:44.9	1.7	12.4 ± 6	37.3 ± 17
214	2:18:40.81	57:02:20.1	0.9	9.6 ± 5	28.9 ± 16
215	2:18:41.00	57:06:26.1	0.4	3.4 ± 2	10.3 ± 7
216	2:18:40.95	57:15:15.2	1.8	70.7 ± 11	212.2 ± 34
217	2:18:41.03	57:07:36.6	0.7	16.3 ± 5	49.0 ± 15
218	2:18:41.09	57:06:08.4	0.5	45.8 ± 6	137.6 ± 17
219	2:18:41.20	57:01:09.6	1.2	10.7 ± 5	32.0 ± 15
220	2:18:41.22	57:11:51.3	2.1	18.0 ± 6	54.1 ± 17
221	2:18:41.60	57:04:15.0	0.4	137.1 ± 10	411.8 ± 29
222	2:18:41.64	57:06:42.6	0.6	32.3 ± 5	97.0 ± 14
223	2:18:41.66	57:08:49.0	0.6	12.6 ± 4	37.7 ± 13
224	2:18:41.85	57:10:56.4	0.7	23.0 ± 4	69.1 ± 13
225	2:18:41.91	57:08:29.2	0.4	3.6 ± 3	10.9 ± 8
226	2:18:42.01	57:01:51.8	1.2	9.6 ± 4	28.7 ± 11
227	2:18:42.02	57:10:14.6	0.8	12.7 ± 4	38.3 ± 13
228	2:18:42.23	57:09:19.9	0.4	3.5 ± 3	10.6 ± 9
229	2:18:42.29	57:09:14.1	0.6	7.5 ± 3	22.5 ± 9
230	2:18:42.36	57:07:35.5	0.3	5.6 ± 3	16.8 ± 9
231	2:18:42.44	57:06:01.6	0.4	20.6 ± 4	61.8 ± 11
232	2:18:42.45	57:10:06.1	1.1	12.0 ± 4	36.0 ± 12
233	2:18:42.49	57:06:05.5	0.9	8.9 ± 3	26.9 ± 10
234	2:18:42.50	57:06:14.6	0.7	5.1 ± 2	15.2 ± 7
235	2:18:42.55	57:05:38.4	0.4	37.7 ± 6	113.3 ± 17
236	2:18:42.60	57:06:03.9	0.5	5.1 ± 2	15.3 ± 7
237	2:18:42.76	57:14:15.7	2.5	51.4 ± 13	154.3 ± 40
238	2:18:42.86	57:04:22.7	0.7	5.2 ± 2	15.5 ± 7
239	2:18:42.95	57:07:33.5	0.7	5.5 ± 3	16.5 ± 8
240	2:18:42.97	57:08:08.2	1.1	12.0 ± 4	36.2 ± 12
241	2:18:42.97	57:09:24.5	0.6	26.0 ± 5	78.1 ± 15
242	2:18:43.21	57:07:23.1	0.5	15.2 ± 5	45.8 ± 15
243	2:18:43.28	57:02:20.6	0.9	11.6 ± 7	34.9 ± 20
244	2:18:43.56	57:03:39.0	0.9	8.9 ± 4	26.7 ± 11
245	2:18:43.78	57:13:35.2	1.2	16.8 ± 7	50.4 ± 22
246	2:18:43.88	57:10:53.5	0.7	5.0 ± 2	15.0 ± 7
247	2:18:43.89	57:13:21.0	3.0	25.2 ± 8	75.7 ± 24
248	2:18:44.03	57:06:36.4	0.4	4.0 ± 3	11.9 ± 8
249	2:18:44.06	57:08:55.8	0.7	15.7 ± 3	47.1 ± 9
250	2:18:44.14	57:12:47.2	1.6	15.1 ± 5	45.4 ± 16
251	2:18:44.22	57:07:46.8	0.4	34.6 ± 5	103.8 ± 15

Table 1. continued.

X source ID	RA (J2000)	DEC (J2000)	Pos. err. (″)	Count rate (10^{-5} cts s^{-1})	Flux (10^{-8} ph s^{-1} cm^{-2})
252	2:18:44.23	57:06:46.2	0.6	9.9 ± 4	29.6 ± 11
253	2:18:44.28	57:06:24.3	0.4	3.8 ± 2	11.3 ± 7
254	2:18:44.28	57:11:39.4	1.4	23.8 ± 7	71.5 ± 21
255	2:18:44.35	57:01:30.6	1.1	7.8 ± 5	23.5 ± 14
256	2:18:44.49	57:09:46.0	1.0	15.8 ± 5	47.6 ± 15
257	2:18:44.51	57:08:00.9	0.4	4.9 ± 3	14.9 ± 8
258	2:18:44.48	57:14:04.1	1.7	19.3 ± 8	57.9 ± 24
259	2:18:44.61	57:10:02.4	1.0	5.9 ± 3	17.8 ± 8
260	2:18:44.70	57:09:18.3	0.6	20.3 ± 4	60.9 ± 12
261	2:18:44.88	57:07:08.2	0.5	8.2 ± 5	24.6 ± 15
262	2:18:44.98	57:05:22.3	0.4	4.5 ± 2	13.5 ± 7
263	2:18:44.99	57:10:04.1	0.5	4.4 ± 2	13.1 ± 6
264	2:18:45.02	57:09:24.4	0.4	27.5 ± 5	82.4 ± 15
265	2:18:45.08	57:06:43.7	0.7	4.9 ± 2	14.8 ± 7
266	2:18:45.24	57:00:41.0	1.7	13.9 ± 5	41.9 ± 15
267	2:18:45.43	57:06:47.4	0.6	4.3 ± 2	12.9 ± 7
268	2:18:45.48	57:10:07.0	0.4	3.7 ± 2	11.1 ± 7
269	2:18:45.80	57:04:53.5	0.4	4.0 ± 3	12.2 ± 9
270	2:18:46.00	57:06:42.8	0.5	4.0 ± 2	11.9 ± 6
271	2:18:46.02	57:08:09.2	0.6	8.6 ± 3	25.8 ± 10
272	2:18:46.07	57:07:27.1	0.4	4.2 ± 3	12.5 ± 10
273	2:18:46.21	57:00:01.6	0.8	44.8 ± 7	134.5 ± 21
274	2:18:46.16	57:09:45.3	0.6	6.4 ± 3	19.1 ± 8
275	2:18:46.31	57:07:46.0	0.7	5.8 ± 3	17.5 ± 8
276	2:18:46.32	57:05:01.7	0.4	3.8 ± 3	11.4 ± 8
277	2:18:46.37	57:04:54.5	0.4	3.7 ± 3	11.0 ± 9
278	2:18:46.46	57:07:56.8	0.4	4.4 ± 3	13.3 ± 9
279	2:18:46.45	57:13:54.1	2.5	38.9 ± 10	116.7 ± 31
280	2:18:46.55	57:08:14.4	0.4	15.7 ± 5	47.2 ± 15
281	2:18:46.63	57:04:33.4	0.4	4.0 ± 2	11.9 ± 7
282	2:18:46.65	57:04:58.6	0.5	5.3 ± 2	15.9 ± 7
283	2:18:46.69	57:08:06.1	0.7	5.0 ± 2	14.9 ± 7
284	2:18:46.80	57:03:52.8	0.9	19.3 ± 3	57.9 ± 10
285	2:18:46.93	57:03:06.8	1.7	11.2 ± 4	33.6 ± 12
286	2:18:47.01	57:06:50.7	0.4	13.6 ± 4	40.8 ± 13
287	2:18:47.04	57:05:27.0	0.4	3.7 ± 2	11.2 ± 7
288	2:18:47.07	57:07:32.5	0.4	4.3 ± 2	12.8 ± 7
289	2:18:47.10	57:11:23.8	0.7	6.3 ± 3	18.8 ± 9
290	2:18:47.17	57:09:11.9	0.4	48.4 ± 6	145.3 ± 17
291	2:18:47.24	57:07:51.9	0.4	52.1 ± 8	156.4 ± 23
292	2:18:47.30	57:04:18.2	0.6	9.0 ± 3	27.1 ± 10
293	2:18:47.39	57:08:42.3	0.5	14.6 ± 5	43.7 ± 14
294	2:18:47.44	57:01:37.8	1.2	13.8 ± 5	41.6 ± 15
295	2:18:47.69	57:04:34.6	0.5	12.9 ± 4	38.6 ± 13
296	2:18:47.80	57:08:42.2	0.5	5.4 ± 2	16.1 ± 7
297	2:18:47.87	57:05:52.5	0.6	12.0 ± 4	36.0 ± 13
298	2:18:47.89	57:04:42.0	0.5	21.9 ± 6	65.6 ± 18
299	2:18:47.92	57:04:02.2	0.7	5.8 ± 3	17.3 ± 8
300	2:18:47.94	57:06:55.5	0.4	3.3 ± 2	9.9 ± 6
301	2:18:47.97	57:06:16.5	0.3	24.2 ± 4	72.8 ± 12
302	2:18:48.03	57:11:27.4	1.7	14.0 ± 5	42.1 ± 15
303	2:18:48.03	57:13:59.2	2.2	19.7 ± 6	59.1 ± 19
304	2:18:48.28	57:13:29.4	1.3	9.4 ± 5	28.1 ± 16
305	2:18:48.34	57:04:24.3	0.4	3.7 ± 2	11.0 ± 7
306	2:18:48.43	57:07:40.1	0.3	6.6 ± 3	19.9 ± 8
307	2:18:48.50	57:03:46.6	0.7	6.1 ± 3	18.2 ± 8
308	2:18:48.53	57:06:45.1	0.3	6.0 ± 3	18.0 ± 8
309	2:18:48.62	57:10:46.4	1.1	15.4 ± 5	46.3 ± 15
310	2:18:48.67	57:08:58.7	0.5	11.7 ± 4	35.2 ± 12
311	2:18:48.70	57:07:18.9	0.5	15.0 ± 7	44.9 ± 21
312	2:18:48.82	57:04:25.4	0.5	5.1 ± 2	15.2 ± 7
313	2:18:48.82	57:07:54.7	0.5	8.3 ± 4	24.9 ± 11
314	2:18:48.83	57:09:55.1	0.7	16.2 ± 5	48.6 ± 15
315	2:18:48.90	57:07:41.5	0.4	7.3 ± 3	22.1 ± 9
316	2:18:48.94	57:12:38.0	1.1	6.3 ± 4	19.0 ± 12
317	2:18:49.00	57:07:23.6	0.4	90.2 ± 11	271.0 ± 33
318	2:18:49.12	57:11:11.6	1.4	10.8 ± 5	32.4 ± 15
319	2:18:49.18	57:01:26.9	0.8	61.3 ± 10	184.0 ± 29
320	2:18:49.19	57:09:09.4	0.7	6.2 ± 3	18.7 ± 8
321	2:18:49.20	57:08:10.2	0.7	7.0 ± 3	20.9 ± 9
322	2:18:49.33	57:05:23.7	0.4	40.2 ± 6	120.8 ± 18
323	2:18:49.46	57:12:55.2	2.3	15.6 ± 5	46.8 ± 16
324	2:18:49.57	57:07:10.6	0.5	31.9 ± 9	95.8 ± 27
325	2:18:49.63	57:08:58.6	0.4	14.3 ± 4	42.9 ± 13
326	2:18:49.64	57:11:25.4	0.9	14.3 ± 5	43.1 ± 16
327	2:18:49.71	57:09:16.1	0.5	11.2 ± 4	33.8 ± 11
328	2:18:49.92	57:01:12.1	0.8	14.3 ± 6	43.0 ± 17
329	2:18:49.93	57:06:37.1	0.4	46.4 ± 5	139.2 ± 15
330	2:18:50.02	56:58:37.8	1.7	25.4 ± 10	76.2 ± 31
331	2:18:50.03	57:02:19.0	1.5	21.5 ± 7	64.5 ± 20
332	2:18:50.17	56:59:24.0	1.9	13.0 ± 6	39.0 ± 17
333	2:18:50.18	57:07:33.2	0.4	5.1 ± 3	15.3 ± 9
334	2:18:50.35	57:06:37.4	0.5	5.5 ± 2	16.6 ± 7
335	2:18:50.47	57:04:26.4	0.5	5.0 ± 2	14.9 ± 7

Table 1. continued.

X source ID	RA (J2000)	DEC (J2000)	Pos. err. (″)	Count rate (10^{-5} cts s^{-1})	Flux (10^{-8} ph s^{-1} cm^{-2})
336	2:18:50.67	57:07:01.2	0.4	7.8 ± 3	23.5 ± 9
337	2:18:50.72	57:03:17.7	0.6	7.6 ± 3	22.7 ± 9
338	2:18:50.88	57:07:07.4	0.3	25.2 ± 4	75.7 ± 13
339	2:18:50.88	57:06:15.7	0.6	8.3 ± 3	25.0 ± 10
340	2:18:50.92	57:11:43.2	0.9	29.0 ± 6	87.1 ± 17
341	2:18:50.99	57:07:21.9	0.4	10.7 ± 5	32.1 ± 15
342	2:18:51.07	57:07:60.0	0.5	5.6 ± 3	16.9 ± 8
343	2:18:51.39	57:04:12.7	0.4	35.9 ± 6	107.9 ± 18
344	2:18:51.37	57:11:16.0	1.2	14.8 ± 5	44.4 ± 16
345	2:18:51.60	57:10:37.1	0.4	7.0 ± 4	20.9 ± 12
346	2:18:51.80	57:06:25.6	0.3	56.8 ± 6	170.6 ± 18
347	2:18:51.81	57:11:14.3	0.7	5.1 ± 3	15.4 ± 9
348	2:18:51.85	57:11:36.5	1.1	13.1 ± 4	39.4 ± 13
349	2:18:51.88	57:09:34.5	0.7	6.9 ± 3	20.7 ± 10
350	2:18:51.98	57:06:56.5	0.7	7.1 ± 3	21.2 ± 9
351	2:18:52.34	57:04:35.0	0.9	8.4 ± 3	25.3 ± 10
352	2:18:52.47	57:10:07.5	0.3	11.4 ± 5	34.2 ± 16
353	2:18:52.55	57:06:40.4	0.4	5.3 ± 3	16.1 ± 8
354	2:18:52.56	57:04:25.2	0.5	24.0 ± 7	72.0 ± 20
355	2:18:52.56	57:13:12.5	2.2	17.1 ± 6	51.3 ± 17
356	2:18:52.65	57:05:23.2	0.3	7.7 ± 3	23.2 ± 10
357	2:18:52.72	57:08:43.6	0.4	9.3 ± 3	28.1 ± 10
358	2:18:52.73	57:11:29.0	0.9	23.8 ± 4	71.5 ± 12
359	2:18:52.83	57:07:42.5	0.4	9.2 ± 4	27.6 ± 11
360	2:18:52.94	57:09:39.7	0.6	18.0 ± 6	54.1 ± 19
361	2:18:52.95	57:12:49.9	1.0	73.1 ± 8	219.5 ± 23
362	2:18:52.98	57:07:22.4	0.6	12.9 ± 5	38.7 ± 15
363	2:18:53.12	57:08:46.9	0.4	3.5 ± 2	10.7 ± 6
364	2:18:53.36	57:07:57.7	0.5	8.1 ± 3	24.3 ± 10
365	2:18:53.38	57:03:09.6	0.6	37.9 ± 6	113.9 ± 17
366	2:18:53.39	57:02:00.1	1.1	17.1 ± 5	51.2 ± 16
367	2:18:53.65	57:10:03.8	0.6	13.5 ± 5	40.7 ± 14
368	2:18:53.69	57:07:04.2	0.9	7.2 ± 3	21.5 ± 9
369	2:18:53.82	57:07:43.9	0.5	20.2 ± 6	60.7 ± 18
370	2:18:53.87	57:01:34.1	1.0	7.9 ± 4	23.8 ± 12
371	2:18:53.88	57:10:19.9	0.4	28.1 ± 7	84.3 ± 22
372	2:18:53.92	57:08:22.3	0.5	5.3 ± 3	15.9 ± 8
373	2:18:53.94	57:06:50.2	0.3	6.1 ± 3	18.4 ± 9
374	2:18:53.97	57:04:40.2	0.5	18.6 ± 5	55.8 ± 16
375	2:18:53.96	57:09:33.4	0.5	26.3 ± 8	78.9 ± 24
376	2:18:54.07	57:10:24.9	0.4	4.1 ± 2	12.2 ± 7
377	2:18:54.23	57:08:13.5	0.6	6.0 ± 3	18.1 ± 10
378	2:18:54.24	57:09:45.5	0.5	5.2 ± 3	15.6 ± 8
379	2:18:54.34	57:08:00.6	0.4	13.4 ± 4	40.3 ± 13
380	2:18:54.37	57:09:50.9	0.7	6.0 ± 3	17.9 ± 8
381	2:18:54.41	57:03:04.7	0.4	4.1 ± 3	12.5 ± 9
382	2:18:54.83	57:05:06.2	0.4	4.3 ± 3	12.8 ± 8
383	2:18:54.84	57:03:38.8	0.6	10.8 ± 4	32.5 ± 11
384	2:18:54.87	57:05:31.3	0.4	15.7 ± 5	47.3 ± 15
385	2:18:54.97	57:05:02.7	0.5	13.5 ± 4	40.5 ± 13
386	2:18:55.10	57:08:52.2	0.4	23.0 ± 8	69.0 ± 24
387	2:18:55.13	57:07:08.6	0.4	12.8 ± 4	38.4 ± 13
388	2:18:55.14	57:06:21.9	0.5	24.4 ± 7	73.3 ± 21
389	2:18:55.12	57:15:21.8	1.9	12.2 ± 5	36.6 ± 16
390	2:18:55.23	57:11:28.5	0.8	12.2 ± 4	36.7 ± 12
391	2:18:55.33	57:04:30.1	0.4	4.1 ± 3	12.3 ± 8
392	2:18:55.35	57:06:33.0	0.5	4.5 ± 2	13.5 ± 7
393	2:18:55.50	57:03:58.3	0.3	23.6 ± 7	70.9 ± 20
394	2:18:55.53	57:04:32.7	0.5	14.8 ± 4	44.4 ± 13
395	2:18:55.77	56:59:07.3	2.2	63.9 ± 10	191.8 ± 29
396	2:18:55.76	57:04:58.2	0.4	29.3 ± 5	88.1 ± 15
397	2:18:55.79	57:07:05.5	0.5	17.1 ± 5	51.4 ± 16
398	2:18:55.85	57:01:25.9	1.7	13.0 ± 5	39.0 ± 14
399	2:18:55.87	57:08:45.2	0.5	6.2 ± 3	18.7 ± 9
400	2:18:55.95	57:07:15.6	0.5	4.3 ± 2	12.8 ± 6
401	2:18:55.96	57:06:17.6	0.4	13.0 ± 4	39.1 ± 13
402	2:18:55.99	57:05:06.1	0.5	7.0 ± 3	21.1 ± 9
403	2:18:56.03	57:00:01.6	3.8	43.3 ± 12	130.1 ± 36
404	2:18:56.02	57:09:51.1	0.6	12.1 ± 4	36.4 ± 12
405	2:18:56.03	57:07:22.2	0.3	36.7 ± 6	110.1 ± 18
406	2:18:56.27	57:07:01.9	0.4	4.9 ± 3	14.8 ± 8
407	2:18:56.31	57:04:08.9	0.4	3.5 ± 2	10.6 ± 7
408	2:18:56.36	57:00:42.8	0.8	152.0 ± 11	456.5 ± 34
409	2:18:56.35	57:05:48.5	0.7	5.1 ± 2	15.4 ± 7
410	2:18:56.50	57:10:03.1	0.4	23.1 ± 4	69.5 ± 12
411	2:18:56.67	57:10:21.4	0.7	6.3 ± 3	19.0 ± 9
412	2:18:56.67	57:08:50.7	0.5	4.6 ± 2	13.7 ± 7
413	2:18:56.71	57:09:01.3	0.5	13.4 ± 4	40.1 ± 13
414	2:18:56.84	57:04:42.1	0.4	8.0 ± 3	24.0 ± 9
415	2:18:56.84	57:12:30.1	1.0	19.9 ± 6	59.7 ± 18
416	2:18:56.85	57:06:54.0	0.5	21.8 ± 6	65.5 ± 19
417	2:18:56.88	57:03:16.1	0.7	17.4 ± 5	52.2 ± 16
418	2:18:56.87	57:10:51.1	0.6	23.1 ± 4	69.4 ± 11
419	2:18:56.96	57:10:39.3	0.4	3.4 ± 2	10.1 ± 6

Table 1. continued.

X source ID	RA (J2000)	DEC (J2000)	Pos. err. (″)	Count rate (10^{-5} cts s^{-1})	Flux (10^{-8} ph s^{-1} cm^{-2})
420	2:18:57.17	57:09:36.0	0.5	20.6 ± 6	62.0 ± 17
421	2:18:57.25	57:11:15.5	0.8	13.5 ± 5	40.6 ± 15
422	2:18:57.29	57:09:12.5	0.5	4.1 ± 2	12.3 ± 6
423	2:18:57.29	57:05:04.3	0.4	4.5 ± 2	13.6 ± 7
424	2:18:57.32	57:05:18.5	0.3	5.8 ± 3	17.5 ± 8
425	2:18:57.32	57:08:27.3	0.4	9.9 ± 3	29.7 ± 10
426	2:18:57.43	57:08:39.5	0.3	20.4 ± 6	61.1 ± 17
427	2:18:57.47	57:08:22.4	0.4	4.8 ± 3	14.3 ± 8
428	2:18:57.50	57:07:59.3	0.4	15.6 ± 6	46.8 ± 18
429	2:18:57.58	57:06:14.1	0.4	4.6 ± 3	13.7 ± 8
430	2:18:57.58	57:12:21.8	0.9	9.6 ± 4	28.9 ± 12
431	2:18:57.63	57:06:12.1	0.7	6.9 ± 3	20.8 ± 9
432	2:18:57.65	57:09:17.5	0.5	4.1 ± 2	12.3 ± 7
433	2:18:57.65	57:03:31.6	0.8	14.6 ± 5	44.0 ± 14
434	2:18:57.75	57:11:52.2	1.1	13.2 ± 4	39.6 ± 13
435	2:18:57.88	57:09:00.1	0.3	5.6 ± 3	16.8 ± 8
436	2:18:57.94	57:05:53.8	0.6	4.1 ± 2	12.2 ± 6
437	2:18:57.95	57:06:46.3	1.7	15.8 ± 6	47.6 ± 18
438	2:18:57.97	57:08:17.4	0.5	22.4 ± 7	67.2 ± 20
439	2:18:58.03	57:09:01.4	0.4	3.6 ± 2	10.9 ± 7
440	2:18:58.05	57:04:18.9	0.4	3.8 ± 2	11.4 ± 7
441	2:18:58.06	57:12:03.4	1.4	20.6 ± 6	62.0 ± 18
442	2:18:58.07	57:09:22.4	0.9	8.3 ± 3	24.9 ± 10
443	2:18:58.10	57:05:41.1	0.4	7.5 ± 3	22.6 ± 9
444	2:18:58.17	57:12:28.5	1.0	6.8 ± 5	20.3 ± 14
445	2:18:58.18	57:09:38.3	0.8	10.3 ± 4	30.8 ± 11
446	2:18:58.20	57:09:41.1	0.7	5.5 ± 2	16.5 ± 7
447	2:18:58.26	57:01:39.8	1.1	15.9 ± 5	47.8 ± 16
448	2:18:58.31	57:06:57.7	0.3	18.2 ± 8	54.6 ± 23
449	2:18:58.39	57:06:30.1	0.4	24.5 ± 8	73.6 ± 23
450	2:18:58.43	57:06:10.9	0.4	13.7 ± 4	41.2 ± 13
451	2:18:58.49	57:09:13.3	0.5	21.8 ± 4	65.5 ± 12
452	2:18:58.50	57:05:28.2	2.4	13.1 ± 5	39.3 ± 14
453	2:18:58.49	57:13:37.8	2.2	20.0 ± 6	60.1 ± 19
454	2:18:58.58	57:07:00.8	0.4	34.4 ± 11	103.4 ± 32
455	2:18:58.62	57:04:42.4	0.3	7.3 ± 3	21.9 ± 9
456	2:18:58.64	57:11:32.3	0.7	7.8 ± 4	23.6 ± 12
457	2:18:58.66	57:09:08.9	0.4	4.1 ± 2	12.2 ± 7
458	2:18:58.72	57:07:54.6	0.4	13.2 ± 5	39.7 ± 14
459	2:18:58.79	57:03:06.0	0.9	7.6 ± 3	22.8 ± 9
460	2:18:58.96	57:06:35.9	0.4	36.1 ± 11	108.4 ± 33
461	2:18:58.97	57:10:25.6	0.7	8.4 ± 3	25.1 ± 10
462	2:18:59.08	57:04:23.5	0.7	17.6 ± 3	52.8 ± 10
463	2:18:59.13	57:10:39.3	0.8	9.9 ± 4	29.7 ± 11
464	2:18:59.15	57:03:25.5	1.2	9.4 ± 4	28.1 ± 11
465	2:18:59.24	57:08:32.9	0.3	9.9 ± 4	29.7 ± 11
466	2:18:59.26	57:09:09.2	0.7	6.5 ± 3	19.5 ± 8
467	2:18:59.39	57:07:15.3	0.4	10.6 ± 4	32.0 ± 13
468	2:18:59.39	57:10:12.3	0.4	4.3 ± 3	12.9 ± 8
469	2:18:59.41	57:07:52.0	0.3	28.1 ± 5	84.5 ± 16
470	2:18:59.49	57:08:43.8	0.3	7.2 ± 3	21.5 ± 10
471	2:18:59.56	57:07:30.1	0.4	22.3 ± 7	66.9 ± 21
472	2:18:59.56	57:02:27.9	0.8	5.1 ± 4	15.4 ± 11
473	2:18:59.57	57:09:37.7	0.5	5.0 ± 2	15.0 ± 7
474	2:18:59.62	57:10:17.0	0.6	10.0 ± 4	30.0 ± 11
475	2:18:59.66	57:09:55.3	0.7	5.3 ± 2	15.9 ± 7
476	2:18:59.82	57:09:03.8	0.4	10.0 ± 3	30.0 ± 10
477	2:18:59.86	57:09:10.8	1.0	5.7 ± 3	17.3 ± 8
478	2:18:59.94	57:03:59.0	0.6	9.4 ± 3	28.2 ± 10
479	2:18:60.00	57:06:04.6	0.5	13.8 ± 6	41.4 ± 18
480	2:19:0 0.12	57:01:35.7	1.0	6.7 ± 3	20.1 ± 10
481	2:19:0 0.20	57:06:27.7	0.7	8.7 ± 4	26.0 ± 12
482	2:19:0 0.46	57:09:16.5	0.5	18.0 ± 3	54.0 ± 10
483	2:19:0 0.49	57:09:05.2	0.4	22.2 ± 4	66.7 ± 11
484	2:19:0 0.62	57:13:02.3	1.3	76.0 ± 8	228.4 ± 23
485	2:19:0 0.66	57:10:19.7	0.4	51.4 ± 8	154.2 ± 23
486	2:19:0 0.67	57:07:09.3	0.4	11.2 ± 4	33.5 ± 11
487	2:19:0 0.87	57:08:28.8	0.4	13.7 ± 5	41.1 ± 15
488	2:19:0 0.89	57:01:44.6	0.9	8.5 ± 4	25.6 ± 13
489	2:19:0 0.93	57:04:48.6	0.6	8.7 ± 3	26.1 ± 10
490	2:19:0 0.94	57:07:23.5	0.4	13.8 ± 4	41.4 ± 13
491	2:19:0 0.96	57:15:30.1	2.6	35.8 ± 10	107.5 ± 29
492	2:19:0 1.03	57:09:15.7	0.5	12.3 ± 4	37.0 ± 12
493	2:19:0 1.07	57:08:36.6	0.4	6.3 ± 4	19.1 ± 11
494	2:19:0 1.07	57:06:27.8	0.7	7.6 ± 3	22.8 ± 10
495	2:19:0 1.12	57:09:57.9	0.5	6.0 ± 3	17.9 ± 8
496	2:19:0 1.18	57:14:14.5	2.9	27.1 ± 8	81.3 ± 24
497	2:19:0 1.31	57:04:07.7	0.4	3.2 ± 2	9.8 ± 7
498	2:19:0 1.34	57:05:49.3	0.7	10.7 ± 5	32.0 ± 14
499	2:19:0 1.35	57:05:34.5	0.5	10.6 ± 5	31.8 ± 14
500	2:19:0 1.38	57:07:51.2	0.3	18.2 ± 7	54.8 ± 22
501	2:19:0 1.39	57:06:50.0	0.7	6.4 ± 3	19.2 ± 8
502	2:19:0 1.50	57:06:10.5	0.5	7.2 ± 3	21.7 ± 10
503	2:19:0 1.55	57:00:11.0	1.1	49.5 ± 7	148.6 ± 21

Table 1. continued.

X source ID	RA (J2000)	DEC (J2000)	Pos. err. (″)	Count rate (10^{-5} cts s^{-1})	Flux (10^{-8} ph s^{-1} cm^{-2})
504	2:19:0 1.66	57:05:59.8	0.3	15.6 ± 5	47.0 ± 16
505	2:19:0 1.72	57:07:11.5	0.3	6.2 ± 3	18.6 ± 9
506	2:19:0 1.74	57:12:28.6	0.5	217.4 ± 13	652.9 ± 40
507	2:19:0 1.82	57:09:05.0	0.6	11.7 ± 4	35.2 ± 13
508	2:19:0 1.88	57:09:44.3	0.5	4.8 ± 2	14.4 ± 7
509	2:19:0 1.88	57:07:23.0	0.4	8.7 ± 3	26.2 ± 10
510	2:19:0 1.95	57:10:08.1	0.5	16.8 ± 3	50.4 ± 10
511	2:19:0 1.99	57:13:29.8	2.3	14.1 ± 5	42.4 ± 15
512	2:19:0 2.00	57:10:53.0	0.9	6.2 ± 2	18.5 ± 7
513	2:19:0 2.24	57:04:13.9	0.5	5.0 ± 3	15.1 ± 8
514	2:19:0 2.38	57:06:21.7	0.5	5.3 ± 2	15.8 ± 7
515	2:19:0 2.53	57:14:31.2	3.5	48.1 ± 12	144.4 ± 38
516	2:19:0 2.55	57:08:26.6	0.3	9.0 ± 4	27.1 ± 13
517	2:19:0 2.58	57:08:14.8	0.4	6.2 ± 3	18.5 ± 9
518	2:19:0 2.66	57:06:35.8	0.4	12.3 ± 4	36.9 ± 12
519	2:19:0 2.79	57:07:52.1	0.4	30.0 ± 10	90.2 ± 31
520	2:19:0 2.81	57:09:35.4	0.4	14.7 ± 5	44.1 ± 15
521	2:19:0 2.89	57:08:06.1	0.4	3.9 ± 2	11.6 ± 7
522	2:19:0 2.96	57:08:24.9	0.4	5.7 ± 3	17.2 ± 9
523	2:19:0 2.97	57:08:33.7	0.5	18.2 ± 6	54.6 ± 17
524	2:19:0 3.04	57:13:00.6	1.4	20.8 ± 6	62.4 ± 19
525	2:19:0 3.05	57:07:02.2	0.4	4.0 ± 2	11.9 ± 7
526	2:19:0 3.05	57:03:00.2	0.6	174.1 ± 14	522.7 ± 41
527	2:19:0 3.06	57:04:51.6	0.8	18.2 ± 7	54.6 ± 20
528	2:19:0 3.15	57:06:24.3	0.3	27.6 ± 4	82.9 ± 13
529	2:19:0 3.18	57:09:08.8	0.4	9.7 ± 4	29.1 ± 11
530	2:19:0 3.21	57:10:01.1	1.1	13.3 ± 4	39.8 ± 13
531	2:19:0 3.22	57:08:01.6	0.6	4.3 ± 2	12.9 ± 7
532	2:19:0 3.23	57:12:14.5	0.9	7.3 ± 3	22.1 ± 9
533	2:19:0 3.27	57:07:25.7	0.3	20.3 ± 4	61.0 ± 11
534	2:19:0 3.30	57:06:17.2	0.4	10.8 ± 4	32.3 ± 12
535	2:19:0 3.30	57:03:00.9	0.4	16.6 ± 6	49.9 ± 19
536	2:19:0 3.38	57:08:42.2	0.4	11.3 ± 4	33.9 ± 12
537	2:19:0 3.43	57:08:47.4	0.4	4.5 ± 2	13.5 ± 7
538	2:19:0 3.48	57:07:33.8	0.3	9.5 ± 4	28.7 ± 13
539	2:19:0 3.57	57:02:57.3	0.6	51.6 ± 9	154.9 ± 27
540	2:19:0 3.60	57:04:02.8	0.4	27.4 ± 8	82.4 ± 25
541	2:19:0 3.66	57:05:55.2	0.4	4.3 ± 2	12.9 ± 6
542	2:19:0 3.70	57:05:21.6	0.7	6.0 ± 3	17.9 ± 8
543	2:19:0 3.77	57:02:25.1	0.9	6.8 ± 3	20.4 ± 9
544	2:19:0 3.88	57:07:51.7	0.6	21.8 ± 8	65.4 ± 25
545	2:19:0 3.90	57:10:58.2	0.6	34.1 ± 5	102.3 ± 14
546	2:19:0 4.01	57:05:47.6	0.6	7.3 ± 3	21.9 ± 9
547	2:19:0 4.07	57:06:43.5	0.4	4.0 ± 2	12.0 ± 7
548	2:19:0 4.09	57:08:43.7	0.4	4.0 ± 2	12.1 ± 7
549	2:19:0 4.23	57:05:24.9	0.3	20.9 ± 3	62.8 ± 10
550	2:19:0 4.24	57:07:31.4	0.5	15.7 ± 5	47.0 ± 14
551	2:19:0 4.29	57:09:43.2	0.5	20.5 ± 6	61.5 ± 18
552	2:19:0 4.30	57:06:39.2	0.4	3.8 ± 2	11.3 ± 7
553	2:19:0 4.44	57:00:44.3	1.4	9.1 ± 5	27.4 ± 15
554	2:19:0 4.71	57:05:25.1	0.8	11.7 ± 4	35.1 ± 12
555	2:19:0 5.04	57:08:19.2	0.3	24.0 ± 4	72.0 ± 13
556	2:19:0 5.25	57:15:14.8	1.4	25.9 ± 8	77.7 ± 23
557	2:19:0 5.36	57:07:40.6	0.3	47.0 ± 7	141.1 ± 21
558	2:19:0 5.38	57:09:01.4	0.4	24.0 ± 4	72.0 ± 11
559	2:19:0 5.48	57:01:12.5	1.9	27.7 ± 8	83.2 ± 24
560	2:19:0 5.52	57:11:19.1	1.0	8.1 ± 4	24.4 ± 11
561	2:19:0 5.57	57:08:12.9	0.5	5.2 ± 2	15.5 ± 7
562	2:19:0 5.59	57:10:48.8	0.4	4.2 ± 2	12.6 ± 7
563	2:19:0 5.57	57:02:09.5	0.7	5.6 ± 3	16.9 ± 9
564	2:19:0 5.62	57:10:25.2	0.4	5.4 ± 3	16.1 ± 8
565	2:19:0 5.61	57:02:51.4	0.7	109.8 ± 11	329.6 ± 34
566	2:19:0 5.65	57:00:39.4	1.7	14.2 ± 5	42.6 ± 15
567	2:19:0 5.95	57:09:20.1	0.6	10.2 ± 3	30.5 ± 10
568	2:19:0 5.96	57:06:33.8	0.5	6.2 ± 3	18.7 ± 8
569	2:19:0 5.99	57:09:44.4	0.4	33.5 ± 5	100.6 ± 14
570	2:19:0 6.04	57:10:18.6	0.5	16.8 ± 5	50.6 ± 16
571	2:19:0 6.21	57:14:20.3	1.4	25.1 ± 5	75.4 ± 15
572	2:19:0 6.25	57:04:41.4	0.6	11.7 ± 4	35.0 ± 12
573	2:19:0 6.30	57:08:37.3	0.3	30.3 ± 4	91.1 ± 13
574	2:19:0 6.30	57:00:02.9	1.3	30.7 ± 6	92.2 ± 17
575	2:19:0 6.48	57:08:13.6	0.7	6.0 ± 3	18.1 ± 8
576	2:19:0 6.78	57:05:54.4	0.4	3.6 ± 2	10.8 ± 7
577	2:19:0 6.89	57:02:10.9	1.2	34.7 ± 6	104.1 ± 18
578	2:19:0 6.90	57:01:10.7	1.0	6.4 ± 3	19.3 ± 10
579	2:19:0 6.98	57:09:04.3	0.4	3.5 ± 2	10.4 ± 5
580	2:19:0 7.07	57:04:19.1	0.7	6.4 ± 3	19.3 ± 8
581	2:19:0 7.29	57:07:34.8	0.4	4.2 ± 3	12.7 ± 8
582	2:19:0 7.31	57:05:35.4	0.7	7.2 ± 3	21.7 ± 9
583	2:19:0 7.38	57:07:23.0	0.3	7.8 ± 3	23.3 ± 10
584	2:19:0 7.42	57:04:47.3	0.4	5.4 ± 3	16.2 ± 8
585	2:19:0 7.57	57:12:33.7	1.0	21.5 ± 6	64.7 ± 20
586	2:19:0 7.56	57:06:55.7	1.0	6.5 ± 3	19.5 ± 9
587	2:19:0 7.57	57:07:47.5	0.9	9.5 ± 4	28.7 ± 11

Table 1. continued.

X source ID	RA (J2000)	DEC (J2000)	Pos. err. (″)	Count rate (10^{-5} cts s^{-1})	Flux (10^{-8} ph s^{-1} cm^{-2})
588	2:19:0 7.58	57:09:13.4	0.7	5.2 ± 2	15.8 ± 7
589	2:19:0 7.58	57:06:09.0	0.4	36.0 ± 5	108.2 ± 14
590	2:19:0 7.66	57:11:03.1	1.1	14.3 ± 5	42.8 ± 15
591	2:19:0 7.77	57:06:34.8	0.5	5.2 ± 3	15.7 ± 8
592	2:19:0 7.83	57:06:45.0	0.4	14.6 ± 5	43.7 ± 15
593	2:19:0 7.90	57:03:28.0	0.6	11.8 ± 4	35.4 ± 13
594	2:19:0 7.95	57:08:26.8	0.4	5.0 ± 3	15.1 ± 8
595	2:19:0 7.96	57:06:51.4	0.3	8.6 ± 3	25.7 ± 10
596	2:19:0 7.98	57:08:52.9	0.4	5.9 ± 3	17.7 ± 9
597	2:19:0 8.01	57:05:32.3	0.5	4.3 ± 2	12.9 ± 7
598	2:19:0 8.06	57:11:12.5	1.7	11.6 ± 4	34.8 ± 13
599	2:19:0 8.06	57:09:55.9	0.3	6.3 ± 3	18.9 ± 9
600	2:19:0 8.08	57:06:08.4	0.3	17.0 ± 3	51.0 ± 10
601	2:19:0 8.13	57:08:41.0	1.0	6.3 ± 3	19.0 ± 8
602	2:19:0 8.15	57:05:11.1	0.4	3.9 ± 2	11.6 ± 6
603	2:19:0 8.17	57:09:12.1	0.7	5.6 ± 2	16.9 ± 7
604	2:19:0 8.19	57:07:05.1	0.5	4.9 ± 2	14.9 ± 7
605	2:19:0 8.21	57:03:26.9	0.4	5.8 ± 3	17.3 ± 10
606	2:19:0 8.21	57:03:48.2	1.0	7.3 ± 3	22.0 ± 9
607	2:19:0 8.40	57:10:39.5	0.4	3.9 ± 3	11.7 ± 8
608	2:19:0 8.62	57:11:20.6	0.6	34.3 ± 5	103.1 ± 16
609	2:19:0 8.61	57:05:16.8	0.6	7.0 ± 3	20.9 ± 8
610	2:19:0 8.66	57:03:48.8	1.2	12.8 ± 4	38.6 ± 13
611	2:19:0 8.71	57:06:20.4	0.5	5.5 ± 2	16.4 ± 7
612	2:19:0 8.73	57:07:51.7	0.5	9.1 ± 4	27.3 ± 13
613	2:19:0 8.76	57:10:24.7	0.6	8.6 ± 3	25.8 ± 10
614	2:19:0 8.78	57:08:43.3	0.5	6.5 ± 3	19.4 ± 9
615	2:19:0 8.79	57:04:16.4	0.7	5.9 ± 3	17.6 ± 8
616	2:19:0 8.86	57:06:58.7	0.3	28.5 ± 4	85.5 ± 13
617	2:19:0 8.91	57:03:57.1	0.4	22.6 ± 4	67.7 ± 13
618	2:19:0 8.94	57:10:13.0	0.4	7.0 ± 4	20.9 ± 13
619	2:19:0 9.07	57:08:34.9	0.5	4.2 ± 2	12.6 ± 7
620	2:19:0 9.07	57:07:19.9	0.4	11.4 ± 4	34.2 ± 11
621	2:19:0 9.13	57:05:56.7	0.7	5.5 ± 2	16.5 ± 7
622	2:19:0 9.21	57:04:36.3	0.5	5.2 ± 3	15.5 ± 8
623	2:19:0 9.29	57:08:06.2	0.4	7.6 ± 4	22.7 ± 13
624	2:19:0 9.35	57:07:55.9	0.4	15.8 ± 6	47.5 ± 18
625	2:19:0 9.37	57:07:32.9	0.5	16.6 ± 6	50.0 ± 17
626	2:19:0 9.46	57:08:45.8	0.7	5.7 ± 2	17.0 ± 7
627	2:19:0 9.48	57:09:55.5	0.9	6.7 ± 3	20.3 ± 8
628	2:19:0 9.48	57:08:17.9	0.4	4.3 ± 3	12.9 ± 8
629	2:19:0 9.65	57:02:33.5	0.8	5.1 ± 3	15.4 ± 8
630	2:19:0 9.78	57:15:21.3	1.9	32.3 ± 9	97.0 ± 27
631	2:19:0 9.80	57:06:22.6	0.4	4.2 ± 2	12.7 ± 6
632	2:19:0 9.86	57:12:12.1	1.0	8.3 ± 5	25.0 ± 14
633	2:19:0 9.84	57:08:20.1	0.5	4.9 ± 2	14.8 ± 7
634	2:19:10.07	57:06:42.5	0.4	4.0 ± 2	11.9 ± 7
635	2:19:10.09	57:06:11.3	0.4	9.1 ± 3	27.4 ± 10
636	2:19:10.15	57:04:46.1	0.5	19.7 ± 6	59.1 ± 17
637	2:19:10.17	57:07:36.7	0.3	6.0 ± 3	17.9 ± 8
638	2:19:10.21	57:06:09.3	0.4	13.1 ± 4	39.3 ± 13
639	2:19:10.29	57:09:08.9	0.4	22.0 ± 4	65.9 ± 11
640	2:19:10.34	57:07:37.5	0.4	27.2 ± 5	81.7 ± 14
641	2:19:10.43	57:11:37.7	1.0	7.6 ± 4	22.9 ± 11
642	2:19:10.41	57:05:33.1	0.4	3.8 ± 2	11.5 ± 7
643	2:19:10.47	57:07:50.0	0.3	29.4 ± 5	88.2 ± 14
644	2:19:10.55	57:00:58.2	1.3	16.1 ± 8	48.3 ± 25
645	2:19:10.59	57:03:55.5	0.7	6.9 ± 3	20.6 ± 9
646	2:19:10.63	57:02:28.8	1.0	6.5 ± 3	19.5 ± 9
647	2:19:10.81	57:07:12.6	0.5	5.1 ± 2	15.5 ± 7
648	2:19:10.82	57:05:25.4	0.6	7.9 ± 3	23.8 ± 9
649	2:19:10.92	57:09:40.3	0.8	5.5 ± 3	16.4 ± 8
650	2:19:10.99	57:07:30.7	0.5	5.4 ± 2	16.2 ± 7
651	2:19:11.02	57:09:29.1	0.5	11.6 ± 4	34.9 ± 11
652	2:19:11.01	57:04:43.8	0.5	12.7 ± 4	38.2 ± 12
653	2:19:11.07	57:09:32.0	0.4	31.4 ± 5	94.2 ± 14
654	2:19:11.17	57:15:55.2	1.8	38.1 ± 11	114.5 ± 33
655	2:19:11.23	57:16:14.0	2.6	15.8 ± 7	47.5 ± 21
656	2:19:11.27	57:08:23.5	0.4	15.5 ± 5	46.6 ± 15
657	2:19:11.36	57:09:52.7	0.6	10.5 ± 4	31.4 ± 11
658	2:19:11.47	57:07:24.8	0.3	6.8 ± 3	20.6 ± 10
659	2:19:11.54	57:08:13.5	0.4	7.0 ± 5	21.1 ± 15
660	2:19:11.64	57:06:45.5	0.4	4.8 ± 2	14.5 ± 7
661	2:19:11.78	57:07:01.2	0.6	6.3 ± 3	18.9 ± 8
662	2:19:11.80	57:07:29.0	0.9	7.7 ± 3	23.2 ± 9
663	2:19:11.90	57:10:44.7	0.8	11.2 ± 4	33.6 ± 12
664	2:19:11.90	57:07:06.0	0.5	4.9 ± 3	14.7 ± 8
665	2:19:11.94	57:10:22.9	0.4	3.8 ± 3	11.5 ± 8
666	2:19:11.95	57:09:44.5	0.5	6.9 ± 3	20.8 ± 9
667	2:19:12.03	57:04:38.6	0.5	4.9 ± 2	14.7 ± 7
668	2:19:12.13	57:07:44.0	0.4	18.7 ± 3	56.3 ± 10
669	2:19:12.22	57:07:40.4	0.4	3.5 ± 2	10.6 ± 7
670	2:19:12.31	57:05:07.1	0.4	11.1 ± 4	33.5 ± 12
671	2:19:12.41	57:06:44.5	0.4	3.6 ± 3	10.9 ± 8

Table 1. continued.

X source ID	RA (J2000)	DEC (J2000)	Pos. err. (″)	Count rate (10^{-5} cts s^{-1})	Flux (10^{-8} ph s^{-1} cm^{-2})
672	2:19:12.46	57:08:08.5	0.5	9.9 ± 5	29.7 ± 14
673	2:19:12.50	57:06:55.6	0.6	7.8 ± 3	23.4 ± 9
674	2:19:12.54	57:08:20.5	0.4	17.8 ± 6	53.4 ± 17
675	2:19:12.63	57:12:12.7	0.9	27.0 ± 4	81.1 ± 13
676	2:19:12.69	57:03:51.9	0.4	34.4 ± 6	103.2 ± 18
677	2:19:12.74	57:03:54.2	0.6	4.5 ± 2	13.4 ± 7
678	2:19:12.93	57:12:22.2	1.0	19.5 ± 6	58.5 ± 18
679	2:19:12.98	57:07:17.4	0.4	10.6 ± 4	32.0 ± 11
680	2:19:13.07	57:12:35.1	1.0	27.7 ± 8	83.2 ± 23
681	2:19:13.10	57:09:42.5	0.4	28.5 ± 4	85.7 ± 13
682	2:19:13.25	57:10:21.2	0.6	8.1 ± 3	24.4 ± 10
683	2:19:13.23	57:03:59.9	1.3	8.5 ± 4	25.4 ± 11
684	2:19:13.56	57:11:47.9	1.0	8.4 ± 4	25.2 ± 13
685	2:19:13.78	57:06:39.4	0.7	6.9 ± 3	20.8 ± 9
686	2:19:13.88	57:06:47.8	0.5	15.0 ± 5	45.0 ± 14
687	2:19:13.87	57:05:32.2	0.7	5.3 ± 2	16.0 ± 7
688	2:19:13.97	57:10:09.1	0.5	16.8 ± 5	50.5 ± 15
689	2:19:13.96	57:06:25.8	0.7	4.8 ± 2	14.4 ± 7
690	2:19:14.05	57:06:53.5	0.5	4.5 ± 2	13.5 ± 7
691	2:19:14.15	57:11:04.9	1.3	76.2 ± 8	228.8 ± 23
692	2:19:14.14	57:01:47.5	0.9	84.0 ± 8	252.2 ± 24
693	2:19:14.45	57:04:12.1	0.5	4.9 ± 2	14.8 ± 7
694	2:19:14.58	57:07:15.4	0.4	3.7 ± 2	11.2 ± 7
695	2:19:14.58	57:06:06.4	0.4	11.9 ± 4	35.8 ± 13
696	2:19:14.59	57:06:45.6	0.3	6.1 ± 3	18.2 ± 8
697	2:19:14.69	57:07:51.0	0.5	14.9 ± 5	44.7 ± 14
698	2:19:14.72	57:06:50.4	0.5	15.0 ± 4	44.9 ± 13
699	2:19:14.85	57:10:11.1	0.7	15.0 ± 5	44.9 ± 15
700	2:19:14.98	57:09:21.7	0.7	15.1 ± 5	45.3 ± 14
701	2:19:15.01	57:09:04.8	0.5	14.7 ± 5	44.3 ± 14
702	2:19:15.10	57:12:45.0	1.6	43.3 ± 6	130.0 ± 19
703	2:19:15.22	57:13:06.4	1.4	27.6 ± 8	82.9 ± 23
704	2:19:15.27	57:11:23.3	0.7	21.5 ± 4	64.5 ± 12
705	2:19:15.29	57:03:59.6	0.7	5.6 ± 3	16.9 ± 8
706	2:19:15.44	57:05:38.1	0.8	13.9 ± 4	41.7 ± 13
707	2:19:15.51	57:10:39.6	0.5	23.2 ± 4	69.8 ± 13
708	2:19:15.59	57:08:41.0	0.5	4.4 ± 2	13.2 ± 7
709	2:19:15.61	57:06:54.1	0.4	3.7 ± 2	11.2 ± 6
710	2:19:15.84	57:13:02.8	1.2	12.4 ± 5	37.1 ± 15
711	2:19:15.87	57:02:59.5	1.3	8.6 ± 3	25.8 ± 10
712	2:19:15.88	57:03:15.3	0.7	5.4 ± 4	16.3 ± 11
713	2:19:15.92	57:06:53.2	0.3	25.3 ± 4	76.1 ± 12
714	2:19:15.94	57:09:03.2	0.5	15.4 ± 5	46.2 ± 15
715	2:19:16.01	57:03:46.1	0.9	23.2 ± 5	69.7 ± 14
716	2:19:16.08	57:09:19.8	0.4	4.2 ± 3	12.6 ± 8
717	2:19:16.19	57:10:44.8	0.9	6.5 ± 3	19.6 ± 8
718	2:19:16.17	57:05:23.2	0.7	5.5 ± 3	16.6 ± 8
719	2:19:16.37	57:05:46.8	0.5	4.0 ± 2	12.1 ± 6
720	2:19:16.55	57:12:31.5	1.5	16.7 ± 5	50.3 ± 16
721	2:19:16.53	57:05:33.2	0.4	7.7 ± 3	23.2 ± 9
722	2:19:16.64	57:13:40.6	1.1	15.0 ± 5	45.1 ± 16
723	2:19:16.70	57:07:13.5	0.4	3.9 ± 2	11.8 ± 7
724	2:19:16.74	57:02:01.2	0.6	132.9 ± 11	399.1 ± 33
725	2:19:16.85	57:04:19.5	0.5	6.6 ± 3	19.7 ± 8
726	2:19:16.89	57:03:10.4	0.9	22.5 ± 6	67.7 ± 19
727	2:19:16.95	57:04:31.2	0.5	14.8 ± 4	44.4 ± 13
728	2:19:17.01	57:04:11.3	1.1	14.7 ± 5	44.0 ± 14
729	2:19:17.12	57:14:58.3	1.2	46.4 ± 8	139.5 ± 23
730	2:19:17.14	57:09:07.6	0.5	16.0 ± 5	48.0 ± 15
731	2:19:17.17	57:08:41.2	0.4	6.8 ± 3	20.3 ± 8
732	2:19:17.30	57:08:22.0	0.4	17.9 ± 7	53.7 ± 22
733	2:19:17.29	57:05:54.6	0.6	8.6 ± 3	25.7 ± 10
734	2:19:17.33	57:02:43.0	2.1	20.8 ± 6	62.5 ± 19
735	2:19:17.41	57:03:03.2	1.2	9.6 ± 4	28.8 ± 11
736	2:19:17.45	57:07:20.0	0.7	6.2 ± 3	18.6 ± 8
737	2:19:17.45	57:07:11.4	0.4	4.4 ± 2	13.4 ± 7
738	2:19:17.52	57:08:46.0	0.7	7.6 ± 3	22.7 ± 9
739	2:19:17.56	57:08:07.5	0.4	53.5 ± 6	160.5 ± 19
740	2:19:17.75	57:09:02.0	0.3	99.4 ± 9	298.5 ± 26
741	2:19:17.90	57:10:25.7	0.7	7.9 ± 3	23.6 ± 10
742	2:19:17.96	57:05:09.4	0.9	8.2 ± 3	24.5 ± 10
743	2:19:18.07	57:07:33.3	0.5	6.0 ± 3	17.9 ± 8
744	2:19:18.23	57:10:23.3	0.6	11.7 ± 4	35.0 ± 12
745	2:19:18.18	57:01:32.6	1.3	10.0 ± 5	30.0 ± 14
746	2:19:18.26	57:05:59.7	0.5	7.1 ± 3	21.3 ± 9
747	2:19:18.33	57:10:36.4	0.7	24.3 ± 4	73.1 ± 13
748	2:19:18.35	57:08:35.6	0.7	6.0 ± 3	18.0 ± 8
749	2:19:18.37	57:04:56.0	0.5	6.1 ± 3	18.2 ± 9
750	2:19:18.63	57:09:49.7	0.4	7.1 ± 3	21.4 ± 9
751	2:19:18.70	57:05:10.5	0.7	6.1 ± 3	18.2 ± 8
752	2:19:18.74	57:07:59.5	0.5	18.8 ± 3	56.4 ± 10
753	2:19:18.69	57:01:38.9	0.9	32.7 ± 6	98.1 ± 19
754	2:19:18.82	57:09:57.0	0.7	5.0 ± 2	15.1 ± 7
755	2:19:18.87	57:07:33.7	0.7	5.5 ± 2	16.6 ± 7

Table 1. continued.

X source ID	RA (J2000)	DEC (J2000)	Pos. err. (″)	Count rate (10^{-5} cts s^{-1})	Flux (10^{-8} ph s^{-1} cm^{-2})
756	2:19:18.97	57:09:15.9	0.6	7.7 ± 3	23.0 ± 9
757	2:19:19.05	57:12:54.4	1.3	10.8 ± 5	32.4 ± 15
758	2:19:19.03	57:08:41.9	0.7	6.8 ± 3	20.5 ± 9
759	2:19:19.13	57:03:18.8	1.1	15.1 ± 5	45.3 ± 15
760	2:19:19.24	57:07:59.7	0.7	5.0 ± 2	15.1 ± 7
761	2:19:19.27	57:00:13.0	3.1	25.5 ± 8	76.5 ± 25
762	2:19:19.52	57:14:29.0	1.8	36.8 ± 7	110.4 ± 21
763	2:19:19.48	57:08:04.7	0.4	4.2 ± 3	12.5 ± 8
764	2:19:19.58	57:07:57.4	0.7	16.1 ± 5	48.3 ± 14
765	2:19:19.62	57:08:41.5	0.5	6.5 ± 3	19.4 ± 9
766	2:19:19.68	57:12:07.9	1.1	18.2 ± 6	54.7 ± 19
767	2:19:19.61	57:03:26.4	1.1	13.8 ± 5	41.4 ± 14
768	2:19:19.78	57:05:24.5	0.5	12.6 ± 4	38.0 ± 12
769	2:19:19.80	57:07:03.3	0.5	6.3 ± 3	18.9 ± 8
770	2:19:19.86	57:04:35.8	0.5	15.6 ± 5	47.0 ± 14
771	2:19:20.03	57:08:45.9	0.8	11.8 ± 4	35.5 ± 12
772	2:19:20.33	57:11:50.1	1.6	46.3 ± 8	139.2 ± 24
773	2:19:20.34	57:07:33.7	0.6	8.0 ± 3	24.2 ± 9
774	2:19:20.37	57:08:02.7	0.7	4.7 ± 2	14.2 ± 7
775	2:19:20.44	57:06:35.5	0.7	5.6 ± 3	16.9 ± 8
776	2:19:20.43	57:04:39.1	0.5	20.9 ± 6	62.7 ± 18
777	2:19:20.56	57:09:25.1	0.4	25.6 ± 4	76.7 ± 13
778	2:19:20.87	57:07:09.6	0.5	4.9 ± 2	14.8 ± 7
779	2:19:20.93	57:13:12.1	2.0	25.9 ± 8	77.8 ± 23
780	2:19:20.94	57:12:01.1	0.9	7.7 ± 3	23.2 ± 10
781	2:19:20.92	57:05:26.9	0.7	5.0 ± 2	14.9 ± 7
782	2:19:20.98	57:09:49.0	0.8	12.1 ± 4	36.4 ± 12
783	2:19:21.07	57:07:28.8	0.6	10.7 ± 4	32.2 ± 11
784	2:19:21.06	57:05:04.5	1.0	6.4 ± 3	19.1 ± 9
785	2:19:21.23	57:09:56.0	0.6	8.0 ± 3	24.0 ± 9
786	2:19:21.25	57:07:48.9	0.5	23.3 ± 4	70.1 ± 12
787	2:19:21.38	57:05:14.5	0.5	22.7 ± 4	68.3 ± 12
788	2:19:21.69	57:13:13.8	1.8	13.3 ± 5	39.9 ± 15
789	2:19:21.72	57:11:12.6	1.0	8.9 ± 5	26.6 ± 14
790	2:19:21.82	57:07:06.9	0.4	3.8 ± 2	11.6 ± 7
791	2:19:21.93	57:02:07.1	1.1	18.0 ± 6	54.1 ± 17
792	2:19:22.03	57:10:25.6	0.8	31.0 ± 5	93.1 ± 15
793	2:19:22.05	57:02:59.3	0.9	30.2 ± 6	90.8 ± 17
794	2:19:22.16	57:04:15.7	0.8	10.1 ± 4	30.2 ± 11
795	2:19:22.26	57:13:55.5	1.3	76.2 ± 8	228.9 ± 23
796	2:19:22.19	57:06:20.9	0.5	4.4 ± 2	13.1 ± 7
797	2:19:22.42	57:09:08.0	0.5	28.9 ± 5	86.8 ± 16
798	2:19:22.65	57:13:09.5	1.8	35.5 ± 7	106.5 ± 20
799	2:19:22.65	57:09:52.6	0.7	15.3 ± 5	45.9 ± 14
800	2:19:22.77	57:06:21.3	0.4	55.4 ± 6	166.3 ± 19
801	2:19:22.98	57:10:58.7	0.9	9.9 ± 4	29.8 ± 12
802	2:19:23.00	57:11:26.9	1.0	7.2 ± 5	21.7 ± 15
803	2:19:23.21	57:06:11.3	0.4	3.7 ± 2	11.1 ± 7
804	2:19:23.24	57:04:58.9	0.7	4.8 ± 2	14.3 ± 7
805	2:19:23.34	57:11:24.2	1.2	27.4 ± 5	82.4 ± 15
806	2:19:23.27	57:01:30.8	1.9	11.2 ± 5	33.6 ± 14
807	2:19:23.39	57:05:04.7	0.5	6.1 ± 3	18.5 ± 8
808	2:19:23.49	57:04:26.4	1.6	14.8 ± 5	44.4 ± 15
809	2:19:23.53	57:02:57.6	1.0	7.9 ± 5	23.8 ± 14
810	2:19:23.58	57:05:35.5	0.4	3.8 ± 2	11.5 ± 7
811	2:19:23.79	57:03:01.0	1.3	7.8 ± 3	23.5 ± 10
812	2:19:23.99	57:09:08.1	0.7	6.1 ± 3	18.4 ± 8
813	2:19:24.04	57:10:01.0	1.0	18.5 ± 6	55.6 ± 17
814	2:19:24.00	57:03:54.8	0.7	6.5 ± 4	19.5 ± 11
815	2:19:24.00	57:02:40.1	1.0	17.8 ± 5	53.6 ± 16
816	2:19:24.01	57:00:15.9	1.3	87.5 ± 9	262.8 ± 28
817	2:19:24.06	57:01:36.4	1.3	27.7 ± 5	83.0 ± 16
818	2:19:24.28	57:04:18.6	1.6	12.6 ± 4	37.8 ± 13
819	2:19:24.34	57:05:56.0	0.8	11.0 ± 4	33.0 ± 11
820	2:19:24.40	57:03:20.2	1.0	7.4 ± 5	22.3 ± 14
821	2:19:24.52	57:09:00.7	0.6	10.1 ± 4	30.2 ± 11
822	2:19:24.65	57:15:36.4	3.3	22.9 ± 8	68.8 ± 25
823	2:19:24.56	57:06:38.9	0.7	5.9 ± 3	17.7 ± 8
824	2:19:24.62	57:03:12.7	1.1	16.4 ± 5	49.3 ± 16
825	2:19:24.77	57:10:18.7	1.0	20.4 ± 7	61.2 ± 20
826	2:19:25.06	57:06:39.7	3.1	17.9 ± 6	53.7 ± 18
827	2:19:25.16	57:09:47.9	0.5	66.0 ± 7	198.3 ± 20
828	2:19:25.23	57:02:37.2	1.0	16.8 ± 5	50.4 ± 16
829	2:19:25.27	57:06:09.9	1.3	7.6 ± 3	23.0 ± 9
830	2:19:25.48	57:06:41.3	0.9	9.5 ± 4	28.6 ± 11
831	2:19:25.60	57:09:13.1	0.7	6.2 ± 3	18.7 ± 10
832	2:19:25.61	57:08:20.0	0.7	14.6 ± 5	43.7 ± 14
833	2:19:25.61	57:05:46.9	0.9	9.8 ± 4	29.3 ± 11
834	2:19:25.80	57:09:24.0	0.9	22.7 ± 4	68.1 ± 13
835	2:19:25.96	57:04:02.6	0.8	5.3 ± 3	15.9 ± 8
836	2:19:26.07	57:05:45.5	0.6	8.2 ± 3	24.6 ± 9
837	2:19:26.19	57:05:11.1	0.8	12.8 ± 4	38.5 ± 13
838	2:19:26.45	57:08:54.0	0.8	5.6 ± 3	16.9 ± 10
839	2:19:26.54	57:06:22.2	0.5	13.7 ± 4	41.1 ± 13

Table 1. continued.

X source ID	RA (J2000)	DEC (J2000)	Pos. err. (″)	Count rate (10^{-5} cts s^{-1})	Flux (10^{-8} ph s^{-1} cm^{-2})
840	2:19:26.62	57:09:37.1	1.1	15.2 ± 5	45.6 ± 15
841	2:19:26.67	57:11:05.0	1.2	9.8 ± 4	29.5 ± 11
842	2:19:26.94	57:07:00.0	0.5	18.2 ± 5	54.7 ± 16
843	2:19:27.13	57:08:55.4	0.7	6.4 ± 4	19.3 ± 11
844	2:19:27.28	57:06:31.5	0.7	7.2 ± 3	21.6 ± 9
845	2:19:27.32	57:05:33.2	1.2	8.9 ± 3	26.6 ± 10
846	2:19:27.42	57:08:33.9	0.7	8.3 ± 4	25.0 ± 13
847	2:19:27.37	57:03:59.9	1.0	7.3 ± 3	21.9 ± 10
848	2:19:27.47	57:07:45.1	0.7	6.4 ± 3	19.3 ± 8
849	2:19:27.47	57:08:17.2	0.8	14.1 ± 4	42.3 ± 13
850	2:19:27.48	57:02:31.5	0.9	8.0 ± 4	24.1 ± 12
851	2:19:27.53	57:06:03.2	0.6	11.4 ± 4	34.1 ± 12
852	2:19:27.77	57:09:00.8	0.7	7.0 ± 3	21.0 ± 10
853	2:19:27.96	57:04:37.5	1.0	7.0 ± 3	20.9 ± 9
854	2:19:28.09	57:07:47.0	0.7	5.7 ± 3	17.2 ± 8
855	2:19:28.13	57:09:48.9	1.2	11.0 ± 4	33.0 ± 12
856	2:19:28.14	57:08:55.2	1.3	10.2 ± 4	30.5 ± 12
857	2:19:28.26	57:07:04.3	0.9	9.8 ± 4	29.4 ± 11
858	2:19:28.83	57:13:48.8	2.6	39.0 ± 11	117.2 ± 32
859	2:19:28.78	57:07:53.1	1.5	13.6 ± 4	40.8 ± 13
860	2:19:28.91	57:10:55.4	1.4	21.0 ± 6	63.0 ± 19
861	2:19:28.97	57:10:39.4	1.1	14.9 ± 5	44.8 ± 14
862	2:19:28.93	57:04:51.2	0.7	5.0 ± 3	15.1 ± 8
863	2:19:28.89	57:01:15.1	1.3	11.6 ± 5	34.8 ± 16
864	2:19:28.99	57:05:04.0	0.7	20.2 ± 6	60.8 ± 19
865	2:19:29.05	57:09:16.1	0.9	25.8 ± 5	77.6 ± 14
866	2:19:29.07	57:09:40.0	1.0	6.7 ± 3	20.0 ± 9
867	2:19:29.25	57:09:48.1	0.9	19.6 ± 4	58.8 ± 11
868	2:19:29.37	57:04:25.3	1.1	18.6 ± 6	55.8 ± 18
869	2:19:29.45	57:05:09.7	1.1	13.6 ± 4	40.8 ± 14
870	2:19:29.51	57:06:53.8	1.2	9.3 ± 4	28.1 ± 11
871	2:19:29.66	57:05:42.9	0.6	27.0 ± 4	81.0 ± 13
872	2:19:29.72	57:10:14.3	1.0	21.0 ± 6	63.1 ± 19
873	2:19:29.74	57:07:47.7	0.9	23.4 ± 4	70.3 ± 12
874	2:19:30.21	57:10:44.8	1.3	8.7 ± 3	26.0 ± 10
875	2:19:30.40	57:07:58.8	0.7	19.2 ± 6	57.6 ± 17
876	2:19:30.47	57:10:18.3	1.0	21.3 ± 6	64.1 ± 19
877	2:19:30.48	57:01:09.2	1.6	17.5 ± 6	52.6 ± 17
878	2:19:30.60	57:04:45.0	0.8	30.4 ± 5	91.3 ± 14
879	2:19:31.06	57:14:33.5	4.2	30.2 ± 10	90.6 ± 29
880	2:19:30.99	57:09:22.5	1.4	21.8 ± 6	65.5 ± 19
881	2:19:31.10	57:12:26.4	1.5	23.4 ± 7	70.4 ± 22
882	2:19:31.17	57:15:19.3	2.1	72.1 ± 10	216.7 ± 29
883	2:19:31.18	57:10:31.9	0.8	12.2 ± 5	36.5 ± 14
884	2:19:31.09	57:01:45.3	1.3	30.9 ± 6	92.9 ± 17
885	2:19:31.32	57:04:27.5	1.0	7.1 ± 4	21.4 ± 11
886	2:19:31.45	57:09:11.1	0.7	20.8 ± 4	62.4 ± 12
887	2:19:31.50	57:07:20.4	0.7	17.7 ± 5	53.3 ± 16
888	2:19:31.58	57:08:57.0	0.9	37.3 ± 7	112.0 ± 21
889	2:19:31.60	57:05:02.1	0.7	45.9 ± 5	137.8 ± 17
890	2:19:31.63	57:05:05.4	0.7	5.8 ± 3	17.4 ± 10
891	2:19:31.80	57:08:00.1	1.0	5.6 ± 3	16.9 ± 8
892	2:19:31.85	57:07:44.6	1.7	9.9 ± 4	29.8 ± 11
893	2:19:32.05	57:07:18.5	0.9	23.4 ± 7	70.3 ± 20
894	2:19:32.15	57:06:26.2	0.9	8.0 ± 4	24.0 ± 11
895	2:19:32.25	57:06:49.0	0.6	76.5 ± 7	229.9 ± 21
896	2:19:32.27	57:03:09.2	0.9	28.6 ± 5	85.8 ± 15
897	2:19:32.78	57:05:43.7	0.7	53.8 ± 6	161.7 ± 19
898	2:19:32.79	57:03:57.7	0.8	13.0 ± 5	39.1 ± 15
899	2:19:32.81	57:04:47.3	0.8	10.6 ± 4	31.8 ± 13
900	2:19:32.93	57:06:01.5	0.9	17.4 ± 3	52.2 ± 10
901	2:19:33.13	57:09:43.4	0.8	17.9 ± 6	53.9 ± 18
902	2:19:33.20	57:08:03.0	1.3	8.3 ± 3	24.9 ± 10
903	2:19:33.59	57:07:24.0	0.7	18.1 ± 4	54.3 ± 11
904	2:19:33.81	57:06:44.7	1.2	8.7 ± 3	26.1 ± 10
905	2:19:33.99	57:11:29.1	1.4	9.3 ± 5	28.1 ± 15
906	2:19:33.99	57:11:21.1	1.2	10.9 ± 4	32.8 ± 13
907	2:19:34.08	57:15:28.2	3.0	33.4 ± 11	100.4 ± 32
908	2:19:34.00	57:06:21.0	1.1	14.4 ± 5	43.1 ± 14
909	2:19:33.98	57:03:30.9	0.9	21.8 ± 4	65.4 ± 13
910	2:19:34.72	57:13:44.0	2.0	28.1 ± 8	84.5 ± 25
911	2:19:34.62	57:05:05.8	0.9	25.3 ± 7	76.0 ± 21
912	2:19:35.25	57:04:14.4	1.3	10.2 ± 4	30.6 ± 13
913	2:19:35.46	57:11:18.4	1.0	20.6 ± 6	61.8 ± 18
914	2:19:35.44	57:07:00.6	2.3	14.2 ± 5	42.7 ± 15
915	2:19:35.51	57:02:10.7	1.6	14.6 ± 5	43.9 ± 15
916	2:19:35.62	57:03:53.3	1.3	9.1 ± 4	27.2 ± 11
917	2:19:36.13	57:08:29.1	1.2	9.4 ± 3	28.3 ± 10
918	2:19:36.29	57:06:18.8	0.6	45.4 ± 6	136.2 ± 18
919	2:19:36.50	57:02:52.9	2.3	17.8 ± 6	53.6 ± 18
920	2:19:36.67	57:08:22.4	1.1	11.4 ± 4	34.2 ± 12
921	2:19:36.66	57:06:30.9	1.1	12.6 ± 4	37.9 ± 13
922	2:19:36.80	57:03:16.3	1.4	28.2 ± 8	84.6 ± 24
923	2:19:37.35	57:10:29.5	1.3	8.6 ± 4	25.7 ± 11

Table 1. continued.

X source ID	RA (J2000)	DEC (J2000)	Pos. err. (″)	Count rate (10^{-5} cts s^{-1})	Flux (10^{-8} ph s^{-1} cm^{-2})
924	2:19:37.35	57:02:15.8	1.2	11.2 ± 5	33.8 ± 15
925	2:19:37.66	57:09:36.0	1.8	10.8 ± 4	32.5 ± 13
926	2:19:37.62	57:04:37.2	0.9	10.2 ± 4	30.7 ± 13
927	2:19:37.83	57:13:27.9	2.4	16.5 ± 6	49.5 ± 19
928	2:19:37.77	57:04:27.4	1.0	8.1 ± 4	24.4 ± 13
929	2:19:38.14	57:12:33.3	1.9	29.4 ± 8	88.3 ± 25
930	2:19:38.06	57:07:04.4	1.0	21.0 ± 6	62.9 ± 18
931	2:19:38.11	57:08:07.4	1.0	7.2 ± 3	21.5 ± 9
932	2:19:38.57	57:06:43.8	0.9	11.0 ± 6	32.9 ± 19
933	2:19:38.53	57:01:12.8	2.2	20.7 ± 7	62.1 ± 21
934	2:19:39.02	57:06:52.9	0.9	8.4 ± 3	25.3 ± 10
935	2:19:39.40	57:09:45.1	1.4	31.3 ± 9	93.9 ± 26
936	2:19:39.68	57:03:34.9	0.9	112.3 ± 9	337.2 ± 27
937	2:19:40.21	57:09:26.5	1.6	12.6 ± 5	37.9 ± 14
938	2:19:40.15	57:03:54.6	1.4	9.1 ± 4	27.4 ± 13
939	2:19:40.18	57:01:10.5	2.3	18.4 ± 7	55.3 ± 20
940	2:19:40.49	57:05:14.2	1.0	22.8 ± 7	68.4 ± 20
941	2:19:40.52	57:04:48.1	1.3	10.8 ± 5	32.5 ± 16
942	2:19:40.55	57:05:06.4	1.0	6.9 ± 4	20.7 ± 12
943	2:19:40.76	57:07:04.9	1.0	6.3 ± 3	18.9 ± 9
944	2:19:41.04	57:05:19.9	0.8	14.0 ± 5	41.9 ± 16
945	2:19:41.14	57:07:52.6	1.0	7.2 ± 3	21.8 ± 10
946	2:19:41.63	57:05:02.4	1.8	11.7 ± 5	35.2 ± 14
947	2:19:41.71	57:06:12.9	0.9	25.6 ± 5	77.0 ± 14
948	2:19:41.78	57:08:33.1	1.4	7.8 ± 4	23.3 ± 12
949	2:19:42.00	57:08:04.3	0.8	30.3 ± 5	90.9 ± 15
950	2:19:42.21	57:06:42.1	1.4	21.8 ± 6	65.3 ± 19
951	2:19:42.89	57:03:26.2	1.0	242.1 ± 14	727.1 ± 41
952	2:19:43.12	57:10:55.5	0.9	104.9 ± 10	315.1 ± 29
953	2:19:43.08	57:06:01.7	0.8	166.8 ± 12	500.8 ± 37
954	2:19:43.28	57:02:01.6	1.7	16.7 ± 8	50.1 ± 24
955	2:19:43.65	57:02:14.1	1.8	35.1 ± 7	105.4 ± 20
956	2:19:43.72	57:02:52.6	1.5	22.4 ± 7	67.2 ± 22
957	2:19:44.60	57:10:47.5	1.6	14.1 ± 5	42.4 ± 16
958	2:19:44.82	57:05:00.2	1.6	17.7 ± 6	53.2 ± 18
959	2:19:45.49	57:10:24.2	1.1	60.5 ± 8	181.7 ± 23
960	2:19:45.67	57:09:34.9	1.4	10.1 ± 5	30.2 ± 16
961	2:19:45.53	57:02:53.4	1.7	34.3 ± 6	102.9 ± 19
962	2:19:46.06	57:07:53.4	3.1	19.8 ± 7	59.5 ± 20
963	2:19:46.03	57:05:46.9	1.6	44.2 ± 7	132.6 ± 20
964	2:19:46.30	57:12:07.1	2.7	40.5 ± 11	121.6 ± 34
965	2:19:46.49	57:06:39.9	1.3	9.3 ± 4	27.9 ± 13
966	2:19:46.53	57:04:44.8	1.2	41.7 ± 6	125.1 ± 19
967	2:19:46.72	57:11:31.8	2.2	19.8 ± 7	59.6 ± 20
968	2:19:47.35	57:03:56.4	1.8	35.7 ± 6	107.1 ± 19
969	2:19:47.62	57:08:44.7	1.7	38.5 ± 6	115.7 ± 19
970	2:19:47.84	57:08:11.9	1.2	12.0 ± 6	36.1 ± 18
971	2:19:47.89	57:02:22.2	1.4	28.4 ± 8	85.4 ± 25
972	2:19:48.86	57:00:52.3	2.5	20.3 ± 11	60.9 ± 33
973	2:19:48.90	57:02:17.6	1.5	55.8 ± 8	167.5 ± 25
974	2:19:49.49	57:10:19.0	1.7	14.1 ± 6	42.3 ± 19
975	2:19:49.84	57:03:19.5	1.4	25.6 ± 8	77.0 ± 23
976	2:19:50.30	57:06:16.9	2.3	15.5 ± 5	46.5 ± 16
977	2:19:50.43	57:10:49.8	2.5	32.0 ± 6	96.2 ± 18
978	2:19:50.46	57:05:17.5	1.2	119.8 ± 10	359.7 ± 31
979	2:19:50.83	57:11:55.5	1.8	102.4 ± 11	307.6 ± 32
980	2:19:51.21	57:07:35.5	1.7	13.0 ± 5	38.9 ± 14
981	2:19:51.55	57:10:00.3	2.1	23.8 ± 7	71.5 ± 22
982	2:19:51.52	57:08:34.8	2.4	14.6 ± 5	43.7 ± 16
983	2:19:51.81	57:03:40.7	1.8	12.9 ± 5	38.8 ± 16
984	2:19:51.92	57:06:46.0	1.2	35.9 ± 6	107.7 ± 18
985	2:19:52.79	57:07:12.9	1.2	122.9 ± 11	369.1 ± 32
986	2:19:53.00	57:06:53.9	1.9	30.8 ± 9	92.6 ± 26
987	2:19:53.06	57:08:16.9	1.7	14.2 ± 5	42.5 ± 16
988	2:19:53.27	57:09:27.4	1.9	13.6 ± 7	40.9 ± 21
989	2:19:53.95	57:06:17.7	1.5	18.5 ± 6	55.5 ± 18
990	2:19:54.09	57:04:52.0	2.4	15.9 ± 6	47.6 ± 18
991	2:19:54.27	57:03:48.4	1.8	13.3 ± 7	39.8 ± 20
992	2:19:55.46	57:10:27.0	2.2	73.7 ± 10	221.4 ± 31
993	2:19:55.80	57:06:50.9	1.7	14.0 ± 6	41.9 ± 17
994	2:19:56.11	57:02:50.7	1.8	143.1 ± 15	429.7 ± 44
995	2:19:57.62	57:07:29.0	2.3	15.2 ± 5	45.8 ± 16
996	2:19:58.13	57:03:14.8	1.9	42.8 ± 8	128.7 ± 25
997	2:19:58.99	57:03:37.3	3.0	33.0 ± 10	99.1 ± 31
998	2:19:59.11	57:02:30.6	2.1	36.3 ± 12	109.2 ± 36
999	2:20:0 0.47	57:03:30.2	2.1	33.1 ± 11	99.4 ± 32
1000	2:20:0 3.23	57:01:40.9	2.3	65.8 ± 11	197.6 ± 33
1001	2:20:0 3.90	57:02:01.5	2.6	60.2 ± 16	180.9 ± 49
1002	2:20:0 4.34	57:03:26.9	2.2	32.5 ± 11	97.5 ± 33

Table 2. X-ray source identified as h Per members.

X memb ID	X src ID	Moraux2013[a] ID	Currie2010[b] ID	$\log L_X^c$	m_V^d	m_I^d	$\log T_{\rm eff}$	$\log L_{\rm bol}/L_\odot$	Period[e] (d)	Mass[e] ($M_\odot$)	$\log\tau$ (d)
1	1	···	1056	$30.64^{+0.12}_{-0.16}$	17.763	16.274	3.777±0.010	0.46±0.02	···	···	···
2a	4	···	13614	$30.51^{+0.13}_{-0.19}$	12.410	···	4.242±0.106	3.01±0.25	···	···	···
2b	4	···	79	$30.53^{+0.14}_{-0.21}$	12.444	11.976	4.404±0.192	3.41±0.53	···	···	···
3	7	···	772	$30.59^{+0.12}_{-0.17}$	16.607	15.414	3.799±0.014	0.63±0.02	···	···	···
4	8	121	···	$30.70^{+0.09}_{-0.12}$	···	···	···	···	0.82	1.39	···
5	10	45	1019	$30.73^{+0.07}_{-0.09}$	17.739	16.067	3.701±0.018	0.48±0.03	2.55	1.33	2.33±0.25
6	13	···	1180	$30.21^{+0.15}_{-0.23}$	18.468	16.880	3.693±0.018	0.07±0.03	···	···	···
7	14	424	1476	$29.98^{+0.17}_{-0.27}$	20.298	18.109	3.621±0.014	−0.48±0.13	6.52	0.89	2.60±0.25
8	17	···	694	$30.61^{+0.10}_{-0.12}$	16.589	15.215	3.787±0.028	0.74±0.13	···	···	···
9	21	···	278	$29.95^{+0.18}_{-0.30}$	14.566	13.910	4.014±0.056	1.72±0.11	···	···	···
10	23	310	1875	$30.26^{+0.14}_{-0.20}$	21.984	19.146	3.553±0.008	−0.82±0.14	0.77	0.55	3.05±0.05
11	24	81	1028	$30.44^{+0.12}_{-0.16}$	17.552	16.116	3.769±0.014	0.43±0.02	0.46	1.33	1.55±0.22
12	28	189	1145	$30.57^{+0.07}_{-0.09}$	18.437	16.695	3.674±0.018	0.15±0.04	1.19	1.24	2.49±0.26
13	29	364	1205	$30.15^{+0.16}_{-0.24}$	18.716	17.054	3.760±0.011	0.22±0.02	3.88	1.19	1.70±0.17
14	32	250	1704	$30.26^{+0.18}_{-0.31}$	21.330	18.751	3.577±0.011	−0.68±0.14	0.55	0.66	3.05±0.09
15	34	···	405	$30.58^{+0.11}_{-0.14}$	15.300	14.509	3.923±0.031	1.31±0.02	···	···	···
16	36	26	···	$30.60^{+0.09}_{-0.11}$	···	···	···	···	0.13	1.18	···
17	38	···	1457	$29.99^{+0.16}_{-0.25}$	20.400	18.047	3.601±0.013	−0.44±0.14	···	···	···
18	39	501	1832	$30.05^{+0.15}_{-0.24}$	21.746	19.045	3.566±0.011	−0.79±0.14	0.54	0.56	3.05±0.05
19	43	···	1601	$30.30^{+0.14}_{-0.20}$	20.866	18.468	3.596±0.013	−0.60±0.14	···	···	···
20	46	509	1111	$30.62^{+0.07}_{-0.08}$	18.079	16.546	3.762±0.009	0.45±0.02	3.40	1.27	1.63±0.13
21	48	···	43	$30.51^{+0.07}_{-0.08}$	11.364	10.956	4.386±0.134	3.77±0.33	···	···	···
22	51	152	918	$30.63^{+0.11}_{-0.14}$	17.168	15.707	3.773±0.012	0.67±0.02	0.39	1.38	1.38±0.19
23	52	578	···	$30.22^{+0.13}_{-0.19}$	···	···	···	···	0.27	0.61	···
24	53	403	1473	$29.87^{+0.19}_{-0.33}$	20.114	18.115	3.644±0.013	−0.47±0.13	4.61	0.92	2.40±0.13
25	54	6	1084	$30.73^{+0.11}_{-0.14}$	18.157	16.396	3.764±0.013	0.57±0.02	0.36	1.29	1.58±0.20
26	55	194	1429	$30.01^{+0.17}_{-0.29}$	20.126	17.988	3.627±0.014	−0.42±0.13	0.82	0.95	2.57±0.22
27	56	···	207	$30.28^{+0.11}_{-0.16}$	13.980	13.474	4.073±0.053	1.95±0.12	···	···	···
28	59	···	13583	$30.48^{+0.06}_{-0.08}$	12.238	···	4.350±0.141	3.35±0.34	···	···	···
29	61	···	13569	$30.55^{+0.06}_{-0.07}$	10.579	9.873	4.381±0.082	4.06±0.20	···	···	···
30	63	···	13702	$30.22^{+0.13}_{-0.18}$	16.830	15.707	3.802±0.012	0.57±0.02	···	···	···
31	64	178	···	$30.27^{+0.14}_{-0.21}$	18.646	17.066	3.762±0.008	0.16±0.02	3.36	1.19	1.65±0.13
32	67	···	1827	$30.44^{+0.13}_{-0.18}$	22.148	18.986	3.540±0.004	−0.74±0.14	···	···	···
33	69	···	540	$30.30^{+0.14}_{-0.21}$	15.679	14.912	3.927±0.026	1.14±0.02	···	···	···
34	70	125	837	$30.42^{+0.12}_{-0.17}$	16.800	15.549	3.800±0.012	0.71±0.02	0.49	1.42	0.87±0.32
35	72	···	525	$30.15^{+0.15}_{-0.22}$	15.740	14.852	3.890±0.026	1.06±0.02	···	···	···
36	75	54	1030	$30.63^{+0.06}_{-0.08}$	17.543	16.134	3.766±0.007	0.42±0.02	0.67	1.33	1.58±0.11
37	76	153	1003	$30.28^{+0.12}_{-0.17}$	17.342	15.996	3.780±0.014	0.45±0.02	2.93	1.35	1.35±0.26
38	78	59	···	$30.60^{+0.13}_{-0.18}$	···	···	···	···	1.19	1.29	···
39	80	···	2467	$29.99^{+0.15}_{-0.24}$	24.036	20.146	3.517±0.008	−1.10±0.20	···	···	···
40	83	422	1404	$30.32^{+0.14}_{-0.20}$	19.962	17.901	3.637±0.013	−0.38±0.13	0.42	0.99	2.51±0.17
41	84	···	703	$30.03^{+0.14}_{-0.20}$	16.442	15.253	3.794±0.014	0.68±0.02	···	···	···
42	86	···	274	$30.13^{+0.14}_{-0.20}$	14.474	13.891	4.005±0.045	1.67±0.09	···	···	···
43	87	···	979	$30.51^{+0.11}_{-0.15}$	17.324	15.905	3.763±0.005	0.53±0.02	···	···	···
44	88	···	273	$30.02^{+0.14}_{-0.21}$	14.475	13.888	4.069±0.054	1.87±0.12	···	···	···
45	89	547	1458	$29.98^{+0.15}_{-0.23}$	20.368	18.053	3.605±0.013	−0.45±0.14	0.46	0.93	2.83±0.35
46	90	···	1599	$30.19^{+0.14}_{-0.20}$	21.227	18.417	3.556±0.008	−0.54±0.14	···	···	···
47	91	···	2437	$30.04^{+0.15}_{-0.23}$	23.504	20.149	3.534±0.006	−1.17±0.17	···	···	···
48	93	92	1739	$29.95^{+0.16}_{-0.26}$	21.547	18.819	3.563±0.010	−0.70±0.14	0.41	0.66	3.05±0.05
49	95	···	13706	$30.30^{+0.12}_{-0.16}$	18.054	16.668	3.762±0.008	0.28±0.02	···	···	···
50	97	···	743	$30.65^{+0.06}_{-0.07}$	16.647	15.342	3.785±0.013	0.76±0.02	···	···	···
51	101	505	···	$30.36^{+0.13}_{-0.18}$	···	···	···	···	3.79	0.45	···
52	105	138	1388	$30.34^{+0.13}_{-0.18}$	19.776	17.849	3.652±0.013	−0.35±0.13	2.38	0.99	2.40±0.14
53	107	···	2040	$30.36^{+0.13}_{-0.20}$	22.793	19.435	3.534±0.004	−0.89±0.15	···	···	···
54	110	···	462	$29.93^{+0.17}_{-0.27}$	15.665	14.693	3.899±0.027	1.22±0.02	···	···	···
55	111	···	107	$29.84^{+0.15}_{-0.23}$	12.881	12.388	4.126±0.044	2.56±0.10	···	···	···
56	113	82	759	$30.44^{+0.12}_{-0.17}$	16.772	15.379	3.782±0.031	0.67±0.13	0.39	1.49	1.25±0.60
57	119	···	3	$30.63^{+0.06}_{-0.07}$	7.787	7.358	4.449±0.026	5.37±0.07	···	···	···
58	124	171	1255	$30.33^{+0.12}_{-0.18}$	19.072	17.276	3.670±0.020	−0.11±0.13	0.89	1.14	2.40±0.23
59	125	57	1075	$30.35^{+0.12}_{-0.17}$	17.887	16.394	3.772±0.013	0.41±0.02	0.53	1.30	1.50±0.21
60	127	18	1222	$30.55^{+0.11}_{-0.15}$	18.864	17.126	3.736±0.015	0.03±0.02	4.26	1.15	1.94±0.15
61	128	406	1542	$30.12^{+0.14}_{-0.20}$	20.600	18.288	3.606±0.013	−0.55±0.14	0.76	0.85	2.73±0.55
62	129	···	13556	$30.47^{+0.06}_{-0.07}$	9.415	···	···	···	···	···	···
63	130	···	2429	$29.78^{+0.17}_{-0.28}$	23.515	20.136	3.533±0.006	−1.17±0.17	···	···	···
64	132	···	604	$30.24^{+0.13}_{-0.19}$	16.115	15.037	3.864±0.035	0.90±0.12	···	···	···
65	133	41	1080	$30.46^{+0.11}_{-0.14}$	17.862	16.415	3.773±0.013	0.44±0.02	3.88	1.30	1.48±0.21
66	134	···	399	$30.21^{+0.12}_{-0.16}$	15.349	14.486	3.909±0.029	1.26±0.02	···	···	···
67	135	446	···	$29.92^{+0.15}_{-0.23}$	···	···	···	···	5.26	0.70	···
68	136	88	1333	$30.01^{+0.16}_{-0.25}$	19.430	17.673	3.677±0.021	−0.27±0.13	8.20	1.07	2.27±0.15
69	138	5	1022	$30.91^{+0.04}_{-0.05}$	17.571	16.101	3.774±0.015	0.56±0.02	0.54	1.34	1.41±0.24
70	140	128	1073	$30.46^{+0.12}_{-0.16}$	17.881	16.382	3.772±0.012	0.37±0.02	0.59	1.30	1.49±0.19
71	141	96	1139	$30.08^{+0.13}_{-0.18}$	18.343	16.686	3.674±0.018	0.10±0.04	2.93	1.26	2.49±0.20
72	142	418	2052	$30.04^{+0.15}_{-0.24}$	22.350	19.508	3.553±0.008	−0.97±0.14	0.64	0.45	3.05±0.05
73	145	367	756	$29.93^{+0.15}_{-0.24}$	16.545	15.400	3.830±0.017	0.81±0.02	1.86	1.45	−0.26±0.95
74	147	···	182	$30.46^{+0.06}_{-0.07}$	13.706	13.200	4.052±0.055	2.04±0.12	···	···	···
75	148	···	1904	$29.89^{+0.18}_{-0.31}$	22.111	19.206	3.551±0.006	−0.84±0.14	···	···	···
76	149	551	···	$29.87^{+0.16}_{-0.25}$	···	···	···	···	0.36	0.34	···
77	151	112	1159	$30.55^{+0.11}_{-0.15}$	18.506	16.732	3.739±0.022	0.34±0.03	5.32	1.24	1.96±0.27
78	152	401	1669	$30.27^{+0.13}_{-0.18}$	21.426	18.642	3.558±0.009	−0.63±0.14	0.54	0.70	3.05±0.05

Table 2. continued.

X memb ID	X src ID	Moraux2013[a] ID	Currie2010[b] ID	$\log L_X^c$	m_V^d	m_I^d	$\log T_{\rm eff}$	$\log L_{\rm bol}/L_\odot$	Period[e] (d)	Mass[e] ($M_\odot$)	$\log \tau$ d
79	153	552	···	$30.26^{+0.10}_{-0.13}$	···	···	···	···	6.94	0.80	···
80	155	···	722	$29.72^{+0.17}_{-0.29}$	16.453	15.316	3.808±0.015	0.71±0.02	···	···	···
81	156	···	2321	$29.90^{+0.16}_{-0.25}$	23.309	19.926	3.533±0.005	−1.08±0.16	···	···	···
82	160	109	1534	$30.27^{+0.13}_{-0.19}$	20.492	18.281	3.618±0.014	−0.55±0.13	0.42	0.85	2.58±0.24
83	162	188	1147	$30.33^{+0.12}_{-0.17}$	18.267	16.714	3.765±0.008	0.34±0.02	0.55	1.25	1.61±0.11
84	166	292	1616	$30.04^{+0.15}_{-0.22}$	20.746	18.524	3.617±0.014	−0.64±0.13	5.90	0.77	2.53±0.20
85	168	···	93	$30.18^{+0.13}_{-0.20}$	12.609	12.218	4.231±0.067	2.87±0.16	···	···	···
86	171	···	1506	$29.84^{+0.15}_{-0.23}$	20.672	18.168	3.584±0.012	−0.45±0.14	···	···	···
87	173	···	720	$29.96^{+0.14}_{-0.20}$	16.418	15.318	3.833±0.019	0.80±0.02	···	···	···
88	175	47	1142	$30.25^{+0.16}_{-0.27}$	18.339	16.688	3.756±0.011	0.41±0.02	0.32	1.25	1.73±0.15
89	177	530	···	$30.01^{+0.14}_{-0.21}$	···	···	···	···	1.68	1.01	···
90	179	14	1081	$30.50^{+0.06}_{-0.08}$	17.913	16.420	3.767±0.010	0.37±0.02	2.30	1.27	1.58±0.16
91	180	···	167	$30.75^{+0.05}_{-0.06}$	13.598	13.036	4.068±0.061	2.17±0.14	···	···	···
92	185	162	···	$30.07^{+0.14}_{-0.21}$	···	···	···	···	0.41	0.67	···
93	186	···	2355	$29.87^{+0.16}_{-0.25}$	23.313	20.005	3.535±0.005	−1.12±0.16	···	···	···
94a	187	21	···	$30.51^{+0.13}_{-0.19}$	···	···	···	···	3.47	1.22	···
94b	187	417	···	$30.51^{+0.13}_{-0.19}$	···	···	···	···	6.76	0.75	···
95	190	···	1528	$30.01^{+0.15}_{-0.23}$	20.598	18.256	3.602±0.013	−0.53±0.14	···	···	···
96	192	···	1880	$30.18^{+0.13}_{-0.19}$	22.271	19.123	3.541±0.005	−0.79±0.14	···	···	···
97	193	···	1094	$30.14^{+0.13}_{-0.18}$	17.968	16.481	3.767±0.006	0.42±0.02	···	···	···
98	197	···	2019	$29.57^{+0.22}_{-0.46}$	22.337	19.441	3.551±0.006	−0.94±0.14	···	···	···
99	198	···	984	$30.42^{+0.09}_{-0.12}$	17.253	15.946	3.798±0.026	0.47±0.13	···	···	···
100	200	···	1272	$30.27^{+0.10}_{-0.13}$	19.003	17.369	3.703±0.025	−0.14±0.13	···	···	···
101	201	···	217	$30.37^{+0.12}_{-0.17}$	14.136	13.539	4.093±0.049	2.07±0.11	···	···	···
102	203	···	1184	$30.46^{+0.11}_{-0.16}$	18.509	16.903	3.708±0.029	0.05±0.13	···	···	···
103	204	···	775	$30.45^{+0.10}_{-0.13}$	16.704	15.419	3.766±0.009	0.61±0.02	···	···	···
104	205	···	1070	$30.45^{+0.07}_{-0.09}$	17.874	16.375	3.774±0.014	0.41±0.02	···	···	···
105	206	···	1855	$29.77^{+0.16}_{-0.27}$	21.850	19.106	3.562±0.010	−0.82±0.14	···	···	···
106	209	···	1154	$30.08^{+0.14}_{-0.20}$	18.445	16.720	3.766±0.022	0.32±0.02	···	···	···
107	210	···	14	$29.92^{+0.14}_{-0.20}$	8.474	8.066	4.376±0.030	4.86±0.07	···	···	···
108	211	···	1186	$30.36^{+0.09}_{-0.12}$	18.617	16.903	3.687±0.022	0.04±0.13	···	···	···
109	213	···	1440	$30.08^{+0.17}_{-0.28}$	20.620	17.968	3.570±0.010	−0.37±0.14	···	···	···
110	217	···	1519	$30.20^{+0.13}_{-0.19}$	20.613	18.227	3.597±0.013	−0.50±0.14	···	···	···
111	220	···	1221	$30.38^{+0.12}_{-0.17}$	18.843	17.126	3.738±0.021	0.13±0.03	···	···	···
112	230	···	1879	$29.74^{+0.19}_{-0.34}$	21.878	19.164	3.564±0.011	−0.84±0.14	···	···	···
113	231	···	111	$30.26^{+0.07}_{-0.08}$	12.862	12.434	4.188±0.058	2.68±0.14	···	···	···
114	235	···	1068	$30.56^{+0.09}_{-0.11}$	17.857	16.364	3.744±0.039	0.26±0.13	···	···	···
115	237	580	991	$30.74^{+0.10}_{-0.13}$	17.266	15.976	3.794±0.014	0.54±0.02	2.89	1.35	1.09±0.31
116	239	377	1325	$29.73^{+0.18}_{-0.31}$	19.722	17.595	3.629±0.014	−0.27±0.13	12.05	1.07	2.69±0.31
117	242	204	1143	$30.33^{+0.12}_{-0.17}$	18.256	16.699	3.770±0.009	0.40±0.02	1.88	1.19	1.53±0.14
118	246	···	2505	$29.69^{+0.18}_{-0.32}$	24.223	20.205	3.513±0.008	−1.10±0.21	···	···	···
119	247	275	1426	$30.39^{+0.13}_{-0.19}$	20.420	17.932	3.585±0.012	−0.36±0.14	15.87	0.95	3.05±0.05
120	249	73	1215	$30.18^{+0.10}_{-0.13}$	18.748	17.099	3.700±0.022	−0.04±0.13	8.26	1.14	2.23±0.16
121	250	462	1228	$30.17^{+0.14}_{-0.21}$	18.814	17.170	3.701±0.023	−0.06±0.13	3.82	1.17	2.22±0.17
122	252	···	810	$29.93^{+0.13}_{-0.20}$	16.654	15.510	3.805±0.013	0.61±0.02	···	···	···
123	254	172	···	$30.36^{+0.13}_{-0.18}$	···	···	···	···	4.98	1.19	···
124	256	···	1555	$30.19^{+0.13}_{-0.19}$	21.152	18.280	3.552±0.006	−0.48±0.14	···	···	···
125	259	···	854	$29.74^{+0.16}_{-0.26}$	16.718	15.590	3.834±0.023	0.64±0.02	···	···	···
126	260	409	1760	$30.29^{+0.10}_{-0.13}$	21.825	18.839	3.547±0.005	−0.69±0.14	10.53	0.64	3.05±0.05
127	261	···	2060	$29.90^{+0.21}_{-0.42}$	22.607	19.503	3.543±0.005	−0.95±0.14	···	···	···
128	264	···	676	$30.42^{+0.07}_{-0.08}$	16.432	15.184	3.803±0.013	0.79±0.02	···	···	···
129	265	···	1798	$29.68^{+0.18}_{-0.30}$	21.599	18.972	3.572±0.011	−0.77±0.14	···	···	···
130	266	···	2326	$30.13^{+0.15}_{-0.22}$	23.276	19.941	3.535±0.005	−1.09±0.16	···	···	···
131	268	···	636	$29.55^{+0.22}_{-0.47}$	16.239	15.112	3.848±0.035	0.85±0.12	···	···	···
132a	273	···	13593	$30.59^{+0.06}_{-0.08}$	10.869	10.469	4.321±0.131	3.77±0.31	···	···	···
132b	273	···	24	$30.64^{+0.09}_{-0.11}$	10.857	10.469	4.538±0.161	4.41±0.53	···	···	···
133	274	···	903	$29.84^{+0.15}_{-0.23}$	17.053	15.674	3.786±0.014	0.65±0.02	···	···	···
134	279	76	1210	$30.65^{+0.10}_{-0.13}$	18.928	17.054	3.676±0.018	0.06±0.04	4.48	1.19	2.44±0.19
135	286	···	585	$30.12^{+0.13}_{-0.19}$	16.249	14.976	3.803±0.024	0.87±0.13	···	···	···
136	290	293	···	$30.77^{+0.05}_{-0.06}$	18.624	16.972	3.766±0.014	0.12±0.02	1.85	1.19	1.61±0.20
137	293	247	···	$30.15^{+0.13}_{-0.19}$	···	···	···	···	7.69	1.16	···
138	294	69	987	$30.22^{+0.13}_{-0.19}$	17.389	15.938	3.778±0.015	0.60±0.02	0.38	1.36	1.32±0.29
139	297	···	139	$30.05^{+0.14}_{-0.20}$	13.223	12.767	4.180±0.057	2.55±0.13	···	···	···
140	298	···	1197	$30.47^{+0.10}_{-0.14}$	18.655	17.002	3.759±0.029	0.20±0.03	···	···	···
141	299	···	8	$29.78^{+0.16}_{-0.25}$	8.222	7.688	4.369±0.031	5.06±0.07	···	···	···
142	303	74	1136	$30.44^{+0.12}_{-0.17}$	18.384	16.658	3.766±0.008	0.34±0.02	3.56	1.25	1.59±0.13
143	306	106	···	$29.81^{+0.16}_{-0.25}$	···	···	···	···	5.35	1.07	···
144	309	···	791	$30.16^{+0.12}_{-0.17}$	16.665	15.448	3.820±0.017	0.67±0.02	···	···	···
145	310	···	1376	$30.06^{+0.14}_{-0.20}$	19.907	17.802	3.631±0.014	−0.35±0.13	···	···	···
146	312	···	312	$29.74^{+0.17}_{-0.28}$	14.910	14.094	3.934±0.030	1.50±0.03	···	···	···
147	315	577	1965	$29.85^{+0.16}_{-0.26}$	22.034	19.351	3.567±0.017	−0.92±0.16	3.31	0.48	3.07±0.10
148	318	11	1007	$30.18^{+0.17}_{-0.28}$	17.573	16.003	3.797±0.010	0.65±0.02	0.39	1.34	0.97±0.23
149	325	187	1131	$30.26^{+0.12}_{-0.16}$	18.330	16.637	3.739±0.015	0.30±0.02	3.38	1.26	1.96±0.19
150	326	···	770	$30.16^{+0.14}_{-0.20}$	16.591	15.413	3.829±0.020	0.74±0.02	···	···	···
151	328	200	1155	$30.23^{+0.14}_{-0.21}$	18.229	16.753	3.762±0.008	0.26±0.02	3.12	1.25	1.67±0.13
152	332	···	1270	$30.19^{+0.15}_{-0.24}$	19.171	17.337	3.698±0.021	−0.04±0.04	···	···	···
153	337	···	13663	$29.91^{+0.14}_{-0.22}$	14.710	···	3.975±0.024	1.61±0.04	···	···	···
154	339	235	1456	$29.91^{+0.15}_{-0.24}$	20.036	18.078	3.649±0.014	−0.45±0.13	4.42	0.95	2.37±0.14
155	340	···	276	$30.53^{+0.08}_{-0.09}$	14.610	13.901	4.042±0.048	1.85±0.10	···	···	···

Table 2. continued.

X memb ID	X src ID	Moraux2013[a] ID	Currie2010[b] ID	$\log L_X^c$	m_V^d	m_I^d	$\log T_{\rm eff}$	$\log L_{\rm bol}/L_\odot$	Period[e] (d)	Mass[e] ($M_\odot$)	$\log \tau$ d
156	343	479	···	$30.54^{+0.09}_{-0.11}$	···	···	···	···	7.63	0.82	···
157	344	291	1172	$30.16^{+0.14}_{-0.22}$	18.381	16.845	3.721±0.034	0.08±0.13	5.38	1.23	2.10±0.34
158	347	227	881	$29.76^{+0.20}_{-0.37}$	17.113	15.610	3.765±0.009	0.65±0.02	0.37	1.39	1.51±0.14
159	350	210	1355	$29.84^{+0.16}_{-0.25}$	19.724	17.738	3.645±0.013	−0.31±0.13	4.95	1.03	2.48±0.16
160	351	272	1260	$30.15^{+0.14}_{-0.22}$	19.143	17.292	3.751±0.017	0.22±0.02	0.25	1.14	1.83±0.24
161	354	385	···	$30.37^{+0.12}_{-0.17}$	···	···	···	···	0.44	1.40	···
162	355	···	13622	$30.21^{+0.12}_{-0.18}$	12.532	···	4.205±0.059	2.91±0.14	···	···	···
163	358	20	936	$30.46^{+0.07}_{-0.08}$	17.290	15.750	3.777±0.014	0.65±0.02	0.45	1.39	1.32±0.24
164	360	···	363	$30.32^{+0.13}_{-0.18}$	15.246	14.292	3.921±0.031	1.41±0.02	···	···	···
165	361	···	13704	$30.87^{+0.04}_{-0.05}$	17.352	16.128	3.777±0.014	0.48±0.02	···	···	···
166	365	···	1021	$30.63^{+0.06}_{-0.07}$	17.523	16.103	3.778±0.012	0.49±0.02	···	···	···
167	367	98	1156	$30.12^{+0.14}_{-0.21}$	18.434	16.733	3.689±0.022	0.10±0.13	0.34	1.23	2.33±0.26
168	370	267	···	$29.89^{+0.19}_{-0.33}$	···	···	···	···	8.43	1.23	···
169	371	···	1138	$30.60^{+0.10}_{-0.13}$	18.356	16.676	3.769±0.010	0.37±0.02	···	···	···
170	372	···	15	$29.68^{+0.17}_{-0.29}$	8.526	8.065	4.342±0.103	4.79±0.24	···	···	···
171	373	···	13627	$29.74^{+0.17}_{-0.27}$	13.117	···	4.175±0.052	2.56±0.12	···	···	···
172	374	···	2087	$30.26^{+0.13}_{-0.18}$	22.723	19.549	3.540±0.005	−0.96±0.15	···	···	···
173	377	···	13666	$29.78^{+0.19}_{-0.33}$	15.134	···	3.963±0.045	1.36±0.06	···	···	···
174	383	49	1292	$30.19^{+0.13}_{-0.18}$	19.212	17.439	3.733±0.024	0.06±0.03	0.66	1.11	1.99±0.27
175	384	127	1462	$30.18^{+0.13}_{-0.19}$	20.430	18.055	3.599±0.015	−0.44±0.15	2.94	0.92	3.02±0.05
176	387	···	1053	$30.09^{+0.14}_{-0.20}$	17.864	16.248	3.706±0.028	0.31±0.13	···	···	···
177	388	···	1454	$30.47^{+0.11}_{-0.15}$	20.506	18.023	3.603±0.030	−0.32±0.13	···	···	···
178	389	302	1224	$30.20^{+0.16}_{-0.25}$	19.134	17.109	3.680±0.018	0.08±0.03	5.59	1.17	2.41±0.19
179	390	65	1289	$30.31^{+0.12}_{-0.17}$	19.322	17.411	3.742±0.035	0.15±0.04	2.62	1.11	1.91±0.35
180	392	306	2127	$29.64^{+0.18}_{-0.32}$	23.139	19.595	3.528±0.005	−0.93±0.15	3.94	0.41	3.05±0.05
181	394	···	326	$30.20^{+0.12}_{-0.16}$	15.003	14.159	3.923±0.028	1.45±0.02	···	···	···
182	398	···	26	$30.10^{+0.15}_{-0.23}$	11.122	10.537	4.191±0.215	3.45±0.49	···	···	···
183	402	···	1299	$29.83^{+0.16}_{-0.26}$	19.257	17.491	3.675±0.022	−0.20±0.13	···	···	···
184	404	···	1171	$30.07^{+0.14}_{-0.20}$	18.392	16.836	3.717±0.034	0.08±0.13	···	···	···
185	405	113	1090	$30.69^{+0.07}_{-0.08}$	18.046	16.450	3.765±0.016	0.44±0.02	0.55	1.28	1.59±0.25
186	407	···	1124	$29.67^{+0.21}_{-0.43}$	18.128	16.627	3.774±0.008	0.38±0.02	···	···	···
187	410	···	1191	$30.35^{+0.09}_{-0.12}$	18.504	16.965	3.720±0.034	0.03±0.13	···	···	···
188	411	···	588	$29.79^{+0.17}_{-0.30}$	16.232	14.981	3.806±0.027	0.87±0.13	···	···	···
189	415	···	1216	$30.40^{+0.12}_{-0.16}$	18.785	17.104	3.751±0.015	0.10±0.02	···	···	···
190	417	···	699	$30.23^{+0.13}_{-0.18}$	16.563	15.227	3.794±0.024	0.75±0.13	···	···	···
191	418	···	40	$30.35^{+0.07}_{-0.08}$	11.381	10.890	4.351±0.032	3.71±0.07	···	···	···
192	421	464	···	$30.12^{+0.15}_{-0.23}$	···	···	···	···	0.48	1.17	···
193	422	···	13623	$29.58^{+0.17}_{-0.29}$	12.573	···	4.201±0.051	2.87±0.12	···	···	···
194	424	···	1732	$29.75^{+0.17}_{-0.27}$	22.957	18.656	3.504±0.004	−0.46±0.15	···	···	···
195	433	27	···	$30.15^{+0.14}_{-0.20}$	···	···	···	···	0.36	1.29	···
196	446	317	···	$29.73^{+0.17}_{-0.28}$	···	···	···	···	6.14	1.03	···
197	447	42	···	$30.19^{+0.14}_{-0.20}$	···	···	···	···	1.88	1.17	···
198	450	362	···	$30.12^{+0.13}_{-0.20}$	···	···	···	···	3.73	1.29	···
199	453	169	1335	$30.29^{+0.13}_{-0.20}$	19.509	17.675	3.662±0.018	−0.28±0.13	3.41	1.05	2.35±0.19
200	455	···	13585	$29.92^{+0.14}_{-0.22}$	13.090	12.548	4.345±0.122	3.15±0.29	···	···	···
201	459	···	919	$29.92^{+0.15}_{-0.23}$	17.089	15.721	3.787±0.011	0.64±0.02	···	···	···
202	460	···	849	$30.58^{+0.12}_{-0.16}$	16.962	15.555	3.777±0.014	0.66±0.02	···	···	···
203	462	···	388	$29.92^{+0.07}_{-0.09}$	15.208	14.443	3.794±0.010	0.84±0.02	···	···	···
204	464	···	1745	$29.96^{+0.15}_{-0.24}$	21.206	18.869	3.603±0.013	−0.77±0.14	···	···	···
205	468	···	658	$29.63^{+0.21}_{-0.43}$	16.129	15.191	3.898±0.030	0.93±0.02	···	···	···
206	474	···	1283	$29.99^{+0.15}_{-0.23}$	19.149	17.395	3.678±0.021	−0.16±0.13	···	···	···
207	476	···	1304	$29.99^{+0.14}_{-0.21}$	19.532	17.492	3.639±0.017	−0.22±0.14	···	···	···
208	478	···	148	$30.00^{+0.14}_{-0.20}$	13.433	12.847	4.158±0.051	2.52±0.12	···	···	···
209	481	···	277	$29.91^{+0.17}_{-0.28}$	14.488	13.915	4.050±0.059	1.75±0.13	···	···	···
210	485	195	1104	$30.83^{+0.06}_{-0.07}$	18.105	16.507	3.770±0.010	0.39±0.02	0.81	1.27	1.52±0.16
211	489	427	1074	$30.04^{+0.14}_{-0.20}$	18.002	16.371	3.757±0.012	0.40±0.02	4.05	1.30	1.72±0.17
212	490	···	1238	$30.30^{+0.12}_{-0.17}$	18.790	17.221	3.762±0.019	0.20±0.02	···	···	···
213	491	···	565	$30.51^{+0.10}_{-0.14}$	16.119	14.945	3.811±0.017	0.86±0.02	···	···	···
214	495	456	962	$29.76^{+0.16}_{-0.27}$	17.194	15.860	3.794±0.024	0.49±0.13	10.87	1.36	1.08±0.56
215	496	···	937	$30.42^{+0.13}_{-0.18}$	17.130	15.774	3.791±0.026	0.52±0.13	···	···	···
216	498	···	1740	$30.01^{+0.17}_{-0.27}$	21.575	18.817	3.560±0.009	−0.70±0.14	···	···	···
217	499	···	1583	$30.01^{+0.17}_{-0.27}$	21.113	18.385	3.563±0.010	−0.53±0.14	···	···	···
218	510	···	1250	$30.45^{+0.08}_{-0.09}$	19.197	17.239	3.719±0.014	0.24±0.04	···	···	···
219	511	···	216	$30.20^{+0.13}_{-0.19}$	14.179	13.530	4.129±0.052	2.19±0.12	···	···	···
220	514	···	334	$29.72^{+0.16}_{-0.26}$	14.832	14.200	4.008±0.050	1.57±0.10	···	···	···
221	515	157	1108	$30.73^{+0.10}_{-0.13}$	18.261	16.499	3.703±0.015	0.27±0.03	0.47	1.28	2.28±0.16
222	524	455	1455	$30.30^{+0.13}_{-0.18}$	20.401	18.035	3.600±0.013	−0.43±0.14	3.95	0.93	3.00±0.08
223	526	···	1789	$31.23^{+0.07}_{-0.09}$	22.029	18.912	3.542±0.005	−0.71±0.14	···	···	···
224	527	148	899	$30.33^{+0.13}_{-0.19}$	17.109	15.663	3.786±0.014	0.68±0.02	0.43	1.39	1.18±0.27
225	529	···	1225	$29.97^{+0.15}_{-0.22}$	18.890	17.154	3.682±0.022	−0.06±0.13	···	···	···
226	534	···	1232	$30.02^{+0.15}_{-0.22}$	18.997	17.172	3.664±0.018	−0.07±0.13	···	···	···
227	540	256	790	$30.46^{+0.12}_{-0.16}$	16.636	15.450	3.822±0.017	0.76±0.02	0.54	1.43	0.12±0.81
228	541	···	1658	$29.62^{+0.18}_{-0.32}$	21.169	18.642	3.582±0.011	−0.64±0.14	···	···	···
229	545	···	1041	$30.52^{+0.09}_{-0.11}$	17.708	16.193	3.734±0.037	0.34±0.13	···	···	···
230	546	167	1443	$29.85^{+0.16}_{-0.24}$	20.212	18.016	3.620±0.014	−0.44±0.13	5.75	0.93	2.64±0.31
231	551	···	683	$30.36^{+0.11}_{-0.15}$	16.605	15.182	3.802±0.011	0.84±0.02	···	···	···
232	558	416	···	$30.37^{+0.09}_{-0.11}$	···	···	···	···	0.37	1.32	···
233	559	···	114	$30.43^{+0.11}_{-0.15}$	12.983	12.448	4.201±0.059	2.73±0.14	···	···	···
234	566	191	1274	$30.14^{+0.14}_{-0.22}$	19.130	17.363	3.675±0.021	−0.14±0.13	6.90	1.12	2.34±0.23

Table 2. continued.

X memb ID	X src ID	Moraux2013[a] ID	Currie2010[b] ID	$\log L_X^c$	m_V^d	m_I^d	$\log T_{\rm eff}$	$\log L_{\rm bol}/L_\odot$	Period[e] (d)	Mass[e] ($M_\odot$)	$\log \tau$ d
235	569	···	1087	$30.66^{+0.06}_{-0.07}$	18.004	16.421	3.772±0.011	0.46±0.02	···	···	···
236	570	···	1345	$30.21^{+0.13}_{-0.19}$	19.476	17.731	3.680±0.022	−0.29±0.13	···	···	···
237	572	526	1511	$30.05^{+0.14}_{-0.22}$	20.314	18.213	3.632±0.014	−0.51±0.13	6.25	0.88	2.48±0.15
238	573	222	···	$30.47^{+0.09}_{-0.11}$	···	···	···	···	0.41	1.19	···
239	576	449	1747	$29.54^{+0.22}_{-0.45}$	21.382	18.853	3.582±0.012	−0.73±0.14	7.96	0.65	3.08±0.05
240	577	···	1201	$30.72^{+0.07}_{-0.08}$	18.733	17.039	3.760±0.010	0.27±0.02	···	···	···
241	578	···	901	$29.79^{+0.19}_{-0.25}$	16.894	15.688	3.816±0.033	0.60±0.13	···	···	···
242	579	···	13587	$29.52^{+0.18}_{-0.32}$	10.470	···	···	···	···	···	···
243	583	···	583	$29.95^{+0.16}_{-0.24}$	15.887	15.011	3.927±0.028	1.16±0.02	···	···	···
244	584	···	1963	$29.72^{+0.19}_{-0.34}$	22.173	19.330	3.553±0.010	−0.90±0.16	···	···	···
245	585	···	863	$30.35^{+0.11}_{-0.16}$	16.815	15.606	3.831±0.020	0.69±0.02	···	···	···
246	589	193	824	$30.57^{+0.05}_{-0.06}$	16.920	15.515	3.785±0.014	0.66±0.02	0.47	1.41	1.20±0.26
247	590	100	1279	$30.14^{+0.14}_{-0.21}$	19.284	17.370	3.653±0.014	−0.16±0.13	3.39	1.12	2.53±0.14
248	592	···	1767	$30.15^{+0.14}_{-0.20}$	21.575	18.897	3.568±0.011	−0.74±0.14	···	···	···
249	593	···	387	$30.10^{+0.14}_{-0.20}$	15.125	14.450	4.038±0.048	1.58±0.10	···	···	···
250	595	190	···	$29.92^{+0.15}_{-0.23}$	···	···	···	···	3.36	1.19	···
251	598	295	1061	$30.18^{+0.14}_{-0.21}$	17.876	16.316	3.774±0.013	0.47±0.02	3.57	1.30	1.46±0.22
252	599	···	532	$29.72^{+0.17}_{-0.30}$	16.018	14.839	3.798±0.019	0.85±0.02	···	···	···
253	600	70	1218	$30.22^{+0.10}_{-0.13}$	19.008	17.096	3.654±0.014	−0.05±0.13	0.66	1.16	2.57±0.19
254	608	···	850	$30.68^{+0.06}_{-0.07}$	17.117	15.540	3.782±0.014	0.83±0.02	···	···	···
255	609	···	2044	$29.83^{+0.15}_{-0.24}$	22.960	19.422	3.528±0.004	−0.86±0.15	···	···	···
256	610	···	75	$30.10^{+0.14}_{-0.21}$	12.446	11.865	4.197±0.217	2.93±0.50	···	···	···
257	616	103	954	$30.45^{+0.06}_{-0.07}$	17.142	15.840	3.794±0.014	0.53±0.02	1.50	1.37	1.10±0.30
258	617	155	906	$30.41^{+0.07}_{-0.09}$	17.101	15.677	3.782±0.015	0.67±0.02	0.41	1.38	1.25±0.26
259	620	···	1316	$30.04^{+0.14}_{-0.20}$	19.450	17.577	3.658±0.021	−0.24±0.14	···	···	···
260	621	419	1906	$29.73^{+0.17}_{-0.27}$	22.090	19.214	3.552±0.007	−0.85±0.14	6.85	0.48	3.05±0.05
261	622	544	1342	$29.70^{+0.18}_{-0.32}$	19.661	17.698	3.648±0.013	−0.30±0.13	0.27	1.04	2.47±0.14
262	623	···	13557	$29.95^{+0.19}_{-0.36}$	9.286	···	4.442±0.111	4.91±0.29	···	···	···
263	629	···	2010	$29.70^{+0.19}_{-0.36}$	22.575	19.398	3.540±0.005	−0.90±0.14	···	···	···
264	631	···	105	$29.66^{+0.18}_{-0.31}$	12.956	12.347	4.214±0.100	2.86±0.24	···	···	···
265	634	···	2181	$29.59^{+0.22}_{-0.45}$	23.616	19.663	3.515±0.006	−0.90±0.17	···	···	···
266	636	···	1134	$30.38^{+0.11}_{-0.15}$	18.212	16.665	3.766±0.012	0.28±0.02	···	···	···
267	639	···	785	$30.33^{+0.09}_{-0.12}$	16.808	15.423	3.784±0.029	0.65±0.13	···	···	···
268	640	···	13562	$30.49^{+0.07}_{-0.08}$	9.038	···	···	···	···	···	···
269	643	···	13588	$30.47^{+0.07}_{-0.08}$	8.477	···	···	···	···	···	···
270	645	···	1415	$29.82^{+0.16}_{-0.26}$	20.017	17.921	3.633±0.013	−0.39±0.13	···	···	···
271	648	579	2263	$29.89^{+0.15}_{-0.24}$	23.104	19.852	3.537±0.005	−1.07±0.15	0.25	0.36	3.05±0.05
272	649	···	1434	$29.73^{+0.18}_{-0.32}$	20.165	17.995	3.623±0.014	−0.43±0.13	···	···	···
273	651	515	1246	$30.05^{+0.13}_{-0.20}$	18.946	17.259	3.692±0.022	−0.11±0.13	0.36	1.15	2.25±0.17
274	652	···	2026	$30.09^{+0.13}_{-0.19}$	22.392	19.441	3.549±0.009	−0.93±0.16	···	···	···
275	655	···	1165	$30.24^{+0.16}_{-0.25}$	18.340	16.786	3.747±0.019	0.17±0.02	···	···	···
276	656	···	1336	$30.18^{+0.13}_{-0.19}$	19.624	17.666	3.649±0.013	−0.28±0.13	···	···	···
277	661	···	781	$29.83^{+0.15}_{-0.23}$	16.549	15.446	3.862±0.026	0.80±0.02	···	···	···
278	670	···	2053	$30.03^{+0.14}_{-0.21}$	22.748	19.468	3.536±0.004	−0.91±0.15	···	···	···
279	679	···	1578	$30.01^{+0.14}_{-0.21}$	20.601	18.427	3.623±0.016	−0.60±0.13	···	···	···
280	680	58	···	$30.43^{+0.12}_{-0.17}$	···	···	···	···	0.41	1.36	···
281	683	···	2315	$29.91^{+0.16}_{-0.27}$	23.187	19.933	3.537±0.005	−1.10±0.15	···	···	···
282	687	211	1396	$29.71^{+0.17}_{-0.28}$	19.859	17.880	3.646±0.013	−0.37±0.13	7.46	0.97	2.44±0.13
283	688	···	13604	$30.30^{+0.12}_{-0.16}$	6.700	···	···	···	···	···	···
284	692	97	964	$31.03^{+0.04}_{-0.04}$	17.389	15.845	3.766±0.008	0.65±0.02	0.85	1.36	1.50±0.13
285	695	353	1141	$30.06^{+0.15}_{-0.23}$	18.164	16.705	3.755±0.039	0.13±0.13	0.50	1.24	1.74±0.50
286	700	···	1369	$30.45^{+0.12}_{-0.16}$	19.820	17.778	3.714±0.014	0.11±0.03	···	···	···
287	701	25	···	$30.16^{+0.13}_{-0.19}$	···	···	···	···	0.40	1.34	···
288	702	···	1248	$30.62^{+0.09}_{-0.11}$	18.956	17.260	3.690±0.022	−0.11±0.13	···	···	···
289	703	···	931	$30.42^{+0.11}_{-0.15}$	17.152	15.753	3.767±0.012	0.51±0.02	···	···	···
290	705	···	1695	$29.74^{+0.17}_{-0.30}$	21.106	18.753	3.601±0.013	−0.72±0.14	···	···	···
291	706	···	127	$30.18^{+0.12}_{-0.17}$	13.216	12.614	4.298±0.033	2.94±0.08	···	···	···
292	710	111	···	$30.30^{+0.15}_{-0.23}$	18.793	17.045	3.791±0.009	0.29±0.02	5.35	1.18	1.36±0.21
293	711	···	2358	$29.92^{+0.16}_{-0.25}$	23.062	20.037	3.546±0.006	−1.17±0.15	···	···	···
294	715	···	1618	$30.35^{+0.10}_{-0.13}$	20.997	18.500	3.585±0.012	−0.59±0.14	···	···	···
295	717	···	1590	$29.80^{+0.16}_{-0.26}$	20.736	18.445	3.608±0.016	−0.62±0.14	···	···	···
296	721	···	895	$29.93^{+0.15}_{-0.22}$	16.980	15.670	3.818±0.020	0.67±0.02	···	···	···
297	722	108	1175	$30.16^{+0.14}_{-0.21}$	18.506	16.870	3.702±0.025	0.06±0.13	6.14	1.21	2.23±0.22
298	726	236	1394	$30.34^{+0.12}_{-0.17}$	19.831	17.876	3.649±0.013	−0.37±0.13	1.23	0.99	2.42±0.13
299	727	393	1190	$30.16^{+0.13}_{-0.18}$	18.533	16.929	3.708±0.030	0.04±0.13	7.75	1.20	2.19±0.24
300	734	···	1297	$30.31^{+0.13}_{-0.19}$	19.224	17.481	3.680±0.022	−0.19±0.13	···	···	···
301	735	···	1731	$29.97^{+0.15}_{-0.22}$	21.300	18.827	3.587±0.012	−0.72±0.14	···	···	···
302	736	···	1550	$29.78^{+0.16}_{-0.27}$	20.474	18.337	3.628±0.027	−0.56±0.17	···	···	···
303	740	···	184	$31.04^{+0.04}_{-0.04}$	13.818	13.202	4.180±0.061	2.45±0.14	···	···	···
304	744	···	886	$30.09^{+0.13}_{-0.19}$	16.864	15.649	3.828±0.022	0.68±0.02	···	···	···
305	745	79	···	$29.99^{+0.17}_{-0.29}$	···	···	···	···	0.45	1.03	···
306	746	···	1497	$29.84^{+0.16}_{-0.25}$	20.749	18.120	3.572±0.010	−0.43±0.14	···	···	···
307	748	120	1303	$29.76^{+0.17}_{-0.29}$	19.373	17.491	3.657±0.015	−0.21±0.13	6.62	1.08	2.45±0.16
308	749	487	1656	$29.77^{+0.18}_{-0.30}$	20.990	18.640	3.601±0.013	−0.68±0.14	4.12	0.73	2.68±0.50
309	752	···	1217	$30.26^{+0.09}_{-0.12}$	18.733	17.113	3.705±0.028	−0.04±0.13	···	···	···
310	753	129	1188	$30.67^{+0.08}_{-0.09}$	18.557	16.914	3.763±0.007	0.30±0.02	0.85	1.19	1.64±0.11
311	756	···	680	$29.88^{+0.14}_{-0.22}$	16.469	15.186	3.805±0.014	0.79±0.02	···	···	···
312	757	132	1219	$30.19^{+0.13}_{-0.17}$	18.914	17.106	3.749±0.013	0.17±0.02	0.42	1.16	1.83±0.17
313	758	···	13698	$29.88^{+0.16}_{-0.25}$	16.000	···	3.851±0.023	1.04±0.02	···	···	···

Table 2. continued.

X memb ID	X src ID	Moraux2013[a] ID	Currie2010[b] ID	$\log L_X^c$	m_V^d	m_I^d	$\log T_{\rm eff}$	$\log L_{\rm bol}/L_\odot$	Period[e] (d)	Mass[e] ($M_\odot$)	$\log\tau$ d
314	759	174	1317	$30.25^{+0.12}_{-0.17}$	19.683	17.557	3.634±0.024	−0.11±0.07	0.46	1.07	2.75±0.68
315	760	···	1729	$29.69^{+0.17}_{-0.27}$	21.944	18.757	3.539±0.004	−0.64±0.14	···	···	···
316	761	···	380	$30.43^{+0.12}_{-0.17}$	15.108	14.405	3.992±0.043	1.48±0.08	···	···	···
317	762	···	518	$30.55^{+0.10}_{-0.12}$	15.888	14.812	3.864±0.035	0.99±0.12	···	···	···
318	763	···	1298	$29.61^{+0.14}_{-0.22}$	19.209	17.485	3.684±0.026	−0.20±0.14	···	···	···
319	764	···	1602	$30.19^{+0.13}_{-0.45}$	21.153	18.438	3.564±0.011	−0.55±0.14	···	···	···
320	765	136	···	$29.80^{+0.17}_{-0.18}$	···	···	···	···	3.45	1.02	···
321	766	···	626	$30.25^{+0.14}_{-0.28}$	16.294	15.080	3.813±0.033	0.84±0.13	···	···	···
322	767	···	1654	$30.13^{+0.14}_{-0.22}$	21.534	18.574	3.548±0.005	−0.59±0.14	···	···	···
323	770	173	1227	$30.34^{+0.12}_{-0.20}$	18.895	17.160	3.751±0.015	0.16±0.02	2.29	1.15	1.81±0.21
324	772		···	$30.65^{+0.09}_{-0.16}$	···	···	···	···	2.99	1.21	···
325	775	···	2323	$29.74^{+0.18}_{-0.12}$	23.408	19.923	3.530±0.005	−1.07±0.16	···	···	···
326	776	130	1360	$30.31^{+0.12}_{-0.30}$	19.920	17.742	3.622±0.014	−0.33±0.13	0.66	1.01	2.71±0.37
327	777	34	···	$30.55^{+0.07}_{-0.17}$	18.374	16.764	3.777±0.016	0.33±0.02	3.47	1.25	1.42±0.26
328	779	22	1144	$30.52^{+0.11}_{-0.08}$	18.277	16.711	3.766±0.011	0.31±0.02	4.07	1.25	1.60±0.17
329	780	···	2254	$29.87^{+0.17}_{-0.15}$	23.364	19.810	3.527±0.005	−1.01±0.16	···	···	···
330	783	273	1512	$30.02^{+0.14}_{-0.27}$	20.253	18.225	3.641±0.013	−0.51±0.13	1.83	0.89	2.39±0.13
331	784	···	2230	$29.79^{+0.17}_{-0.21}$	22.836	19.830	3.547±0.005	−1.09±0.14	···	···	···
332	785	···	1436	$29.89^{+0.15}_{-0.29}$	19.921	18.032	3.656±0.015	−0.42±0.13	···	···	···
333	787	40	1103	$30.45^{+0.07}_{-0.24}$	18.089	16.500	3.766±0.033	0.36±0.03	2.42	1.28	1.60±0.46
334	788	142	1115	$30.19^{+0.14}_{-0.09}$	18.131	16.564	3.761±0.016	0.29±0.02	0.67	1.27	1.67±0.25
335	790	503	1489	$29.57^{+0.21}_{-0.21}$	20.218	18.153	3.636±0.013	−0.49±0.13	0.84	0.91	2.45±0.14
336	791	64	807	$30.25^{+0.12}_{-0.40}$	16.810	15.489	3.786±0.013	0.67±0.02	0.46	1.42	1.18±0.25
337	792	···	865	$30.51^{+0.06}_{-0.17}$	16.870	15.604	3.808±0.018	0.67±0.02	···	···	···
338	793	···	1239	$30.47^{+0.10}_{-0.07}$	18.982	17.205	3.673±0.020	−0.08±0.13	···	···	···
339	794	···	1203	$30.11^{+0.14}_{-0.12}$	18.704	17.047	3.745±0.029	0.15±0.03	···	···	···
340	795	243	1044	$30.98^{+0.04}_{-0.20}$	17.749	16.207	3.767±0.039	0.49±0.03	0.90	1.32	1.56±0.64
341	797	375	1069	$30.59^{+0.07}_{-0.05}$	17.911	16.371	3.779±0.013	0.49±0.02	2.99	1.30	1.37±0.22
342	799	358	704	$30.17^{+0.12}_{-0.09}$	16.369	15.272	3.830±0.023	0.80±0.02	0.32	1.59	−0.24±1.27
343	800	146	985	$30.82^{+0.05}_{-0.16}$	17.396	15.932	3.795±0.011	0.58±0.02	1.33	1.35	1.04±0.24
344	804	···	1347	$29.72^{+0.17}_{-0.05}$	19.928	17.686	3.621±0.028	−0.23±0.10	···	···	···
345	805	234	1116	$30.53^{+0.07}_{-0.28}$	18.114	16.576	3.766±0.006	0.33±0.02	1.95	1.24	1.60±0.09
346	808	312	846	$30.23^{+0.13}_{-0.09}$	16.868	15.556	3.804±0.013	0.75±0.02	1.70	1.40	0.74±0.37
347	810	···	1635	$29.57^{+0.21}_{-0.18}$	21.146	18.539	3.574±0.011	−0.60±0.14	···	···	···
348	811	493	1637	$29.88^{+0.16}_{-0.40}$	20.900	18.573	3.604±0.013	−0.66±0.14	6.03	0.74	2.66±0.42
349	812	36	1340	$29.78^{+0.17}_{-0.26}$	19.481	17.712	3.675±0.021	−0.28±0.13	2.20	1.03	2.28±0.16
350	814	···	1839	$29.80^{+0.20}_{-0.29}$	21.722	19.072	3.570±0.011	−0.81±0.14	···	···	···
351	815	···	1096	$30.33^{+0.12}_{-0.40}$	17.961	16.494	3.764±0.022	0.36±0.02	···	···	···
352	817	···	690	$30.43^{+0.10}_{-0.16}$	16.574	15.201	3.787±0.028	0.75±0.13	···	···	···
353	818	457	1276	$30.18^{+0.13}_{-0.19}$	19.288	17.350	3.681±0.018	−0.04±0.03	6.69	1.11	2.33±0.18
354	819	252	1178	$30.26^{+0.13}_{-0.13}$	18.631	16.861	3.764±0.010	0.41±0.02	0.33	1.21	1.61±0.15
355	821	···	1389	$29.99^{+0.15}_{-0.18}$	20.027	17.834	3.621±0.014	−0.37±0.13	···	···	···
356	822	420	1088	$30.37^{+0.13}_{-0.23}$	17.902	16.434	3.763±0.008	0.28±0.02	2.60	1.28	1.65±0.14
357	825	139	1687	$30.30^{+0.13}_{-0.19}$	21.416	18.692	3.564±0.010	−0.65±0.14	0.49	0.67	3.05±0.05
358	827	205	1119	$30.91^{+0.04}_{-0.05}$	18.128	16.596	3.767±0.024	0.32±0.02	1.19	1.26	1.58±0.35
359	828	51	1322	$30.35^{+0.12}_{-0.16}$	19.684	17.583	3.667±0.024	−0.08±0.06	0.67	1.05	2.44±0.32
360	829	···	1421	$29.87^{+0.16}_{-0.25}$	19.999	17.959	3.639±0.013	−0.41±0.13	···	···	···
361	833	359	1344	$29.98^{+0.15}_{-0.23}$	19.616	17.713	3.655±0.014	−0.30±0.13	8.20	1.03	2.41±0.15
362	834	17	1237	$30.56^{+0.07}_{-0.09}$	18.983	17.190	3.755±0.011	0.25±0.02	0.36	1.15	1.77±0.15
363	835	···	1630	$29.71^{+0.18}_{-0.33}$	21.202	18.518	3.567±0.011	−0.58±0.14	···	···	···
364	837	316	···	$30.09^{+0.14}_{-0.21}$	···	···	···	···	3.92	1.10	···
365	839	326	1450	$30.12^{+0.13}_{-0.19}$	20.133	18.044	3.633±0.013	−0.44±0.13	0.53	1.01	2.50±0.17
366	840	270	1114	$30.29^{+0.12}_{-0.17}$	18.142	16.547	3.757±0.010	0.36±0.02	0.38	1.27	1.72±0.14
367	841	216	1433	$29.98^{+0.15}_{-0.23}$	19.980	18.012	3.647±0.013	−0.42±0.13	2.66	0.95	2.39±0.13
368	843	···	1408	$29.80^{+0.20}_{-0.38}$	19.889	17.915	3.647±0.014	−0.38±0.13	···	···	···
369	845	···	2110	$29.94^{+0.15}_{-0.24}$	22.792	19.596	3.539±0.005	−0.98±0.15	···	···	···
370	846	···	247	$30.01^{+0.19}_{-0.33}$	14.479	13.716	4.089±0.050	2.05±0.12	···	···	···
371	847	···	806	$29.94^{+0.16}_{-0.26}$	16.818	15.486	3.811±0.014	0.80±0.02	···	···	···
372	848	···	1914	$29.79^{+0.16}_{-0.25}$	22.275	19.220	3.545±0.007	−0.84±0.16	···	···	···
373	851	···	2199	$30.04^{+0.14}_{-0.21}$	23.741	19.683	3.511±0.006	−0.89±0.17	···	···	···
374	854	···	1620	$29.74^{+0.18}_{-0.32}$	20.863	18.525	3.603±0.016	−0.64±0.15	···	···	···
375a	858	···	13601	$30.62^{+0.10}_{-0.14}$	12.341	11.782	4.284±0.118	3.26±0.28	···	···	···
375b	858	···	71	$30.58^{+0.12}_{-0.17}$	12.341	11.782	4.228±0.231	3.05±0.54	···	···	···
376	859	···	1417	$30.12^{+0.13}_{-0.19}$	20.137	17.920	3.618±0.015	−0.40±0.13	···	···	···
377	861	···	1195	$30.16^{+0.13}_{-0.19}$	18.771	16.982	3.671±0.020	0.01±0.13	···	···	···
378	864	···	900	$30.31^{+0.12}_{-0.16}$	16.878	15.689	3.837±0.020	0.63±0.02	···	···	···
379	865	···	13581	$30.42^{+0.07}_{-0.08}$	11.846	11.174	4.354±0.106	3.57±0.25	···	···	···
380	867	···	56	$30.28^{+0.10}_{-0.12}$	11.895	11.430	4.410±0.191	3.64±0.53	···	···	···
381	868	···	13648	$30.36^{+0.12}_{-0.16}$	13.807	···	4.046±0.052	2.24±0.11	···	···	···
382	869	···	1591	$30.12^{+0.14}_{-0.20}$	20.890	18.429	3.589±0.015	−0.57±0.15	···	···	···
383	871	···	1181	$30.68^{+0.07}_{-0.08}$	18.779	16.849	3.761±0.009	0.43±0.02	···	···	···
384	873	···	1310	$30.36^{+0.09}_{-0.12}$	19.442	17.535	3.654±0.015	−0.23±0.13	···	···	···
385	875	···	945	$30.27^{+0.12}_{-0.18}$	17.313	15.788	3.728±0.035	0.50±0.13	···	···	···
386	876	···	1256	$30.32^{+0.13}_{-0.18}$	18.909	17.304	3.708±0.029	−0.11±0.13	···	···	···
387	877	···	1153	$30.36^{+0.12}_{-0.18}$	18.339	16.728	3.762±0.008	0.31±0.02	···	···	···
388	879	468	1257	$30.56^{+0.12}_{-0.16}$	19.289	17.268	3.668±0.020	−0.03±0.05	1.50	1.13	2.44±0.26
389	880	···	1468	$30.33^{+0.13}_{-0.18}$	20.134	18.100	3.640±0.014	−0.46±0.13	···	···	···
390	881	···	1515	$30.36^{+0.13}_{-0.19}$	20.760	18.183	3.577±0.011	−0.46±0.14	···	···	···
391	884	···	1101	$30.60^{+0.07}_{-0.09}$	18.216	16.477	3.732±0.018	0.36±0.03	···	···	···

Table 2. continued.

X memb ID	X src ID	Moraux2013[a] ID	Currie2010[b] ID	$\log L_X^c$	m_V^d	m_I^d	$\log T_{\rm eff}$	$\log L_{\rm bol}/L_\odot$	Period[e] (d)	Mass[e] ($M_\odot$)	$\log \tau$ d
392	886	241	1259	$30.14^{+0.07}_{-0.09}$	19.338	17.270	3.603±0.010	−0.28±0.05	0.85	1.13	3.08±0.07
393	888	···	1040	$30.60^{+0.08}_{-0.09}$	17.593	16.201	3.777±0.014	0.43±0.02	···	···	···
394	889	307	841	$30.72^{+0.09}_{-0.06}$	16.949	15.537	3.787±0.017	0.72±0.02	0.46	1.40	1.14±0.32
395	893	···	172	$30.36^{+0.12}_{-0.17}$	13.716	13.077	4.005±0.212	1.99±0.25	···	···	···
396	894	···	2086	$29.89^{+0.17}_{-0.29}$	22.623	19.560	3.544±0.005	−0.97±0.14	···	···	···
397	895	···	502	$30.91^{+0.04}_{-0.04}$	15.872	14.785	3.853±0.022	1.06±0.02	···	···	···
398	897	29	1120	$30.88^{+0.05}_{-0.05}$	18.232	16.596	3.769±0.012	0.41±0.02	0.71	1.26	1.54±0.19
399	898	···	158	$30.18^{+0.14}_{-0.21}$	13.635	12.951	4.144±0.050	2.47±0.12	···	···	···
400	900	287	···	$30.37^{+0.08}_{-0.10}$	18.462	16.831	3.767±0.009	0.27±0.02	3.06	1.22	1.59±0.16
401	901	91	1117	$30.38^{+0.12}_{-0.17}$	18.091	16.579	3.772±0.012	0.41±0.02	4.12	1.27	1.49±0.19
402	903	···	1288	$30.24^{+0.10}_{-0.13}$	19.240	17.420	3.665±0.018	−0.17±0.13	···	···	···
403	907	···	613	$30.51^{+0.13}_{-0.19}$	16.323	15.044	3.802±0.024	0.84±0.13	···	···	···
404	908	332	1430	$30.14^{+0.14}_{-0.20}$	20.041	17.997	3.639±0.013	−0.42±0.13	0.32	0.96	2.47±0.15
405	909	263	1017	$30.43^{+0.08}_{-0.09}$	17.611	16.076	3.777±0.013	0.54±0.02	0.33	1.34	1.39±0.21
406	911	154	1179	$30.50^{+0.11}_{-0.14}$	18.578	16.867	3.759±0.007	0.17±0.02	3.05	1.22	1.71±0.11
407	913	230	1047	$30.35^{+0.11}_{-0.15}$	17.642	16.234	3.770±0.012	0.41±0.02	3.36	1.32	1.53±0.19
408	914	199	1483	$30.14^{+0.14}_{-0.21}$	20.348	18.120	3.616±0.014	−0.48±0.13	3.50	0.89	2.65±0.30
409	917	423	2375	$29.96^{+0.15}_{-0.22}$	23.489	20.026	3.530±0.006	−1.11±0.16	1.43	0.32	3.05±0.05
410	919	583	952	$30.30^{+0.13}_{-0.18}$	17.166	15.829	3.810±0.022	0.61±0.02	0.22	1.37	0.66±0.71
411	920	···	1771	$30.04^{+0.14}_{-0.21}$	22.018	18.865	3.541±0.004	−0.69±0.14	···	···	···
412	921	···	2231	$30.09^{+0.14}_{-0.21}$	23.053	19.809	3.538±0.005	−1.05±0.15	···	···	···
413	922	15	1262	$30.62^{+0.11}_{-0.14}$	19.094	17.309	3.737±0.014	0.13±0.02	0.95	1.12	1.98±0.18
414	923	···	166	$29.96^{+0.15}_{-0.24}$	13.666	13.012	4.071±0.053	2.23±0.12	···	···	···
415	926	160	1234	$30.00^{+0.17}_{-0.27}$	18.876	17.190	3.692±0.022	−0.08±0.13	3.62	1.15	2.25±0.17
416	927	341	872	$30.20^{+0.15}_{-0.24}$	16.862	15.617	3.807±0.028	0.62±0.13	0.90	1.39	0.73±0.93
417	929	2	1127	$30.55^{+0.11}_{-0.15}$	18.322	16.626	3.748±0.012	0.26±0.02	0.62	1.25	1.86±0.16
418	930	110	1318	$30.31^{+0.12}_{-0.18}$	19.519	17.587	3.651±0.013	−0.25±0.13	5.59	1.05	2.47±0.14
419	931	···	802	$29.84^{+0.17}_{-0.27}$	16.841	15.475	3.789±0.027	0.64±0.13	···	···	···
420	934	266	1604	$29.91^{+0.16}_{-0.24}$	21.328	18.423	3.551±0.006	−0.53±0.14	0.63	0.75	3.05±0.05
421	935	116	958	$30.59^{+0.11}_{-0.14}$	17.328	15.839	3.784±0.012	0.64±0.02	0.40	1.36	1.21±0.21
422	936	···	625	$31.04^{+0.07}_{-0.09}$	16.512	15.050	3.755±0.039	0.79±0.13	···	···	···
423	937	···	310	$30.11^{+0.13}_{-0.20}$	14.760	14.101	4.011±0.052	1.63±0.10	···	···	···
424	938	201	1435	$29.95^{+0.18}_{-0.31}$	20.270	17.992	3.610±0.014	−0.44±0.14	0.42	0.93	2.78±0.43
425	939	···	666	$30.25^{+0.14}_{-0.22}$	16.496	15.166	3.795±0.024	0.77±0.13	···	···	···
426	941	···	365	$30.11^{+0.18}_{-0.30}$	15.252	14.306	3.931±0.031	1.43±0.03	···	···	···
427	945	576	1536	$29.85^{+0.17}_{-0.28}$	20.898	18.240	3.570±0.011	−0.47±0.14	0.37	0.84	3.05±0.05
428	947	124	···	$30.59^{+0.07}_{-0.09}$	18.352	16.790	3.791±0.008	0.41±0.02	3.13	1.24	1.15±0.17
429	949	···	1062	$30.55^{+0.07}_{-0.08}$	17.754	16.340	3.786±0.010	0.43±0.02	···	···	···
430	955	335	1331	$30.53^{+0.10}_{-0.13}$	19.503	17.639	3.659±0.016	−0.26±0.13	7.41	1.02	2.38±0.18
431	956	442	2114	$30.34^{+0.14}_{-0.20}$	22.754	19.606	3.541±0.005	−0.99±0.14	6.02	0.42	3.05±0.05
432	958	···	2543	$30.24^{+0.14}_{-0.20}$	24.018	20.319	3.523±0.007	−1.19±0.19	···	···	···
433	961	43	1236	$30.51^{+0.07}_{-0.09}$	18.974	17.184	3.672±0.015	−0.10±0.03	1.60	1.14	2.38±0.18
434	962	···	262	$30.35^{+0.12}_{-0.18}$	14.552	13.802	4.023±0.064	1.81±0.13	···	···	···
435	963	80	1099	$30.63^{+0.09}_{-0.11}$	17.989	16.496	3.744±0.039	0.21±0.13	4.31	1.25	1.90±0.40
436	966	···	286	$30.67^{+0.06}_{-0.07}$	14.717	13.969	4.008±0.060	1.70±0.11	···	···	···
437	967	371	1050	$30.37^{+0.13}_{-0.18}$	17.743	16.241	3.774±0.013	0.44±0.02	4.02	1.32	1.47±0.21
438	968	355	1240	$30.54^{+0.09}_{-0.12}$	18.928	17.226	3.689±0.022	−0.09±0.13	0.91	1.12	2.27±0.19
439	971	···	755	$30.52^{+0.11}_{-0.15}$	16.847	15.364	3.773±0.012	0.79±0.02	···	···	···
440	974	460	1858	$30.14^{+0.17}_{-0.28}$	21.931	19.101	3.554±0.008	−0.81±0.14	2.63	0.56	3.05±0.05
441	976	220	1309	$30.18^{+0.14}_{-0.21}$	19.426	17.535	3.656±0.015	−0.23±0.13	4.76	1.10	2.44±0.16
442	977	141	1410	$30.49^{+0.10}_{-0.12}$	20.349	17.868	3.586±0.012	−0.34±0.14	0.50	0.96	3.05±0.05
443	980	294	1610	$30.10^{+0.15}_{-0.22}$	21.183	18.456	3.563±0.010	−0.56±0.14	0.86	0.78	3.05±0.05
444	981	63	···	$30.36^{+0.13}_{-0.19}$	···	···	···	···	5.32	1.11	···
445	982	33	1653	$30.15^{+0.15}_{-0.22}$	21.198	18.605	3.576±0.011	−0.62±0.14	0.74	0.76	3.05±0.07
446	983	568	1835	$30.10^{+0.16}_{-0.25}$	22.260	19.008	3.537±0.004	−0.73±0.14	0.32	0.55	3.05±0.05
447	990	441	···	$30.21^{+0.14}_{-0.21}$	17.503	16.195	3.806±0.013	0.40±0.02	0.80	1.32	1.16±0.34
448	991	62	1173	$30.17^{+0.17}_{-0.29}$	18.505	16.845	3.725±0.017	0.14±0.03	5.88	1.21	2.09±0.17
449	993	221	1348	$30.13^{+0.16}_{-0.25}$	19.624	17.719	3.654±0.014	−0.30±0.13	5.41	1.02	2.41±0.15
450	996	···	2194	$30.62^{+0.10}_{-0.13}$	23.008	19.751	3.537±0.005	−1.03±0.15	···	···	···
451	999	431	10149	$30.51^{+0.13}_{-0.19}$	21.121	18.777	3.602±0.013	−0.74±0.14	0.45	0.66	2.63±0.44
452	1002	···	7786	$30.83^{+0.13}_{-0.18}$	17.906	16.438	3.914±0.027	0.94±0.02	···	···	···
···	···	4	1123	< 30.95	18.098	16.629	3.759±0.010	0.29±0.02	2.85	1.27	1.70±0.14
···	···	7	1054	< 30.13	17.881	16.250	3.763±0.008	0.47±0.02	0.36	1.31	1.62±0.11
···	···	8	1357	< 30.06	19.703	17.748	3.610±0.027	−0.32±0.11	2.97	1.03	2.92±0.19
···	···	9	1287	< 30.25	19.092	17.429	3.709±0.018	−0.06±0.03	5.18	1.12	2.16±0.15
···	···	10	1446	< 30.12	20.230	18.030	3.620±0.014	−0.45±0.13	4.46	0.94	2.64±0.31
···	···	12	···	< 30.50	···	···	···	···	2.87	1.23	···
···	···	16	1414	< 30.38	19.819	17.938	3.657±0.015	−0.39±0.13	10.99	0.96	2.35±0.13
···	···	19	1091	< 30.43	18.020	16.457	3.765±0.018	0.31±0.02	1.53	1.28	1.62±0.28
···	···	23	1278	< 30.38	19.125	17.378	3.679±0.022	−0.15±0.13	7.52	1.09	2.31±0.22
···	···	24	890	< 31.10	17.024	15.659	3.794±0.013	0.66±0.02	0.47	1.39	1.02±0.29
···	···	28	1676	< 30.05	21.058	18.703	3.601±0.013	−0.70±0.14	2.15	0.73	2.67±0.52
···	···	30	···	< 30.30	···	···	···	···	0.37	1.36	···
···	···	31	···	< 30.10	···	···	···	···	0.35	1.30	···
···	···	35	1121	< 30.29	18.286	16.601	3.769±0.011	0.35±0.02	0.40	1.26	1.56±0.18
···	···	37	1370	< 30.16	19.650	17.800	3.660±0.017	−0.33±0.13	5.32	1.00	2.35±0.16
···	···	44	1349	< 30.20	19.543	17.729	3.666±0.019	−0.30±0.13	5.24	1.04	2.32±0.17
···	···	46	···	< 30.09	19.029	17.305	3.761±0.008	0.06±0.02	4.57	1.13	1.67±0.11
···	···	50	1638	< 30.13	20.897	18.576	3.605±0.014	−0.66±0.14	0.37	0.76	2.65±0.45
···	···	52	1503	< 30.05	20.378	18.196	3.622±0.014	−0.51±0.13	0.76	0.88	2.56±0.23

Table 2. continued.

X memb ID	X src ID	Moraux2013[a] ID	Currie2010[b] ID	$\log L_X^c$	m_V^d	m_I^d	$\log T_{\rm eff}$	$\log L_{\rm bol}/L_\odot$	Period[e] (d)	Mass[e] ($M_\odot$)	$\log \tau$ d
...	...	55	1300	< 30.27	19.248	17.495	3.700±0.015	−0.06±0.03	1.10	1.10	2.23±0.10
...	...	60	...	< 30.33	...	...	...	...	0.77	1.00	...
...	...	61	1876	< 30.13	22.416	19.102	3.535±0.004	−0.76±0.14	0.54	0.53	3.05±0.05
...	...	66	978	< 30.68	17.336	15.902	3.767±0.008	0.61±0.02	0.37	1.36	1.51±0.15
...	...	67	1319	< 30.36	19.449	17.596	3.660±0.017	−0.25±0.13	0.30	1.06	2.38±0.19
...	...	68	1358	< 30.33	19.561	17.763	3.669±0.019	−0.31±0.13	4.27	1.04	2.31±0.16
...	...	71	...	< 30.41	18.295	16.788	3.767±0.017	0.16±0.02	3.42	1.22	1.58±0.25
...	...	72	1522	< 30.00	20.465	18.249	3.618±0.014	−0.53±0.13	7.09	0.86	2.59±0.25
...	...	75	...	< 30.50	...	...	...	...	4.93	1.20	...
...	...	83	1368	< 31.21	19.820	17.776	3.639±0.013	−0.33±0.13	0.89	1.01	2.53±0.16
...	...	84	1385	< 30.03	19.667	17.844	3.665±0.018	−0.34±0.13	5.24	1.01	2.32±0.16
...	...	85	9348	< 30.41	20.282	18.165	3.630±0.014	−0.49±0.13	5.29	0.91	2.50±0.17
...	...	86	1329	< 29.97	19.434	17.643	3.671±0.020	−0.26±0.13	3.18	1.05	2.32±0.18
...	...	87	...	< 29.86	17.616	16.286	3.777±0.015	0.37±0.02	5.59	1.31	1.42±0.26
...	...	89	...	< 29.77	...	...	...	...	3.25	0.78	...
...	...	90	...	< 29.84	...	...	...	...	2.12	0.67	...
...	...	93	1866	< 31.08	21.934	19.132	3.556±0.009	−0.82±0.14	4.22	0.56	3.05±0.05
...	...	94	1346	< 30.25	19.700	17.709	3.645±0.014	−0.30±0.13	3.19	1.02	2.50±0.17
...	...	95	1302	< 30.33	19.276	17.500	3.673±0.020	−0.20±0.13	0.58	1.10	2.32±0.20
...	...	99	1537	< 30.07	20.390	18.296	3.633±0.014	−0.54±0.13	7.14	0.87	2.45±0.14
...	...	101	1751	< 30.22	21.612	18.842	3.559±0.009	−0.71±0.14	4.85	0.63	3.05±0.05
...	...	102	...	< 29.92	...	...	...	...	0.42	1.01	...
...	...	104	1122	< 30.65	18.305	16.601	3.728±0.019	0.26±0.03	0.34	1.25	2.06±0.18
...	...	105	1079	< 30.43	17.816	16.415	3.767±0.013	0.32±0.02	2.69	1.30	1.58±0.21
...	...	114	1505	< 30.40	20.231	18.215	3.642±0.013	−0.51±0.13	0.71	0.88	2.39±0.13
...	...	118	1529	< 30.28	20.834	18.233	3.575±0.010	−0.47±0.14	4.41	0.85	3.05±0.05
...	...	119	...	< 29.73	...	...	...	...	0.33	1.00	...
...	...	122	1291	< 30.20	19.362	17.422	3.651±0.013	−0.18±0.13	0.86	1.10	2.53±0.14
...	...	123	...	< 30.00	...	...	...	...	7.25	1.05	...
...	...	126	1463	< 29.99	20.090	18.094	3.644±0.013	−0.46±0.13	0.28	0.94	2.40±0.13
...	...	131	1269	< 30.29	19.131	17.339	3.731±0.016	0.11±0.02	0.35	1.12	2.04±0.18
...	...	133	...	< 30.30	18.890	17.169	3.757±0.012	0.07±0.02	2.66	1.16	1.71±0.17
...	...	134	1362	< 30.33	19.641	17.776	3.659±0.016	−0.32±0.13	2.72	1.02	2.37±0.16
...	...	135	...	< 30.13	...	...	...	...	5.71	0.83	...
...	...	140	1024	< 30.49	17.533	16.110	3.767±0.037	0.37±0.13	0.77	1.33	1.58±0.53
...	...	143	...	< 30.38	...	...	...	...	2.24	0.87	...
...	...	145	7841	< 30.72	18.062	16.491	3.751±0.024	0.33±0.03	4.63	1.28	1.79±0.31
...	...	147	1668	< 30.07	21.156	18.669	3.586±0.012	−0.65±0.14	0.29	0.70	3.07±0.05
...	...	149	...	< 30.28	...	...	...	...	0.95	0.58	...
...	...	150	...	< 30.14	...	...	...	...	0.28	0.55	...
...	...	151	1538	< 30.33	20.438	18.293	3.627±0.014	−0.55±0.13	5.52	0.82	2.50±0.18
...	...	156	818	< 30.09	16.870	15.497	3.765±0.009	0.60±0.02	7.46	1.42	1.54±0.16
...	...	158	13701	< 30.07	16.808	15.530	3.805±0.013	0.72±0.02	0.69	1.41	0.72±0.40
...	...	159	...	< 30.28	20.710	18.636	3.635±0.017	−0.68±0.13	7.30	0.75	2.34±0.22
...	...	161	1692	< 29.77	21.105	18.737	3.599±0.013	−0.71±0.14	0.48	0.68	2.68±0.58
...	...	163	1418	< 30.23	19.831	17.957	3.658±0.015	−0.39±0.13	7.30	0.99	2.34±0.13
...	...	165	1707	< 30.28	21.470	18.749	3.564±0.010	−0.67±0.14	1.42	0.66	3.05±0.05
...	...	166	1366	< 30.19	19.718	17.784	3.651±0.013	−0.33±0.13	6.58	1.00	2.42±0.14
...	...	168	...	< 30.26	...	...	...	...	1.85	0.76	...
...	...	170	9951	< 30.44	20.891	18.659	3.616±0.014	−0.70±0.13	2.92	0.72	2.53±0.16
...	...	175	2187	< 30.11	23.081	19.727	3.534±0.005	−1.01±0.15	0.76	0.38	3.05±0.05
...	...	176	...	< 30.51	...	...	...	...	2.83	0.87	...
...	...	177	1231	< 30.30	18.899	17.182	3.686±0.022	−0.07±0.13	0.41	1.16	2.29±0.21
...	...	179	2038	< 30.02	22.591	19.444	3.541±0.005	−0.92±0.14	0.44	0.47	3.05±0.05
...	...	180	1801	< 30.14	21.789	18.958	3.554±0.008	−0.75±0.14	0.61	0.60	3.05±0.05
...	...	181	1391	< 30.19	19.800	17.872	3.652±0.013	−0.36±0.13	1.85	1.00	2.39±0.14
...	...	182	...	< 29.90	...	...	...	...	5.49	0.52	...
...	...	183	...	< 30.40	...	...	...	...	3.11	1.01	...
...	...	184	1403	< 29.96	19.846	17.911	3.651±0.013	−0.38±0.13	3.19	0.98	2.39±0.13
...	...	185	1491	< 30.34	20.542	18.126	3.594±0.013	−0.46±0.14	0.49	0.88	3.07±0.10
...	...	186	1743	< 30.16	21.343	18.852	3.585±0.012	−0.73±0.14	0.44	0.65	3.02±0.05
...	...	192	1199	< 30.15	18.796	17.012	3.728±0.016	0.14±0.03	0.64	1.18	2.06±0.17
...	...	196	1833	< 30.15	21.675	19.054	3.573±0.011	−0.80±0.14	2.13	0.59	3.05±0.10
...	...	198	1741	< 30.23	21.749	18.802	3.549±0.005	−0.68±0.14	11.76	0.65	3.05±0.05
...	...	202	1328	< 30.10	19.572	17.628	3.650±0.013	−0.27±0.13	0.33	1.06	2.47±0.14
...	...	203	1471	< 30.10	20.194	18.101	3.633±0.013	−0.47±0.13	0.28	0.92	2.49±0.16
...	...	206	1545	< 29.83	20.549	18.301	3.614±0.014	−0.56±0.13	0.30	0.86	2.62±0.33
...	...	208	742	< 29.75	16.413	15.366	3.862±0.028	0.82±0.02	0.81	1.54	−0.90±1.41
...	...	209	1564	< 30.07	20.572	18.374	3.620±0.014	−0.58±0.13	7.14	0.81	2.54±0.21
...	...	212	1588	< 30.57	20.701	18.444	3.612±0.014	−0.61±0.14	10.99	0.78	2.59±0.32
...	...	213	9139	< 30.33	19.988	17.983	3.643±0.013	−0.41±0.13	5.65	0.94	2.43±0.13
...	...	214	1064	< 30.17	17.874	16.340	3.754±0.011	0.40±0.02	0.33	1.30	1.76±0.15
...	...	217	...	< 30.16	...	...	...	...	0.45	0.49	...
...	...	218	1166	< 29.96	18.272	16.801	3.720±0.022	0.08±0.03	4.31	1.24	2.11±0.19
...	...	219	1533	< 30.13	20.541	18.273	3.611±0.014	−0.55±0.14	5.56	0.83	2.66±0.42
...	...	223	...	< 29.79	...	...	...	...	5.21	0.99	...
...	...	224	1383	< 30.14	19.793	17.824	3.647±0.013	−0.35±0.13	2.40	1.00	2.45±0.13
...	...	226	...	< 30.18	...	...	...	...	0.76	0.73	...
...	...	228	...	< 30.07	...	...	...	...	0.34	0.67	...
...	...	229	...	< 29.72	...	...	...	...	6.45	0.82	...
...	...	231	1365	< 30.04	19.977	17.753	3.617±0.014	−0.34±0.13	4.57	1.01	2.77±0.46
...	...	232	1513	< 30.19	20.299	18.221	3.635±0.013	−0.51±0.13	5.00	0.89	2.45±0.14
...	...	233	...	< 29.91	...	...	...	...	3.28	0.50	...
...	...	237	1459	< 30.22	20.300	18.062	3.615±0.014	−0.46±0.13	4.48	0.91	2.68±0.36

Table 2. continued.

X memb ID	X src ID	Moraux2013[a] ID	Currie2010[b] ID	$\log L_X^c$	m_V^d	m_I^d	$\log T_{\rm eff}$	$\log L_{\rm bol}/L_\odot$	Period[e] (d)	Mass[e] ($M_\odot$)	$\log \tau$ d
...	...	238	1314	< 30.38	19.722	17.531	3.621±0.014	−0.25±0.13	1.38	1.06	2.81±0.37
...	...	239	1517	< 30.49	20.338	18.237	3.632±0.014	−0.52±0.13	0.86	0.85	2.47±0.15
...	...	240	1603	< 30.29	20.743	18.483	3.612±0.014	−0.63±0.14	3.30	0.77	2.58±0.31
...	...	242	...	< 30.24	...	...	...	...	0.31	1.09	...
...	...	244	1607	< 29.85	20.803	18.485	3.605±0.013	−0.63±0.14	0.68	0.78	2.67±0.44
...	...	245	1939	< 29.59	22.503	19.243	3.537±0.004	−0.83±0.14	0.75	0.53	3.05±0.05
...	...	246	1451	< 30.33	20.056	18.067	3.645±0.013	−0.45±0.13	3.92	0.94	2.40±0.13
...	...	248	1944	< 30.39	22.560	19.258	3.536±0.004	−0.83±0.14	4.39	0.52	3.05±0.05
...	...	249	1680	< 30.05	21.232	18.692	3.581±0.011	−0.66±0.14	0.83	0.67	3.06±0.11
...	...	251	2045	< 30.28	22.308	19.497	3.555±0.009	−0.97±0.14	2.87	0.47	3.05±0.05
...	...	253	...	< 30.34	...	...	...	...	0.61	0.45	...
...	...	254	1480	< 30.42	20.507	18.091	3.594±0.013	−0.44±0.14	6.10	0.91	3.07±0.09
...	...	255	1493	< 30.39	20.406	18.144	3.612±0.014	−0.50±0.14	1.63	0.88	2.69±0.44
...	...	257	...	< 30.02	...	...	...	...	6.29	0.64	...
...	...	258	...	< 30.66	...	...	...	...	2.50	0.98	...
...	...	259	...	< 30.44	17.645	16.275	3.797±0.011	0.45±0.02	2.29	1.31	1.02±0.25
...	...	260	1709	< 30.42	21.235	18.778	3.589±0.012	−0.71±0.14	3.66	0.67	2.91±0.20
...	...	261	821	< 30.70	16.720	15.526	3.802±0.013	0.68±0.02	1.29	1.41	0.82±0.37
...	...	262	1399	< 30.20	19.823	17.891	3.651±0.013	−0.37±0.13	1.25	0.99	2.39±0.14
...	...	264	...	< 30.18	...	...	...	...	6.33	0.76	...
...	...	265	927	< 30.93	17.130	15.747	3.782±0.010	0.62±0.02	1.96	1.39	1.24±0.18
...	...	268	1508	< 30.31	20.370	18.201	3.624±0.014	−0.51±0.13	0.73	0.87	2.54±0.22
...	...	269	2095	< 30.11	22.638	19.586	3.545±0.005	−0.99±0.14	7.41	0.43	3.05±0.05
...	...	271	1032	< 30.22	17.522	16.141	3.766±0.027	0.33±0.03	3.48	1.32	1.60±0.39
...	...	274	1243	< 30.57	18.989	17.235	3.678±0.021	−0.09±0.13	11.49	1.14	2.34±0.25
...	...	276	...	< 30.45	18.187	16.751	3.777±0.014	0.16±0.02	1.21	1.23	1.55±0.13
...	...	277	...	< 29.88	...	...	...	...	4.46	0.71	...
...	...	278	1566	< 30.33	20.701	18.363	3.603±0.013	−0.57±0.14	6.94	0.83	2.75±0.47
...	...	279	1889	< 29.98	21.881	19.194	3.567±0.011	−0.85±0.14	6.58	0.52	3.05±0.08
...	...	280	...	< 30.30	...	...	...	...	0.85	1.12	...
...	...	281	2067	< 30.07	22.640	19.516	3.542±0.005	−0.95±0.14	8.00	0.43	3.05±0.05
...	...	282	...	< 30.15	...	...	...	...	1.81	0.46	...
...	...	283	1804	< 30.17	21.586	18.986	3.575±0.011	−0.78±0.14	0.32	0.61	3.08±0.07
...	...	285	...	< 30.15	...	...	...	...	5.49	0.70	...
...	...	286	1702	< 30.27	21.257	18.755	3.584±0.012	−0.69±0.14	3.75	0.65	3.08±0.05
...	...	288	...	< 29.98	...	...	...	...	0.89	1.00	...
...	...	289	1452	< 30.01	20.065	18.067	3.644±0.013	−0.45±0.13	5.56	0.94	2.41±0.13
...	...	290	1285	< 30.13	19.088	17.404	3.693±0.022	−0.16±0.13	4.88	1.11	2.22±0.15
...	...	296	1321	< 30.19	19.356	17.617	3.681±0.022	−0.25±0.13	5.08	1.06	2.26±0.15
...	...	297	...	< 30.14	...	...	...	...	0.58	0.92	...
...	...	298	...	< 31.04	...	...	...	...	0.54	0.69	...
...	...	299	1488	< 30.13	20.260	18.142	3.630±0.014	−0.48±0.13	0.33	0.90	2.51±0.17
...	...	300	2109	< 30.32	22.519	19.625	3.551±0.007	−1.01±0.14	0.53	0.44	3.05±0.05
...	...	303	2236	< 30.24	22.925	19.828	3.543±0.005	−1.08±0.15	0.36	0.36	3.05±0.05
...	...	304	1650	< 30.15	20.947	18.621	3.604±0.013	−0.68±0.14	9.43	0.70	2.64±0.40
...	...	305	...	< 30.67	...	...	...	...	2.71	1.15	...
...	...	308	1540	< 29.96	20.402	18.301	3.632±0.014	−0.55±0.13	2.25	0.85	2.45±0.14
...	...	309	1978	< 30.29	22.337	19.354	3.548±0.005	−0.90±0.14	4.02	0.48	3.05±0.05
...	...	311	1211	< 30.78	18.713	17.078	3.732±0.017	0.02±0.03	0.50	1.18	1.98±0.17
...	...	313	1242	< 30.16	19.126	17.218	3.641±0.023	−0.12±0.07	4.72	1.15	2.66±0.80
...	...	315	1441	< 29.75	20.168	18.017	3.626±0.014	−0.44±0.13	1.16	0.90	2.58±0.23
...	...	318	1597	< 30.44	20.744	18.465	3.610±0.014	−0.62±0.14	0.87	0.79	2.61±0.37
...	...	319	877	< 30.33	17.095	15.607	3.746±0.039	0.57±0.13	11.90	1.39	1.80±0.56
...	...	321	...	< 30.23	...	...	...	...	8.20	0.67	...
...	...	322	1460	< 30.30	20.640	18.027	3.574±0.010	−0.39±0.13	0.54	0.91	3.05±0.05
...	...	323	...	< 29.96	17.768	16.407	3.779±0.015	0.31±0.02	6.67	1.30	1.39±0.26
...	...	324	1840	< 30.21	21.697	19.076	3.573±0.011	−0.81±0.14	7.25	0.57	3.05±0.10
...	...	325	1499	< 30.25	20.294	18.181	3.631±0.014	−0.50±0.13	8.62	0.87	2.50±0.16
...	...	327	1282	< 30.23	19.279	17.378	3.655±0.014	−0.16±0.13	4.57	1.11	2.51±0.15
...	...	328	2003	< 30.31	22.457	19.394	3.544±0.005	−0.91±0.14	1.15	0.47	3.05±0.05
...	...	329	1264	< 30.34	19.064	17.315	3.700±0.021	−0.05±0.04	0.75	1.14	2.23±0.15
...	...	330	1837	< 29.93	22.172	19.022	3.541±0.004	−0.75±0.14	2.64	0.57	3.05±0.05
...	...	331	...	< 30.49	...	...	...	...	0.68	0.43	...
...	...	333	716	< 30.22	16.325	15.305	3.847±0.025	0.74±0.02	0.62	1.54	−0.68±1.67
...	...	334	...	< 29.66	...	...	...	...	0.65	0.58	...
...	...	336	2170	< 30.34	23.006	19.714	3.536±0.005	−1.01±0.15	5.65	0.40	3.05±0.05
...	...	338	...	< 30.24	...	...	...	...	5.88	1.34	...
...	...	339	...	< 29.96	...	...	...	...	6.41	0.58	...
...	...	340	708	< 30.32	16.328	15.288	3.842±0.024	0.77±0.02	0.28	1.60	−0.64±1.15
...	...	342	1663	< 30.39	21.046	18.666	3.598±0.013	−0.68±0.14	3.62	0.70	2.73±0.57
...	...	343	1420	< 30.14	19.998	17.951	3.639±0.013	−0.40±0.13	6.85	0.97	2.48±0.15
...	...	344	...	< 30.16	...	...	...	...	0.32	0.52	...
...	...	345	2146	< 30.07	22.764	19.680	3.543±0.005	−1.02±0.14	6.33	0.40	3.05±0.05
...	...	347	...	< 30.23	...	...	...	...	5.56	0.89	...
...	...	348	1759	< 30.30	21.482	18.873	3.574±0.011	−0.73±0.14	0.55	0.62	3.06±0.07
...	...	350	...	< 30.05	...	...	...	...	7.94	0.82	...
...	...	351	...	< 30.34	...	...	...	...	4.02	0.72	...
...	...	352	1416	< 30.27	19.961	17.936	3.641±0.013	−0.40±0.13	9.17	0.96	2.47±0.14
...	...	354	1652	< 30.11	21.198	18.602	3.575±0.011	−0.62±0.14	1.35	0.72	3.05±0.06
...	...	356	1672	< 30.56	21.238	18.666	3.578±0.011	−0.65±0.14	0.32	0.68	3.05±0.09
...	...	357	1492	< 30.33	20.193	18.165	3.641±0.013	−0.49±0.13	0.48	0.90	2.41±0.13
...	...	360	1544	< 30.21	20.561	18.297	3.612±0.014	−0.56±0.14	7.87	0.83	2.65±0.39
...	...	361	1551	< 30.29	20.528	18.334	3.620±0.014	−0.57±0.13	3.88	0.84	2.54±0.22
...	...	363	...	< 30.21	...	...	...	...	0.49	0.68	...

Table 2. continued.

X memb ID	X src ID	Moraux2013[a] ID	Currie2010[b] ID	$\log L_X^c$	m_V^d	m_I^d	$\log T_{\rm eff}$	$\log L_{\rm bol}/L_\odot$	Period[e] (d)	Mass[e] ($M_\odot$)	$\log \tau$ d
...	...	365	1803	< 30.37	21.618	18.982	3.572±0.011	−0.77±0.14	6.49	0.62	3.05±0.08
...	...	366	867	< 29.57	16.893	15.605	3.791±0.014	0.62±0.02	7.46	1.40	1.10±0.28
...	...	368	1665	< 29.92	21.149	18.660	3.585±0.012	−0.65±0.14	15.38	0.70	3.07±0.05
...	...	370	...	< 29.92	...	...	...	...	3.80	1.36	...
...	...	373	...	< 30.14	18.482	16.840	3.765±0.005	0.26±0.02	0.34	1.23	1.62±0.09
...	...	374	...	< 29.82	...	...	...	...	4.65	0.69	...
...	...	376	1689	< 30.35	21.413	18.695	3.564±0.010	−0.65±0.14	6.02	0.70	3.05±0.05
...	...	378	...	< 29.97	...	...	...	...	0.43	0.84	...
...	...	379	1472	< 30.46	20.164	18.106	3.637±0.013	−0.47±0.13	7.46	0.90	2.46±0.14
...	...	380	1378	< 30.03	19.791	17.818	3.647±0.013	−0.34±0.13	0.35	1.01	2.45±0.13
...	...	381	1576	< 30.26	20.824	18.398	3.593±0.012	−0.56±0.14	3.41	0.77	3.02±0.05
...	...	383	...	< 29.98	22.026	19.398	3.572±0.011	−0.94±0.14	0.54	0.49	3.06±0.05
...	...	384	...	< 30.27	...	...	...	...	0.31	1.22	...
...	...	386	1998	< 29.93	22.691	19.353	3.534±0.004	−0.86±0.15	8.00	0.48	3.05±0.05
...	...	388	1373	< 30.21	19.740	17.813	3.652±0.013	−0.34±0.13	1.49	1.01	2.41±0.14
...	...	389	...	< 30.18	...	...	...	...	0.55	0.74	...
...	...	390	2005	< 30.04	22.406	19.403	3.547±0.005	−0.92±0.14	0.66	0.47	3.05±0.05
...	...	392	1467	< 30.40	20.121	18.099	3.641±0.014	−0.46±0.13	2.69	0.92	2.42±0.15
...	...	394	...	< 30.12	...	...	...	...	0.47	0.94	...
...	...	395	...	< 30.38	...	...	...	...	0.33	0.98	...
...	...	396	10204	< 30.55	21.225	18.812	3.594±0.013	−0.73±0.14	4.42	0.65	2.75±0.55
...	...	397	1851	< 29.67	21.772	19.105	3.569±0.011	−0.82±0.14	4.20	0.57	3.05±0.08
...	...	398	...	< 29.63	...	...	...	...	3.21	0.91	...
...	...	399	1770	< 30.00	21.490	18.919	3.578±0.011	−0.75±0.14	6.85	0.63	3.08±0.06
...	...	400	1495	< 30.23	20.230	18.171	3.637±0.013	−0.49±0.13	4.61	0.89	2.44±0.13
...	...	402	1213	< 30.54	18.734	17.092	3.701±0.024	−0.03±0.13	3.69	1.18	2.22±0.17
...	...	404	1026	< 30.25	17.477	16.117	3.790±0.026	0.38±0.13	6.94	1.33	1.19±0.52
...	...	405	...	< 29.99	...	...	...	...	7.25	0.83	...
...	...	407	...	< 29.80	...	...	...	...	0.61	0.61	...
...	...	408	...	< 30.33	...	...	...	...	1.53	0.46	...
...	...	410	...	< 29.94	...	...	...	...	10.87	0.53	...
...	...	412	...	< 30.22	...	...	...	...	0.57	0.37	...
...	...	414	933	< 29.85	17.018	15.772	3.806±0.028	0.56±0.13	2.27	1.38	0.76±0.86
...	...	415	2034	< 30.40	22.479	19.450	3.546±0.005	−0.93±0.14	0.67	0.44	3.05±0.05
...	...	421	...	< 30.25	...	...	...	...	11.24	0.93	...
...	...	425	1921	< 30.46	22.120	19.251	3.552±0.007	−0.86±0.14	0.62	0.52	3.05±0.05
...	...	428	...	< 29.93	18.153	16.733	3.765±0.007	0.18±0.02	7.81	1.24	1.60±0.13
...	...	429	1681	< 30.30	21.358	18.679	3.568±0.011	−0.65±0.14	0.46	0.68	3.05±0.05
...	...	430	1354	< 29.88	19.936	17.711	3.617±0.014	−0.32±0.13	14.49	1.03	2.80±0.43
...	...	432	1813	< 29.69	22.187	18.946	3.538±0.004	−0.71±0.14	0.44	0.59	3.05±0.05
...	...	433	...	< 29.91	...	...	...	...	4.39	1.33	...
...	...	434	10434	< 30.49	21.550	18.946	3.575±0.011	−0.76±0.14	5.52	0.62	3.07±0.08
...	...	435	...	< 30.29	...	...	...	...	4.72	0.58	...
...	...	436	...	< 29.84	...	...	...	...	7.69	0.64	...
...	...	437	1812	< 30.05	21.495	19.019	3.587±0.012	−0.80±0.14	10.20	0.59	2.87±0.26
...	...	438	1942	< 30.48	22.055	19.308	3.561±0.010	−0.90±0.14	3.26	0.51	3.05±0.05
...	...	439	...	< 30.16	...	...	...	...	3.39	1.04	...
...	...	440	...	< 30.28	...	...	...	...	0.34	1.01	...
...	...	443	1996	< 30.22	22.290	19.384	3.551±0.006	−0.92±0.14	7.52	0.48	3.05±0.05
...	...	444	...	< 30.24	...	...	...	...	0.52	0.47	...
...	...	445	...	< 29.96	...	...	...	...	8.62	0.67	...
...	...	447	2213	< 29.98	23.091	19.771	3.535±0.005	−1.03±0.15	4.05	0.38	3.05±0.05
...	...	448	1527	< 30.13	20.471	18.268	3.619±0.014	−0.54±0.13	4.88	0.87	2.57±0.24
...	...	450	...	< 30.10	...	...	...	...	7.52	0.39	...
...	...	452	...	< 30.23	17.670	16.328	3.786±0.014	0.35±0.02	5.05	1.31	1.26±0.26
...	...	453	1182	< 30.21	18.706	16.873	3.675±0.018	0.10±0.04	8.33	1.21	2.47±0.20
...	...	454	2075	< 29.86	22.396	19.554	3.553±0.008	−0.99±0.14	8.26	0.44	3.05±0.05
...	...	458	2119	< 30.41	22.552	19.635	3.550±0.014	−1.01±0.19	0.83	0.44	3.05±0.05
...	...	461	1547	< 30.06	20.505	18.312	3.621±0.014	−0.56±0.13	10.53	0.84	2.55±0.22
...	...	463	796	< 30.20	16.741	15.459	3.731±0.028	0.51±0.04	10.00	1.43	2.02±0.34
...	...	465	1685	< 30.13	21.350	18.689	3.569±0.011	−0.65±0.14	5.41	0.70	3.05±0.05
...	...	466	...	< 30.28	...	...	...	...	7.46	0.81	...
...	...	467	930	< 30.08	16.960	15.773	3.805±0.013	0.57±0.02	3.57	1.38	0.80±0.40
...	...	469	1608	< 29.98	20.871	18.481	3.597±0.013	−0.60±0.14	6.99	0.77	2.85±0.30
...	...	470	...	< 30.26	...	...	...	...	0.42	0.48	...
...	...	471	1170	< 31.00	18.593	16.788	3.668±0.019	0.08±0.13	0.26	1.22	2.53±0.25
...	...	474	1631	< 30.36	21.062	18.533	3.582±0.011	−0.60±0.14	6.10	0.75	3.05±0.10
...	...	475	1280	< 30.02	19.148	17.386	3.676±0.021	−0.15±0.13	6.25	1.11	2.33±0.22
...	...	476	...	< 30.24	...	...	...	...	5.10	0.90	...
...	...	477	896	< 30.29	16.875	15.683	3.810±0.016	0.60±0.02	1.56	1.39	0.66±0.50
...	...	478	1818	< 30.38	21.770	18.997	3.559±0.009	−0.77±0.14	0.47	0.59	3.05±0.05
...	...	480	...	< 29.62	...	...	...	...	5.56	0.40	...
...	...	481	...	< 30.40	...	...	...	...	6.52	1.38	...
...	...	482	...	< 30.24	...	...	...	...	0.26	0.43	...
...	...	483	2166	< 29.84	23.717	19.631	3.511±0.006	−0.86±0.17	0.39	0.41	3.05±0.05
...	...	484	880	< 30.25	16.846	15.638	3.854±0.025	0.76±0.02	0.15	1.39	−0.92±2.05
...	...	485	...	< 29.65	...	...	...	...	2.64	0.87	...
...	...	486	1230	< 30.33	18.850	17.181	3.696±0.022	−0.07±0.13	7.35	1.15	2.24±0.15
...	...	488	1768	< 30.23	21.890	18.864	3.546±0.005	−0.70±0.14	0.54	0.61	3.05±0.05
...	...	489	8785	< 31.40	19.728	17.621	3.631±0.014	−0.28±0.13	4.52	1.05	2.65±0.26
...	...	490	1877	< 30.08	21.977	19.150	3.554±0.008	−0.83±0.14	0.55	0.54	3.05±0.05
...	...	491	1667	< 30.35	21.539	18.625	3.550±0.005	−0.61±0.14	1.30	0.70	3.05±0.05
...	...	495	...	< 30.26	...	...	...	...	2.93	1.02	...
...	...	496	1552	< 30.28	20.898	18.301	3.575±0.011	−0.50±0.14	10.75	0.83	3.05±0.05

Table 2. continued.

X memb ID	X src ID	Moraux2013[a] ID	Currie2010[b] ID	$\log L_X^c$	m_V^d	m_I^d	$\log T_{\rm eff}$	$\log L_{\rm bol}/L_\odot$	Period[e] (d)	Mass[e] ($M_\odot$)	$\log \tau$ d
···	···	497	1988	< 30.43	22.211	19.377	3.554±0.008	−0.92±0.14	8.47	0.48	3.05±0.05
···	···	498	···	< 29.96	···	···	···	···	0.34	0.47	···
···	···	499	1498	< 30.17	20.260	18.180	3.635±0.013	−0.50±0.13	4.88	0.88	2.46±0.14
···	···	500	1802	< 30.33	21.636	18.977	3.569±0.011	−0.77±0.14	0.47	0.61	3.05±0.07
···	···	502	···	< 29.92	···	···	···	···	1.34	0.41	···
···	···	506	1424	< 30.45	20.361	17.935	3.593±0.012	−0.38±0.14	3.33	0.97	3.06±0.09
···	···	507	···	< 30.28	···	···	···	···	1.17	0.60	···
···	···	508	1987	< 30.22	22.287	19.368	3.550±0.006	−0.91±0.14	10.87	0.50	3.05±0.05
···	···	510	···	< 30.18	···	···	···	···	2.16	0.36	···
···	···	511	1530	< 30.22	20.486	18.272	3.618±0.014	−0.54±0.13	0.79	0.83	2.58±0.25
···	···	512	1901	< 30.10	22.140	19.196	3.549±0.005	−0.84±0.14	0.45	0.53	3.05±0.05
···	···	514	1926	< 30.17	22.048	19.271	3.559±0.009	−0.88±0.14	5.41	0.51	3.05±0.05
···	···	516	2241	< 30.22	23.026	19.828	3.539±0.005	−1.07±0.15	0.45	0.36	3.05±0.05
···	···	517	1393	< 30.24	19.732	17.883	3.661±0.017	−0.36±0.13	4.18	0.99	2.34±0.15
···	···	518	1975	< 30.27	22.241	19.357	3.552±0.007	−0.91±0.14	7.75	0.47	3.05±0.05
···	···	519	1924	< 30.35	22.186	19.251	3.550±0.005	−0.86±0.14	1.26	0.51	3.05±0.05
···	···	520	1826	< 30.11	21.970	19.004	3.548±0.005	−0.76±0.14	0.46	0.58	3.05±0.05
···	···	521	1905	< 29.90	22.058	19.216	3.553±0.008	−0.85±0.14	0.81	0.51	3.05±0.05
···	···	522	2004	< 29.90	22.368	19.404	3.548±0.005	−0.92±0.14	7.75	0.52	3.05±0.05
···	···	523	···	< 30.28	···	···	···	···	8.03	1.17	···
···	···	525	···	< 30.47	···	···	···	···	12.50	0.58	···
···	···	527	···	< 30.25	19.024	17.323	3.764±0.009	0.14±0.02	0.26	1.13	1.62±0.15
···	···	528	1848	< 30.20	21.797	19.085	3.565±0.012	−0.81±0.15	1.23	0.56	3.05±0.06
···	···	529	···	< 29.73	···	···	···	···	0.28	0.85	···
···	···	531	959	< 30.10	17.144	15.859	3.786±0.018	0.47±0.02	3.26	1.37	1.24±0.35
···	···	532	1611	< 30.30	20.879	18.492	3.597±0.013	−0.61±0.14	6.45	0.76	2.83±0.33
···	···	533	2039	< 30.37	22.367	19.478	3.551±0.007	−0.95±0.14	3.76	0.45	3.05±0.05
···	···	534	1664	< 29.62	21.072	18.664	3.595±0.013	−0.67±0.14	3.91	0.71	2.80±0.45
···	···	535	1915	< 30.20	22.154	19.234	3.550±0.006	−0.85±0.14	2.23	0.54	3.05±0.05
···	···	536	···	< 30.15	···	···	···	···	4.00	0.55	···
···	···	537	···	< 30.11	···	···	···	···	6.08	1.05	···
···	···	538	···	< 30.35	···	···	···	···	3.77	0.81	···
···	···	539	1908	< 29.90	22.336	19.201	3.541±0.005	−0.83±0.14	6.76	0.53	3.05±0.05
···	···	540	···	< 30.43	···	···	···	···	4.55	0.45	···
···	···	541	1535	< 29.72	20.828	18.247	3.577±0.011	−0.48±0.14	8.13	0.85	3.05±0.05
···	···	542	2365	< 30.58	23.515	19.993	3.528±0.006	−1.09±0.16	3.11	0.34	3.05±0.05
···	···	543	1711	< 30.09	21.164	18.789	3.599±0.013	−0.73±0.14	0.27	0.69	2.68±0.59
···	···	545	···	< 29.71	···	···	···	···	3.25	0.36	···
···	···	546	1679	< 30.16	21.457	18.666	3.557±0.009	−0.64±0.14	7.81	0.69	3.05±0.05
···	···	548	1746	< 30.19	21.436	18.845	3.576±0.011	−0.72±0.14	5.24	0.63	3.06±0.08
···	···	549	1659	< 29.91	21.045	18.656	3.597±0.013	−0.68±0.14	6.72	0.71	2.76±0.54
···	···	550	793	< 30.14	16.497	15.472	3.825±0.020	0.63±0.02	0.31	1.43	0.17±0.80
···	···	553	2006	< 30.31	22.393	19.408	3.547±0.005	−0.92±0.14	5.88	0.46	3.05±0.05
···	···	554	···	< 30.26	···	···	···	···	3.79	0.47	···
···	···	555	1881	< 30.23	22.245	19.126	3.542±0.005	−0.80±0.14	2.93	0.54	3.05±0.05
···	···	556	1742	< 30.05	21.185	18.862	3.605±0.014	−0.77±0.14	3.45	0.66	2.57±0.33
···	···	557	···	< 29.95	···	···	···	···	7.25	0.55	···
···	···	558	1049	< 30.37	17.670	16.248	3.766±0.008	0.36±0.02	6.83	1.31	1.60±0.12
···	···	559	1809	< 29.85	21.844	18.977	3.552±0.007	−0.76±0.14	5.05	0.59	3.05±0.05
···	···	560	1891	< 30.10	21.980	19.185	3.557±0.009	−0.84±0.14	0.63	0.52	3.05±0.05
···	···	561	2031	< 30.49	22.348	19.454	3.551±0.006	−0.94±0.14	11.36	0.44	3.05±0.05
···	···	562	1014	< 30.08	17.732	16.045	3.660±0.021	0.13±0.05	6.85	1.33	2.63±0.58
···	···	563	···	< 30.10	···	···	···	···	0.47	0.34	···
···	···	564	929	< 29.77	17.214	15.742	3.786±0.015	0.64±0.02	2.82	1.38	1.17±0.27
···	···	565	2022	< 30.24	22.469	19.431	3.545±0.005	−0.92±0.14	0.69	0.46	3.05±0.05
···	···	566	1110	< 29.85	18.041	16.543	3.759±0.010	0.34±0.02	10.45	1.28	1.70±0.14
···	···	567	···	< 29.86	···	···	···	···	0.62	0.35	···
···	···	569	2160	< 29.77	23.069	19.681	3.533±0.005	−0.98±0.15	1.37	0.40	3.05±0.05
···	···	570	1935	< 30.19	22.058	19.288	3.559±0.009	−0.89±0.14	6.58	0.49	3.05±0.05
···	···	571	1773	< 30.03	21.581	18.916	3.569±0.011	−0.74±0.14	6.04	0.61	3.05±0.05
···	···	572	2243	< 30.51	22.968	19.836	3.541±0.005	−1.08±0.15	2.25	0.38	3.05±0.05
···	···	573	2172	< 30.39	22.829	19.736	3.543±0.005	−1.04±0.14	1.61	0.39	3.05±0.05
···	···	574	1885	< 29.83	21.987	19.166	3.554±0.008	−0.83±0.14	3.26	0.53	3.05±0.05
···	···	575	1525	< 30.14	20.398	18.272	3.629±0.014	−0.54±0.13	5.18	0.87	2.49±0.16
···	···	581	2129	< 30.40	22.831	19.639	3.539±0.005	−0.99±0.15	3.28	0.39	3.05±0.05
···	···	582	···	< 30.20	···	···	···	···	0.69	0.37	···
···	···	584	2008	< 29.85	22.373	19.415	3.549±0.005	−0.92±0.14	4.48	0.46	3.05±0.05
···	···	586	1579	< 30.21	20.734	18.413	3.605±0.013	−0.60±0.14	3.16	0.81	2.70±0.48

[a] Record ID of h Per members listed in Table 2 of Moraux et al. (2013). [b] Record ID of h Per members listed in Table 6 of Currie et al. (2010). [c] L_X are in erg s^{-1}. [d] Apparent magnitudes in V and I_C band are from Currie et al. (2010). [e] Period and mass values are form Moraux et al. (2013).